Carnegie Mellon University

CARNEGIE INSTITUTE OF TECHNOLOGY

THESIS

SUBMITTED IN PARTIAL FULFILLMENT OF THE REQUIREMENTS

FOR THE DEGREE OF

Doctor of Philosophy

TITLE **Assessing the Costs and Risks of Novel Wind Turbine Applications**

PRESENTED BY **Stephen M. Rose**

ACCEPTED BY THE DEPARTMENT OF

Engineering & Public Policy

Professor Jay Apt, MAJOR PROFESSOR DATE

Professor M. Granger Morgan, DEPARTMENT HEAD DATE

APPROVED BY THE COLLEGE COUNCIL

DEAN DATE

Assessing the Costs and Risks of Novel Wind Turbine Applications

SUBMITTED IN PARTIAL FULFILLMENT OF THE REQUIREMENTS FOR

THE DEGREE OF

DOCTOR OF PHILOSOPHY

IN

ENGINEERING & PUBLIC POLICY

Stephen M. Rose

B.S., Mechanical Engineering, University of California, Berkeley

M.S., Mechanical Engineering, Georgia Institute of Technology

Carnegie Mellon University

Pittsburgh, PA

May 2013

Acknowledgements

I want to thank the people who collaborated with me on this research and those who helped me along the way. Thanks to Jay Apt for spending countless hours advising me in my research, editing my writing, and pushing me to improve my research without getting lost in the pursuit of perfection. Thanks to Mitch Small for teaching me statistics and probability by suggesting which technique I should use and then sending me off to figure it out on my own, and for always pushing me use slightly fancier methods than I needed. Thanks to Paulina Jaramillo for collaborating with me on the hurricane research and giving me research and career advice. Thanks to John Zack for provided his expertise in boundary-layer meteorology and very astute criticisms of the assumptions I made in my research.

Thanks to Kerry Emanuel who provided the simulated hurricanes used in Chapter 5:and lots of patient support in understanding and using them. Thanks to Iris Grossmann for her collaboration and hurricane expertise for the research in Chapter 4:.

Finally, thanks to Lucy for putting up with years of me being stressed, frustrated, or distracted by my research and for helping to teach me statistics.

This work was supported in part by the EPA STAR fellowship program, a grant from the Alfred P. Sloan Foundation and EPRI to the Carnegie Mellon Electricity Industry Center, and by the Doris Duke Charitable Foundation, the R.K. Mellon Foundation and the Heinz Endowments for support of the RenewElec program at Carnegie Mellon University. This research was also supported in part by the Climate and Energy Decision Making (CEDM) center. This Center has been created through a cooperative agreement between the National Science Foundation (SES-0949710) and Carnegie Mellon University.

Abstract

This thesis addresses the cost-effectiveness of curtailing a wind farm to regulate the electrical grid frequency and the hurricane risk to offshore wind farms in the eastern United States. Additionally, this thesis presents a new method to generate long periods of non-stationary wind speed time series data sampled at high rates by combining measured and simulated data.

Paper 1 calculates the cost of curtailing the power output of a wind farm to provide a reserve of power to regulate the electrical grid frequency, as required by grid operators in several countries with high wind-power penetrations. The simulations in Paper 1 show that it is most efficient to curtail a few turbines deeply rather than curtail all turbines in a wind farm equally. Compared to regulation prices in the Texas (ERCOT) market in 2007-2009, a curtailed wind farm would be cost-competitive with conventional generators less than 1% of the time.

Paper 2 supports the simulations in Paper 1 by developing a method to combine long periods of low-frequency wind speed data with realistic simulated high-frequency turbulence. The combined time series of wind speeds retains the non-stationary characteristics of wind speed, such as diurnal variations, the passing of weather fronts, and seasonal variations, but gives a much higher sampling rate.

Papers 3 and 4 estimate the hurricane risks to current designs of offshore wind turbines in the U.S. Paper 3 develops analytical probability distributions based on historical hurricane records to predict the distribution of damages to a single wind farm in a given location. Paper 4 uses simulated hurricanes with realistic statistical properties to estimate the correlated risks to all the wind farms in a region and estimate the distribution of aggregate losses over different periods. Both papers find hurricane risks are small for current turbine designs in New England and the Mid-Atlantic, but the

risks in the Gulf of Mexico and the Southeast are significant enough to warrant new, stronger designs. Hurricane risks could be reduced almost an order of magnitude by ensuring that turbines can continue yawing to track the wind direction even if grid power is lost.

TABLE OF CONTENTS

LIST OF TABLES

LIST OF FIGURES

Chapter 1: INTRODUCTION

The United States pledged at the Copenhagen Accord to reduce greenhouse gas emissions 17% below 2005 levels by 2020 [1]. Electricity generation is likely to contribute significantly to that reduction because it accounts for approximately 40% of United States greenhouse gas emissions [2] and it is easy to regulate—there are relatively few power plants compared to the number of other greenhouse gas (GHG) sources and their emissions can be easily monitored. Greenhouse gas emissions from electric power can be reduce by capturing carbon released during combustion and sequestering it ("CCS"), by switching to technologies that produce less carbon per unit of electricity generated (e.g. natural gas turbines), or by generating electricity without combustion (e.g. nuclear, hydro, wind, solar). Since 2000, most new generation built in the U.S. has been either natural gas turbines or wind power. The wind power's share of new generation peaked at 42% in 2009, when natural gas prices reached record highs [3].

This growth has been fueled by economics, uncertainty about future greenhouse gas policies, and a growing demand for renewable energy to meet Renewables Portfolio Standards that many states have enacted. The economics are particularly compelling-- in many cases, the cost of energy from a new wind power plant is less than that cost of energy from new power plants of most other types [4] and government subsidies make wind even more attractive. As a result, the capacity of wind generators installed in the United States has grown from approximately 8.7 GW in 2005 to more than 47 GW at the end of 2011 [3]. Nationally, approximately 3.3% of electrical energy is generated from wind power, but the penetration is much higher in some states [3]. For example, approximately 22% of the electricity generated in South Dakota and 20% of the electricity generated in Iowa come from wind power [3].

The work in this thesis investigates the feasibility of using current wind turbine designs in ways they were not intended for. Current wind turbines are designed to maximize power capture but grid operators in some areas are asking wind farms to curtail power output to regulate the electrical grid frequency. Similarly, current offshore turbines are designed to survive North Sea storms, but developers are considering installing them in areas prone to hurricanes, which can be stronger. We base our analysis of the feasibility of those activities on deep understanding of the characteristics of wind, which we feel is vital to understanding wind power. Each paper in this thesis incorporates sophisticated models of wind phenomena, from the spectrum of wind turbulence on short time scales to stochastic models of hurricane diameter.

In Chapter 1 we calculate the cost-effectiveness of curtailing a wind farm to regulate the grid frequency. Current turbine designs are capable of curtailing their power output to create a reserve of power that can be used to regulate the grid frequency. We calculate the regulation capacity available and its cost by simulating the active power output of a curtailed 100-MW wind farm with a hybrid of real speed data and simulated high-frequency turbulence. The simulations allow us to estimate the size of reserve as a function of statistical properties of the wind speed and show that a curtailed wind farm can provide secondary frequency regulation capacity at a cost lower than conventional generators in less than 1% of the 1-hour periods studied. Although the operating cost of curtailing a wind farm for frequency regulation capacity is high, the capital cost of installing the hardware and software to enable curtailment for frequency regulation is low, so it is reasonable for grid operators to require wind farms to have the capability as long as it is rarely used. If a wind farm is curtailed, we find it is most efficient to deeply curtail a few turbines than evenly distribute the curtailment to all turbines.

In Chapter 2 we develop a method to generate realistic wind speed data used in the simulations in Chapter 1. Certain applications, such as that in Chapter 1, require long periods (e.g. several years) of wind speed data measured at short intervals (e.g. a few seconds). We develop a method to generate days to years of non-stationary wind speed time series sampled at high rates by combining measured and simulated data. Measured data, typically 10 - 15 minute averages, captures the non-stationary characteristics of wind speed variation: diurnal variations, the passing of weather fronts, and seasonal variations. Simulated wind speed data, generated from spectral models, adds realistic turbulence between the empirical data. The wind speed time series generated with this method agree very well with measured time series, both qualitatively and quantitatively. The power output of a wind turbine simulated with wind data generated by this method demonstrates energy production, ramp rates, and reserve requirements that closely match the power output of a turbine simulated turbine with measured wind data.

In Chapter 3 and Chapter 4, we look at the hurricane risks to offshore wind turbines built to current designs. Current offshore wind turbines are designed to withstand wind speeds equivalent to a Category 2 hurricane, but they are likely to be damaged by stronger winds. No offshore wind projects have been developed in the United States, but there are 10 offshore wind projects in the planning process (with an estimated capacity of 3.8 GW) [3] and more proposed [5], all in areas at risk from Atlantic hurricanes. These risks directly affect the cost of offshore wind power—strengthening current turbine designs to better survive hurricanes will increase their costs and the cost of electricity they produce.

In Chapter 3 we estimate the hurricane risk to a single wind farm in a specific location using probability distributions fit to historical hurricane records. We develop two analytical probability distributions for the expected number of turbines destroyed over the lifetime of a windfarm: one for the case where turbines are not replaced when destroyed and one for the case that turbines are replaced. Those distributions predict that the hurricane risk is low for current turbine designs in the Mid-Atlantic and New England, but is significant in the Gulf of Mexico where more intense hurricanes are frequent. The risk can be reduced by designing turbines for higher maximum wind speeds, or by adding backup power to ensure the turbine nacelle can be turned to point directly into the wind even if grid power is lost.

In Chapter 4, we estimate the correlated hurricane risk to all wind farms in a region using simulated hurricanes with realistic statistical properties. Using simulated hurricanes allows us to estimate the risks of events with return periods longer than the historical record (~ 100 years) and assess the correlation of risks between locations. We estimate the fraction of offshore wind power simultaneously offline and the cumulative damage in a region. In Texas, the most vulnerable region we studied, 11% of offshore wind power could be offline simultaneously due to hurricane damage with a 100-year return period and 5% could be destroyed in any 10-year period. Correlated damage to wind farms in a region is unlikely to significantly affect grid operations, but could cause large losses for companies insuring many wind farms in a region. We also use this method to re-calculate the results in Chapter 3 and find the risks lower than those estimated in Chapter 3, though still significant.

The work presented in this thesis is intended to inform better policies and investment decisions for large-scale wind power development. Wind power is likely to make a significant contribution to reducing GHG emissions from electric power generation if it is developed and used cost-effectively.

1.1 References

[1] "Appendix I to the Copenhagen Accord - Quantified economy-wide emissions targets for 2020 ," United Nations, Copenhagen, FCCC/CP/2009/11/Add.1, Mar. 2010.

[2] EIA, "Electric Power Annual 2010," U.S. Energy Infomation Administration, Washington, DC, Nov. 2011.

[3] R. Wiser and M. Bolinger, “2011 Wind Technologies Market Report,” U.S. Department of Energy, Oak Ridge, TN, DOE/GO-102012-3472, Jul. 2012.

[4] EIA, “Levelized Cost of New Generation Resources in the Annual Energy Outlook 2012,” U.S. Energy Information Administration, Washington DC, Jul. 2012.

[5] “OffshoreWind.net,” *offshorewind.net*. [Online]. Available: http://www.offshorewind.net. [Accessed: 18-Nov-2012].

Chapter 2: THE COST OF CURTAILING WIND TURBINES FOR SECONDARY FREQUENCY REGULATION CAPACITY

Abstract

We analyze the cost of curtailing the active power output of a wind farm to provide secondary frequency regulation capacity. We calculate the regulation capacity available and its cost by simulating the active power output of a curtailed 100-MW wind farm with a hybrid of real speed data and simulated high-frequency turbulence. We find that a curtailed wind farm can provide secondary frequency regulation capacity at a cost lower than conventional generators in less than 1% of the 1440 1-hour periods studied. Although the operating cost of curtailing a wind farm for frequency regulation capacity is high, the capital cost of installing the hardware and software to enable curtailment for frequency regulation is low. For that reason, we suggest that it is reasonable that grid operators require wind farms to have the capability to curtail for frequency regulation, but we recommend that capability should be rarely used.

This paper, written with Jay Apt, was submitted to *Energy Systems* in December 2012.

2.1 Introduction

When large numbers of wind turbines are connected to the electrical grid, the rapid variability of wind power on short time scales can cause the grid frequency to deviate significantly from its nominal value [1], [2]. In the many regions where pumped hydroelectric storage is not available, the grid frequency is typically regulated by adjusting the power output of fast-ramping thermal generators, including gas turbines. Gas turbines can be expensive to operate and produce power less efficiently and with higher levels of NO_x emissions when quickly varying their power output [3]. Other technologies are capable of compensating for the short-term variability of wind power, but they are either currently too expensive to be practical or cannot be scaled large enough to meet the rapidly-increasing penetration of wind power on the electrical power grid. Batteries and flywheels are technically well-suited to rapidly generating or absorbing power but commercially available units are too expensive at the moment on the scale needed for the penetrations of wind power expected in the next 10 – 20 years, although some promising systems are in the development phase. Hydroelectric power, and especially pumped hydro storage, is technically well-suited to rapidly changing power output and is relatively inexpensive. However, little new pumped hydro storage is being developed in the United States.

Denmark, Ireland, Great Britain, and Germany now include requirements in their national grid codes that wind farms be able to increase or decrease their power output to aid in regulating the grid frequency [4]-[7]. The active power output of a wind farm can be decreased by reducing the aerodynamic efficiency of the wind turbines or completely shutting down some turbines, but it is impossible to increase the output of a wind farm beyond the power level provided by the current wind velocity. Operating a wind farm at less than the currently available wind capacity ("curtailing") creates a reserve of power that allows power output to be increased on demand. Prior research has demonstrated the technical feasibility of curtailing the power output of a wind farm to regulate the grid frequency [5], [8]-[10]. Those authors consider primary frequency regulation, in which a generator responds to frequency deviations in a few seconds. In this paper we consider *secondary* frequency regulation, in which the generator responds over tens of seconds or minutes to a dispatch signal from the grid operator. Other research has demonstrated the feasibility of curtailing a wind farm to reduce the variation in power output or limit power ramp rates [11]-[13]. Many modern wind farms already have most or all the equipment necessary to curtail for frequency regulation and many others can be retrofitted inexpensively. However, the revenue a wind farm foregoes due to curtailment may be greater than the cost of procuring the same frequency regulation from traditional sources such as gas turbines or hydroelectric power plants, or using an energy storage technology such as a battery to store a reserve of energy [9], [10].

We calculate the cost and quantity available of frequency upregulation capacity from a curtailed wind farm as a function of wind conditions. Upregulation capacity is the ability of a generator to increase its active power output to increase the grid frequency. We also compare the cost of upregulation from a curtailed wind farm to market prices for upregulation capacity (typically set by gas turbines), though grid operation rules do not generally allow wind power to bid into the market for upregulation capacity (or other ancillary services). This comparison gives a first-order estimate of how often grid operators may call on wind turbines for secondary frequency regulation.

The method of curtailing a wind farm we consider in this research does not reduce the variability of the wind farm power output. We control the wind farm to maintain a constant difference Δ between the possible power P_{poss} and curtailed power P_{curt} outputs, which provides only a reserve of power that the grid operator can use to regulate the supply of power to match demand. There is an alternative curtailment scheme that would reduce the variability of wind power by curtailing the wind farm output to a low fixed amount, but we do not consider it here because the cost would be extremely high and there is still active debate about how much cost wind power variability imposes on a grid operator [14], [15].

2.2 Model

We calculate the amount of upregulation capacity a curtailed wind farm can produce and its cost by simulating the operation of a 100-MW wind farm. The wind farm produces upregulation capacity by curtailing its power output a fixed amount below the power possible in given wind conditions; this creates a reserve of power than can be dispatched on demand. The wind farm we model consists of 20 5-MW pitch-regulated turbines that receive power setpoint commends from a closed-loop wind farm controller that regulates the aggregate power output of the wind farm. The turbines are driven by wind speed data that is a hybrid of measured low-frequency wind speed data and simulated high-frequency turbulence. We analyze the curtailed power output of the wind farm, relative to its uncurtailed output, to calculate how much upregulation capacity it can produce and at what cost.

We create 60 days of wind speed data sampled at 5 Hz for three locations in central North America listed in Table 2.1. We use the method developed by Rose and Apt to create the wind speed data as a hybrid of measured 10-minute data and simulated high-frequency turbulence [16]. This method simulates high-frequency turbulence to "interpolate" between empirical data while maintaining the statistical properties of the empirical data. In this research, the empirical data is 10-minute mean and standard deviation of the wind speed measured at 50-meter height at three locations listed in Table 2.1. We randomly draw 60 days of data from each year and each location; 15 days from each season where possible. The high-frequency turbulence is simulated using Veers' method with the Kaimal spectrum recommended by the IEC wind turbine design standard [17], [18]. We create wind-speed time series for each turbine location in the wind farm. The wind speed time series for each turbine location have identical mean wind speeds, but the turbulences are related to each other by the lateral coherence relation proposed by Sørensen et al. [19] We use only the lateral coherence relation because all the turbines are arranged in a straight line perpendicular to the wind.

We use the hybrid wind speed data to dynamically simulate the power output of each turbine in a 20-turbine wind farm. Dynamically simulating individual turbines is an improvement on steady-state turbine models that relate power output to wind speed with a simple power curve, or aggregate farm models that lump the entire farm into a single equivalent turbine [19]-[21]. Each turbine is a pitch-regulated 5-MW turbine with a 126-meter rotor designed by the National Renewable Energy Laboratory [22]. The turbine rotor is large enough that it has a smoothing effect on the wind turbulence at higher frequencies; we model this smoothing effect with the wind turbine admittance function ($F_{wt}(f)$) proposed by Sørensen et al. [19] The turbines in the wind farm are spaced 5 rotor diameters apart (630 m) in a line perpendicular to the wind direction; the wind direction is constant.

The wind farm simulations are run using the SimWindFarm toolbox (version 0.8) for Matlab, developed as part of the Aeolus project [23]. The active power output of the wind farm is curtailed by a closed-loop controller that reduces the power setpoint for each turbine so the aggregate actual power output is a fixed number of megawatts below the possible power output; the Danish grid code refers to this control scheme as "Delta production constraint", where Δ is the fixed difference between the possible and actual power outputs [24]. Individual turbines are not curtailed equally—each turbine is curtailed proportional to its available power [25]. We do not allow the wind farm controller to command any wind turbine to curtail below its lower operating limit (LOL) of 20% of its rated power, though a turbine's power output may go below that limit when the wind speed is low.

We simulate the power output of the wind farm for levels of curtailment $0 \leq \Delta \leq 30$ MW with identical wind inputs. To limit the number of simulations, we increase curtailment in one-megawatt steps up to 10 MW, two-megawatt steps up to 20 MW, and five-megawatt steps up to 30 MW. We repeat the simulations of all curtailment levels with 60 days of hybrid wind speed data described above. To generalize the results of these experiments, we repeat the simulations with five wind speed data sets of 60 days each, listed in Table 2.1: three sets of wind speed measurements from a wind farm site in west Texas in 2007, 2008, and 2009, a set of measurements from a site in the northern Great Plains of the U.S. in 2008, and a set of measurements from a site in Ontario, Canada in 2008.

Table 2.1: Empirical wind speed data used to simulate wind farm power

Location	Period	Mean wind speed	Turbulence intensity (TI)	Capacity factor
West Texas	29 Mar. 2007 – 8 Dec. 2007	6.8 m/s	13%	29%
	21 Dec. 2007 – 14 Dec. 2008	7.2 m/s	13%	33%
	25 Dec. 2008 – 1 Sept. 2009	7.5 m/s	13%	35%
Northern Great Plains (U.S.)	2 Jan. – 17 Dec. 2008	8.0 m/s	10%	41%
Ontario (Canada)	29 Dec. 2007 – 20 Dec. 2008	6.7 m/s	12%	28%

2.3 Analysis

We calculate the amount of upregulation capacity that a curtailed wind farm can provide by retrospectively analyzing the wind farm simulations described in Section 2.2. The upregulation capacity $R(k \mid \Delta)$ that a wind farm can supply for given curtailment Δ in the k^{th} dispatch interval of length T is the smallest difference between the uncurtailed ("possible") power at time $P_{poss}(t)$ and curtailed power at time $P_{curt}(t)$:

$$R(k|\Delta) = \min\left(P_{poss}(t) - P_{curt}(t|\Delta)\right) \tag{2.1}$$

for t in the k^{th} period: $kT \leq t \leq (k+1)T$.

An example of data for this calculation are shown in Figure 2.1 for a dispatch interval of T = 300 seconds and a curtailment of Δ = 5 MW. During most of the dispatch interval, the curtailed power $P_{\text{curt}}(t \mid \Delta = 5)$ (green line) closely tracks the desired curtailment $P_{\text{ref}}(t)$ - Δ (dashed line), as shown at point A. However, $P_{\text{curt}}(t)$ (green line) is sometimes not curtailed as much as desired, as shown at point B. In this case illustrated by point B, the power output of several of the turbines in the wind farm reached the lower operating limit (LOL = 0.2 p.u.) and could not curtail further. The amount of available upregulation capacity $R(\text{k} \mid \Delta = 5)$ for the interval, shown as the shaded area, is limited by the smallest difference between $P_{\text{poss}}(t)$ and $P_{\text{curt}}(t \mid \Delta = 5)$ in that interval. Upregulation capacity R is always less than or equal to the curtailment Δ. We measure upregulation capacity in megawatts hours (MW-h), which is different from the unit of energy "megawatt hours (MWh)".

We analyze dispatch intervals T of 60 minutes and 15 minutes. Most power systems with markets for frequency regulation use a dispatch interval of 60 minutes, which means market participants bid an amount of regulation capacity they can sustain for the full 60 minutes. We test a dispatch interval of 15 minutes to determine whether a curtailed wind farm can better compete over shorter intervals.

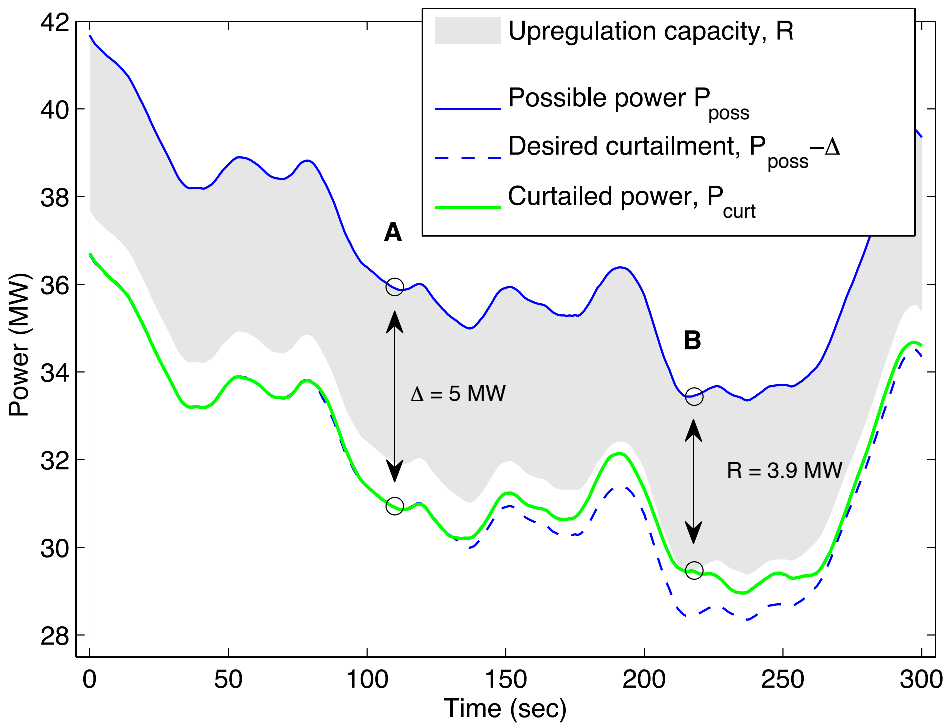

Figure 2.1: Method for calculating the available regulation capacity. In this example, the 100 MW-capacity wind farm is curtailed by Δ = 5 MW, but the available regulation capacity R(k | Δ) is 3.9 MW. R(k | Δ) is the largest curtailment that can be maintained through the entire dispatch interval T, i.e. the smallest difference between the uncurtailed and curtailed power outputs of the wind farm. The limiting condition is shown at point B. Point A shows an example of the turbines tracking their power limit setpoints perfectly—the actual curtailed power is 5 MW less than the uncurtailed power, as it is commanded to be.

The upregulation capacity available in a given dispatch interval, calculated in (2.1) cannot be known in advance without perfect forecasting of future wind conditions. Perfect foresight is an unrealistic assumption, but it sets an upper bound on the amount of regulation capacity available and the opportunity cost, in terms of energy production lost, to produce it. The results in Section 2.4 relax this assumption slightly—there we assume perfect forecasting of only the mean and standard deviation of wind speed in a given dispatch interval, rather than perfect forecasting of the wind speed at every moment.

We calculate the cost of upregulation capacity from a curtailed wind farm by retrospectively analyzing the wind farm simulations described in Section 2.2. The average cost of upregulation capacity $AC(k \mid \Delta)$ in the k^{th} dispatch interval with curtailment Δ is the energy generation lost in that interval due to curtailment $E_{loss}(k \mid \Delta)$ divided by the quantity of upregulation capacity provided during that interval $R(k \mid \Delta)$:

$$AC(k|\Delta) = \frac{E_{loss}(k|\Delta)}{R(k|\Delta)} \tag{2.2}$$

where E_{loss} is measured in MWh and AC is measured in MW-h/MWh. We calculate the marginal cost of upregulation capacity $MC(k \mid \Delta)$ as the additional upregulation capacity divided by the additional energy loss resulting from curtailing one more step. The steps are not always one megawatt; to limit the number of simulations, we increase curtailment in one-megawatt steps up to 10 MW, two-megawatt steps up to 20 MW, and five-megawatt steps up to 30 MW. The average power was often not high enough to simulate curtailment up to 30 MW-- only approximately 20% of the 1-hour intervals we examined produced enough power to curtail by 30 MW.

2.4 Results

We present three results: estimates of the maximum regulation capacity available in given conditions, the cost of regulation capacity in terms of unproduced energy, and the cost premium for curtailment-derived regulation capacity compared to the market price.

2.4.1 Maximum Available Regulation Capacity

The maximum upregulation capacity available by curtailing a wind farm in the k^{th} dispatch interval $R_{max}(k)$ can be modeled by a linear function of the average power over the interval $P_{\mu}(k)$ and coefficient of variation (COV) of power over the interval $P_{COV}(k)$ with a form given by (2.3) and fitted parameters given in Table 2.2. The COV of power $P_{COV}(k)$ is the standard deviation of power in that interval divided by the mean power in that interval.

$$\hat{R}_{max}(k) = a_0 + a_1 P_{\mu}(k) + a_2 P_{COV}(k) \tag{2.3}$$

We fit the linear function in equation (2.3) to data derived from the power output of a 100-MW wind farm described in Section 2.2 simulated with wind speed data from west Texas in 2008. The maximum upregulation capacity $R_{max}(k)$ calculated as the maximum of (2.1) over the range of simulated curtailments. We use Type I Tobit regression [26], [27] to fit the model to the data because $R_{max}(k)$ is both left- and right-censored—it cannot be less than zero and it cannot be greater than the largest curtailment we simulated (30 MW). In practice, we find left- and right-censoring limits of 1 MW and 29 MW, respectively, gave a better fit because R_{max} does not reach the theoretical limits (0 and 30 MW) in many of the simulated intervals. Tobit regression for data that is both left- and right-censored is fit by maximizing the log of the likelihood function given in equation 6.39 in a monograph by Maddala [28].

Table 2.2: Regression coefficients for max regulation capacity in (2.3)

	T = 60 min (n_{cens} = 996)	T = 15 min (n_{cens} = 3764)
Constant (a_0)	-9.40 (0.55)	-13.5 (0.16)
P_μ coeff. (a_1)	0.621 (0.010)	0.770 (0.0037)
P_{COV} coeff. (a_2)	-52.2 (2.2)	-48.4 (0.85)

The a_1 coefficient in Table 2.2 shows that the expected value of R_{max} increases 0.62 MW when the mean power in a 60-minute dispatch interval increases by 1 MW and by 0.77 MW for a 15-minute dispatch interval. The a_2 coefficient shows that the expected value of R_{max} *decreases* very rapidly as the coefficient of variance (COV) of the wind farm power increases. For example, if the COV increases by 0.01 (1% of the mean power) for a 60-minute dispatch interval, R_{max} decreases by 0.52 MW.

These results assume perfect forecasting of the mean and COV of wind farm power for a given interval. This is important because upregulation capacity must typically be bid into the market hours or a full day ahead. If future wind conditions cannot be forecast with perfect accuracy, the wind farm must bid less upregulation capacity into the market than it could theoretically produce or risk being unable to meet its commitment. However, we show in Section 2.4.2 that a wind farm should bid less than the R_{max} because the costs rise steeply as the upregulation capacity approaches its maximum.

2.4.2 Cost of Curtailing for Regulation Capacity

The average and marginal costs of curtailing a wind farm for frequency regulation as a function of regulation capacity are calculated with (2.2) and the results are shown in Figure 2.2 for 15-minute and 60-minute dispatch intervals. We calculate the average cost as the opportunity cost, i.e. the amount of energy production (in MWh) lost to produce 1 MW-h of steady regulation capacity. The marginal cost is the opportunity cost of additional regulation capacity R produced by curtailing the wind farm one additional megawatt. Figure 2.2 plots cost curves for three representative ranges of R_{max}: 5 MW, 10 MW, and 15 MW. The circles denote the median cost and the error bars show the 5^{th} and 95^{th} percentile costs.

We find several trends in the cost of regulation capacity from a curtailed wind farm. First, the cost of regulation capacity is lower in periods with larger maximum available regulation capacity R_{max}. Second, the cost is high for quantities of regulation capacity near zero or near R_{max}. Third, costs are slightly lower for shorter dispatch intervals, e.g. 15-minute intervals vs. 60-minute intervals. These trends are consistent for wind power simulated with wind data from the three sites listed in Table 2.1.

The cost of regulation capacity is lower in intervals with larger R_{max}, as shown in Figure 2.2. The cost curves representing periods with smaller R_{max} (e.g. 5 MW) have higher costs for all levels of regulation capacity then the curves representing periods with larger R_{max} (e.g. 15 MW). For example, minimum median AC for 60-minute dispatch intervals in Figure 2.2C is 1.51 MWh/MW-h when

R_{max} = 5 MW , 1.11 MWh/MW-h when R_{max} = 10 MW, and 1.06 MWh/MW-h when R_{max} = 15 MW.

Similarly, the marginal cost MC decreases as R_{max} increases. For example, the minimum median MC for a 60-minute dispatch interval in Figure 2.2D is 1.31 MWh/MW-h when R_{max} = 5 MW, 1.03 MWh/MW-h when R_{max} = 10 MW, and 1.00 MWh/MW-h when R_{max} = 15 MW.

The cost of regulation capacity is high for quantities of regulation capacity R near zero or near R_{max}. The high cost of regulation capacity near zero ($R \leq 1$ MW) can be seen on the left side of the AC curves in Figure 2.2A and C. For example, Figure 2.2C shows the median AC of 1 MW of regulation

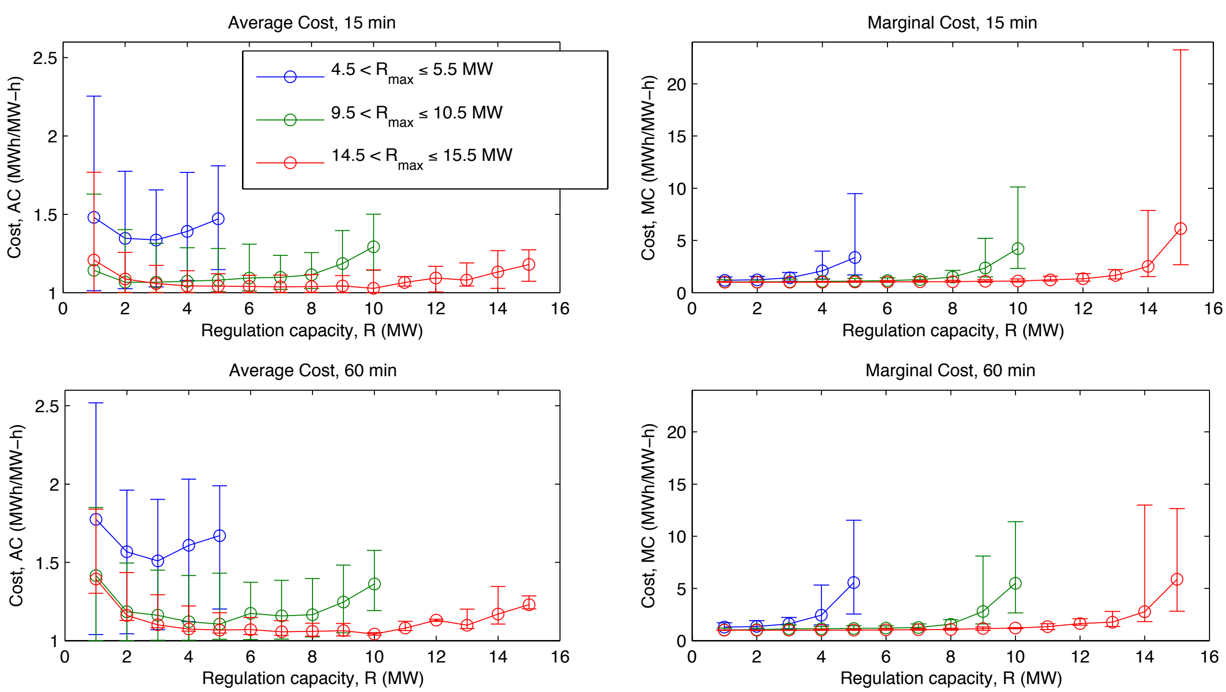

Figure 2.2: The average cost (AC) and marginal costs (MC) of regulation capacity for 15-minute and 60-minute dispatch intervals. Each line represents cost data for dispatch intervals with maximum available regulation capacity in a certain interval described in the figure key. Circles denote the median and error bars show the 5th and 95th percentile costs. These results are calculated for a 100-MW wind farm simulated with wind speed data from west Texas in 2008.

The opportunity cost when R is near zero can be reduced by curtailing a few turbines more deeply instead of curtailing all turbines in the wind farm equally. For example, if all turbines are curtailed equally, the median AC of R = 1 MW is 1.48 MWh/MW-h for a 15-min dispatch interval with R_{max} = 5 MW. If only half the turbines in the wind farm are curtailed, the median AC is 1.12 MWh/MW-h and if a quarter of the turbines are curtailed, the median AC is 1.00 MWh/MW-h. However, concentrating the curtailment on a few turbines reduces the maximum available regulation capacity; for example, concentrating the curtailment on 25% of the turbines reduces R_{max} by a factor of four.

The high cost of regulation capacity near the maximum can be seen on the right side of the AC curves in Figure 2.2A and C and the MC curves in Figure 2.2B and D. For example, Figure 2.2D shows the marginal cost of increasing R from 8 to 9 MW is 1.58 MWh/MW-h and the marginal cost of increasing R from 9 to 10 MW is 2.80 MWh/MW-h in a 60-min period with R_{max} = 10 MW. The cost increases sharply as R approaches R_{max} because individual wind turbines reach the lower operating limit (LOL) of their power output. When turbines reach their LOL, even for a short time, that limits the available regulation capacity R for the entire interval, as described in equation (2.1). However, energy loss E_{loss} is cumulative over the entire interval, so it is not affected much when turbines briefly reach their LOL. Thus the cost of regulation capacity, calculated with equation (2.2), increases sharply when the denominator R decreases (because turbines reach their LOL) but the numerator E_{loss} changes very little.

The results in Figure 2.2 exclude data where the actual regulation capacity is very close to the maximum available regulation capacity ($R_{max} - R < 0.1$ MW) because the costs approach infinity. Excluding those points significantly reduces the 95th percentile cost but changes the median MC very little. In addition to excluding those points, we also exclude dispatch intervals when the mean wind farm power is outside the linear range ($P_{\mu}(k) < 21$ MW or $P_{\mu}(k) > 50$ MW) and dispatch intervals when the maximum available upregulation capacity is near zero ($R_{max}(k) < 0.5$ MW).

The cost of regulation capacity decreases for shorter dispatch intervals, though the difference becomes smaller as R_{max} increases. For example, the results in Figure 2.2A and C show that the median AC of 10 MW of regulation capacity is 1.03 MWh/MW-h for a 15-minute dispatch interval and 1.04 for a 60-minute dispatch interval when R_{max} = 15 MW.

The results in Figure 2.2 are calculated for wind speed data from west Texas in 2008, but results calculated for the other locations and other periods listed in Table 2.1 show the same trends. Results calculated for the Great Plains wind data show lower average and marginal costs than the other sites; we believe the costs are lower because the a wind farm at the Great Plains site has a significantly higher capacity factor than the other two sites—41%, as compared to 33% for the west Texas site in 2008 and 28% for the Ontario site.

2.4.3 Cost-Effectiveness of Curtailing for Frequency Regulation

Curtailing a wind farm can very rarely provide frequency regulation for less than the market price of regulation. We compare the minimum AC in each 1-hour dispatch interval to the market price of upregulation ("MCPCU" = "Market-Clearing Price of Capacity – Up") in the corresponding dispatch interval in the ERCOT (Texas) market [29]. The cost of upregulation capacity from a curtailed wind farm in a given interval is the minimum AC in that interval multiplied by the opportunity cost of a megawatt of wind power production. We plot the results in Figure 2.3 as a cumulative distribution (CDF) of premiums that must be paid for regulation capacity from a curtailed wind farm, above the market price. The results are sensitive to the market price of upregulation and to the opportunity cost of curtailment.

Negative cost premiums in Figure 2.3 correspond to intervals when wind farm curtailment produces upregulation capacity for less the market price. The cost of curtailment-derived upregulation capacity is less than the market price in approximately 1% of the 1440 1-hour dispatch intervals studied in 2008, and approximately 0% of the dispatch intervals in 2007 and 2009. If the grid operator is willing to pay a premium up to $50/MW-h, the wind farm can provide regulation capacity in 8% of the 1-hour dispatch intervals in 2007, 15% in 2008, and 5% in 2009. These results assume an opportunity cost for curtailing the wind farm of $62/MWh, made up of a wholesale energy price of $40/MWh (the only wind power price in Texas reported to Wiser and Bolinger [30]), the federal Production Tax Credit ("PTC") of $21/MWh, and a Renewable Energy Certificate ("REC") price of $1/ MWh estimated by Wiser and Bollinger [30]. To examine the sensitivity of the results to the opportunity cost, we plot in Figure 2.4 the percentage of 1-hour dispatch intervals when upregulation capacity from a curtailed wind farm costs less than the market price against the opportunity cost of curtailment. These results show that a wind farm with a lower opportunity cost will be competitive in the upregulation capacity market more often than a wind farm with higher opportunity costs. The CDF in Figure 2.3 does not reach a cumulative probability of 1 because the wind farm was not able to supply *any* regulation capacity in approximately 55% of the periods analyzed.

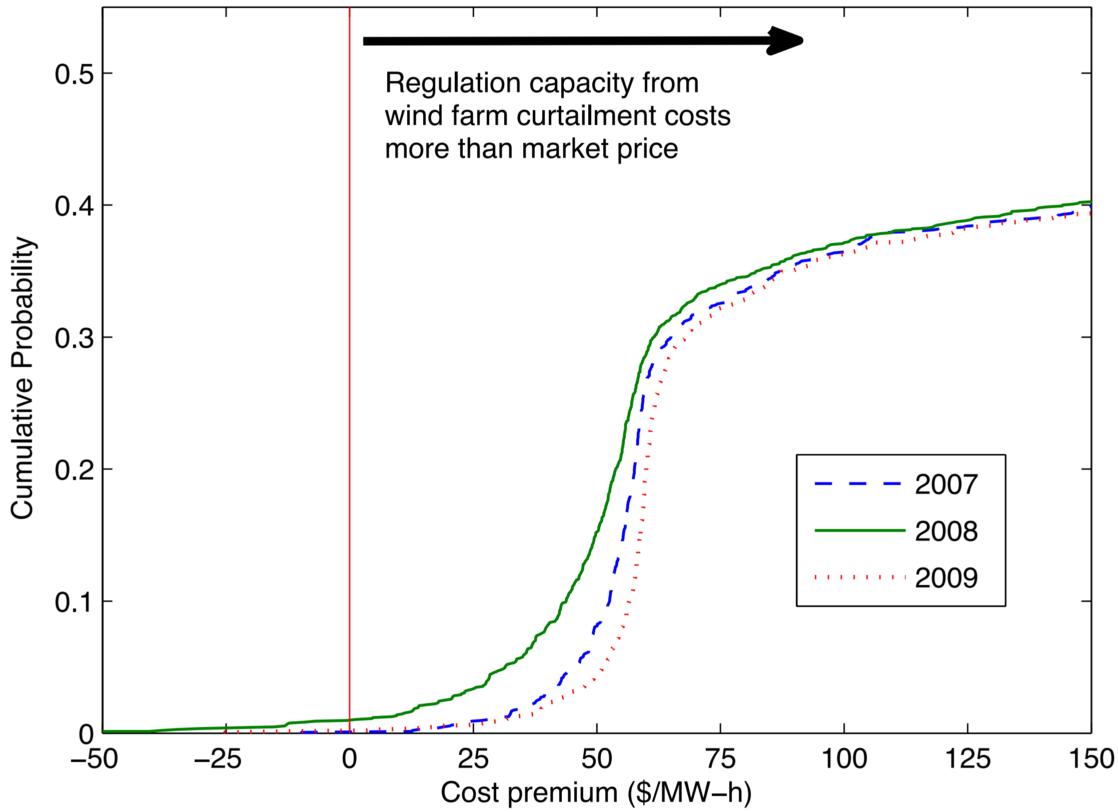

Figure 2.3: A CDF of the cost premium for regulation capacity from a curtailed wind farm, as compared to ERCOT market prices for upregulation. The curtailed wind farm can provide upregulation at less than the market price in fewer than 1% of the 1440 1-hour periods studied and at *any* price in approximately 45% of the periods studied. We assume an opportunity cost for curtailing the wind farm of $62/MWh.

In practice, a wind farm operator may bid less than the full opportunity cost for upregulation capacity because he or she would receive payments for extra energy produced when that upregulation capacity is dispatched, sometimes called upregulation *energy*. Most other players in the upregulation capacity market already bid prices based on expectations of the amount of upregulation energy that will be dispatched.

The results in Figure 2.3 and Figure 2.4 are calculated for wind speed data from west Texas in 2008, but results calculated for the other locations and other periods listed in Table 2.1 show the same trends. We compare regulation capacity costs calculated with wind speed data from the other sites listed in Table 2.1 to regulation capacity market prices from Texas, so the results do not account for any correlation between regulation market prices and wind conditions. Regulation capacity costs calculated with Great Plains wind data are approximately half of costs calculated with wind data from the other two sites, though they are still only competitive with the market price in 3.5% of the periods studied. We believe the costs are lower because the a wind farm at the Great Plains site has a significantly higher capacity factor than the other two sites—41%, as compared to 33% for the west Texas site in 2008 and 28% for the Ontario site.

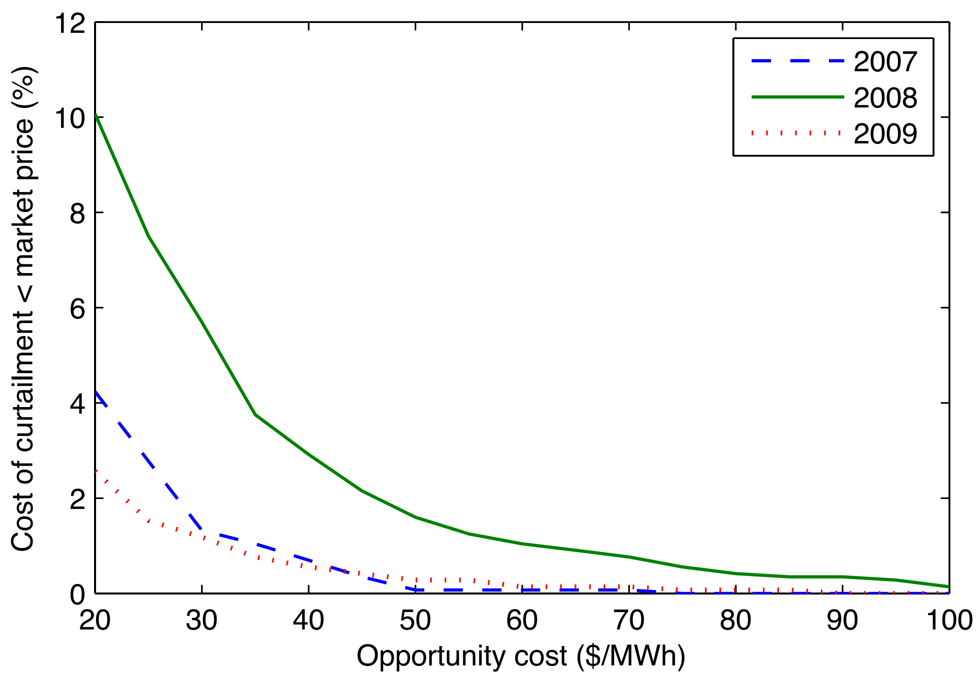

Figure 2.4: Cost-effectiveness of wind farm curtailment for upregulation as a function of opportunity cost of curtailment. As the opportunity cost of curtailment increases, upregulation from curtailment is cheaper than the market price for curtailment in fewer 1-hour dispatch intervals.

These results are best-case scenarios based on the assumption of perfect forecasting. The results are likely to be similar even with imperfect forecasting because Figure 2.2 shows that the cost of upregulation capacity does not diverge much from the minimum when the wind farm is not curtailed by the optimum amount. However, the cost of upregulation capacity from a curtailed wind farm is rarely competitive with Texas market prices.

We show above that, for Texas energy and regulation prices, curtailing a wind farm is rarely cost-competitive. However, curtailing a wind farm may be more or less cost-effective in other power systems depending on the relationship between energy and regulation prices. For example, a system with many large coal power plants and few gas turbines would likely have lower energy costs and higher regulation costs, which would make curtailing a wind farm more cost-competitive.

2.5 Conclusions

A curtailed wind farm can rarely provide frequency upregulation at a cost lower than the present U.S. regulation market price, even if wind conditions can be forecast with perfect accuracy. We find that even with the high prices for upregulation capacity seen in the Texas (ERCOT) market in 2008, a curtailed wind farm with average opportunity costs could produce upregulation capacity at a cost less than the market price only 1% of the time. In other years with lower market prices for upregulation capacity, a curtailed wind farm would almost never be competitive. Curtailing a wind farm for frequency upregulation may be worthwhile in electrical grids where fast-ramping conventional generators are very expensive such as Hawaii, where diesel generators produce most of the regulation.

Several factors put wind farms at a disadvantage in a competitive market for upregulation capacity. First, the structure of some government subsidies for wind energy increase the opportunity cost of unproduced energy. When wind turbines are subsidized based on energy production, a curtailed wind farm loses both the revenue and the subsidy for unproduced energy. Second, thermal generators have lower opportunity costs for unproduced energy because their lost revenue is partially offset by fuel savings. Wind turbines have no significant variable costs, so they receive no offsetting savings for curtailment.

However, it is reasonable for grid operators to require that wind farms install the capability to curtail for frequency regulation. Curtailing a wind farm has a high operating cost, the opportunity cost of unproduced energy, but a very low capital cost. For grid operators, requiring delta curtailment capability from wind farms creates an emergency source of frequency regulation that may become more useful as wind power penetration increases. Wind farm owners already accept the requirement to be able to curtail for frequency regulation as a cost of connecting to the grid in some places.

If it is necessary to curtail a wind farm to provide upregulation capacity, there are several ways to minimize the cost. First, wind farms should be curtailed to approximately half of the maximum available upregulation capacity, as shown in Figure 2.2. If a wind farm is required to provide a small quantity of regulation capacity, it is better to deeply curtail a few of the turbines than evenly spread the curtailment over all the turbines. Some grid codes, such as those for E.On (Germany) and EirGrid (Ireland) require wind farms to curtail by a few percent of their rated power to create reserve power for frequency regulation [5], [7]. Curtailing only a few turbines in each wind farm to meet these requirements would increase the amount of reserve power for a given curtailment and decrease the variability of the size of the reserve. Second, wind farms with low opportunity costs should be curtailed first. Wind farms that sell power on low-price long-term contracts or farms that no longer receive production subsidies are the most likely candidates.

2.6 Acknowledgements

This work was supported in part by the EPA STAR fellowship program, a grant from the Alfred P. Sloan Foundation and EPRI to the Carnegie Mellon Electricity Industry Center, and by the Doris Duke Charitable Foundation, the R.K. Mellon Foundation and the Heinz Endowments for support of the RenewElec program at Carnegie Mellon University. This research was also supported in part by the Climate and Energy Decision Making (CEDM) center. This Center has been created through a cooperative agreement between the National Science Foundation (SES-0949710) and Carnegie Mellon University.

2.7 References

[1] D. Brooks, "Evaluation of the Effectiveness of Automatic Generation Control (AGC) Alterations for Improved Control with Significant Wind Generation," Electric Power Research Institute, Palo Alto, 1018715, May 2009.

[2] "Evaluation of the Impacts of Wind Generation on HELCO AGC and System Performance -- Phase 2," Electric Power Research Institute, Palo Alto, 1018716, May 2009.

[3] W. Katzenstein and J. Apt, "Air Emissions Due To Wind And Solar Power," *Environ. Sci. Technol*, vol. 43, no. 2, pp. 253–258, 2009.

[4] M. Tsili, C. Patsiouras, and S. Papathanassiou, "Grid code requirements for large wind farms: A review of technical regulations and available wind turbine technologies," *Proceedings of EWEC*, 2008.

[5] G. Ramtharan, N. Jenkins, and J. Ekanayake, "Frequency support from doubly fed induction generator wind turbines," *IET Renew. Power Gener.*, vol. 1, no. 1, p. 3, 2007.

[6] B. Singh and S. Singh, "Wind power interconnection into the power system: a review of grid code requirements," *The Electricity Journal*, vol. 22, no. 5, pp. 54–63, 2009.

[7] EirGrid, "EirGrid Grid Code: WFPS1, Controllable Wind Farm Power Statoin Grid Code Provisions, version 3.3," Jan. 2009.

[8] R. de Almeida and J. Lopes, "Participation of Doubly Fed Induction Wind Generators in System Frequency Regulation," *IEEE Transactions on Power Systems*, vol. 22, no. 3, pp. 944–950, 2007.

[9] L. Holdsworth, J. Ekanayake, and N. Jenkins, "Power System Frequency Response from Fixed Speed and Doubly Fed Induction Gernerator-based Wind Turbines," *Wind Energy*, vol. 7, no. 1, pp. 21–35, Mar. 2004.

[10] C. Jecu, A. Teninge, D. Roye, S. Bacha, R. Belhomme, and P. Bousseau, "Contribution to frequency control through wind turbine inertial energy storage," *European Wind Energy Conference 2008*, 2008.

[11] Z. Lubosny and J. Bialek, "Supervisory control of a wind farm," *IEEE Transactions on Power Systems*, vol. 22, no. 3, pp. 985–994, 2007.

[12] B. Rawn, P. Lehn, and M. Maggiore, "Control methodology to mitigate the grid impact of wind turbines," *IEEE Trans. on Energy Conversion*, vol. 22, no. 2, pp. 431–438, 2007.

[13] A. Vigueras-Rodríguez, P. Sørensen, N. A. Cutululis, A. Viedma, E. Gómez-Lázaro, and S. Martin, "Application of ramp limitation regulations for smoothing the power fluctuations from offshore wind farms," *European Wind Energy Conference 2009*.

[14] B. Parsons, M. Milligan, B. Zavadil, and D. Brooks, "Grid impacts of wind power: a summary of recent studies in the United States," *Wind Energy*, vol. 7, pp. 87–108, 2004.

[15] E. Ela, M. Milligan, B. Parsons, D. Lew, and D. Corbus, "The evolution of wind power integration studies: Past, present, and future," presented at the IEEE Power & Energy Society General Meeting, 2009, Calgary, 2009, pp. 1–8.

[16] S. Rose and J. Apt, "Generating wind time series as a hybrid of measured and simulated data," *Wind Energy*, vol. 15, no. 5, pp. 699–715, Jul. 2012.

[17] P. S. Veers, "Three-Dimensional Wind Simulation," *SAND88-0152*, p. 40, Mar. 1988.

[18] "IEC 61400-1: Wind Turbine Design Requirements (ed. 3.0)," *International Electrotechnical Commission*, pp. 22–31, Aug. 2005.

[19] P. Sørensen, N. A. Cutululis, A. Vigueras-Rodríguez, H. Madsen, P. Pinson, L. E. Jensen, J. Hjerrild, and M. H. Donovan, "Modelling of power fluctuations from large offshore wind farms," *Wind Energy*, vol. 11, no. 1, pp. 29–43, 2008.

[20] L. De Tommasi, M. Gibescu, and A. J. Brand, “A dynamic aggregate model for the simulation of short term power fluctuations,” *Procedia Computer Science*, vol. 1, no. 1, pp. 269–278, May 2010.
[21] P. Sørensen, N. A. Cutululis, A. Vigueras-Rodríguez, L. E. Jensen, J. Hjerrild, M. H. Donovan, and H. Madsen, “Power Fluctuations From Large Wind Farms,” *IEEE Transactions on Power Systems*, vol. 22, no. 3, pp. 958–965, 2007.
[22] J. Jonkman, S. Butterfield, W. Musial, and G. Scott, “Definition of a 5-MW reference wind turbine for offshore system development,” National Renewable Energy Laboratory, Golden, CO, NREL/TP-500-38060, Feb. 2009.
[23] J. D. Grunnet, M. Soltani, T. Knudsen, M. Kragelund, and T. Bak, “Aeolus Toolbox for Dynamics Wind Farm Model, Simulation and Control,” presented at the European Wind Energy Conference & Exhibition 2010, Warsaw, 2010, pp. 1–10.
[24] Elkraft and Eltra, “Wind Turbines Connected to Grids with Voltage above 100kV,” Dec. 2004.
[25] A. D. Hansen, P. Sørensen, F. Iov, and F. Blaabjerg, “Centralised power control of wind farm with doubly fed induction generators,” *Renewable Energy*, vol. 31, no. 7, pp. 935–951, 2006.
[26] J. Tobin, “Estimation of Relationships for Limited Dependent Variables,” *Econometrica*, vol. 26, no. 1, pp. 24–36, Jan. 1958.
[27] T. Amemiya, “Tobit Models - a Survey,” *Journal of Econometrics*, vol. 24, pp. 3–61, Jan. 1984.
[28] G. S. Maddala, *Limited-Dependent and Qualitative Variables in Econometrics*. Cambridge: Cambridge University Press, 1983.
[29] ERCOT, “Day-Ahead Ancillary Services Market Clearing Prices for Capacity Archives,” *Electric Reliability Council of Texas*. [Online]. Available: http://www.ercot.com/mktinfo/prices/mcpc. [Accessed: 29-Mar-2012].
[30] R. Wiser and M. Bolinger, “2010 Wind Technologies Market Report,” 2011.

Chapter 3: GENERATING WIND TIME SERIES AS A HYBRID OF MEASURED AND SIMULATED DATA

Abstract

Certain applications, such as analyzing the effect of a wind farm on grid frequency regulation, require several years of wind power data measured at intervals of a few seconds. We have developed a method to generate days to years of non-stationary wind speed time series sampled at high rates by combining measured and simulated data. Measured wind speed data, typically 10 - 15 minute averages, captures the non-stationary characteristics of wind speed variation: diurnal variations, the passing of weather fronts, and seasonal variations. Simulated wind speed data, generated from spectral models, adds realistic turbulence between the empirical data. The wind speed time series generated with this method agree very well with measured time series, both qualitatively and quantitatively. The power output of a wind turbine simulated with wind data generated by this method demonstrates energy production, ramp rates, and reserve requirements that closely match the power output of a turbine simulated turbine with measured wind data.

This paper, written with Jay Apt, was published as S. Rose and J. Apt, "Generating wind time series as a hybrid of measured and simulated data," *Wind Energy*, vol. 15, no. 5, pp. 699–715, Jul. 2012.

3.1 Introduction

Planning for frequency control in a power system with significant amounts of wind power requires both high-frequency data (~1 Hz) to capture fast changes in power output and long periods of data to capture diurnal and seasonal variations. Similarly, simulating the fatigue life of wind turbine mechanical components requires high-frequency data to capture the dynamic effects of control system actions, but long periods of data to compile statistical data to more accurately estimate lifetimes. In both cases, large amounts of data are needed to design systems that are neither overly conservative and inefficient nor unreliable.

Long wind speed data sets sampled at high rates are often difficult to obtain. Empirical data are often sampled at too slow a rate, in the wrong location, or at the wrong height. Government meteorological services record many years of wind speed data, but it is typically sampled at slow rates (2 minute moving average in the USA) with low amplitude resolution (1 knot, 0.51 m/s, in the USA) [1] and at locations that are not valuable for wind power development. Wind farm developers collect several years of data at potential wind power sites, but they typically record 10-15 minute average values that are sufficient to estimate only long-term power production. Special scientific campaigns sometimes collect weeks to years of high-frequency data, but there are few of them because they are expensive to set up and maintain. The measurement instruments on a wind turbine are one of the best sources of this type of data, but the measurements can be confounded by the effects of the turbine and other turbines nearby, and data are frequently not archived at high temporal resolution.

Simulated wind speed data can be created at very high sampling rates, in any location, and at any height desired. However, simulation of periods longer than a few hours is difficult because wind speed variations are non-stationary processes: their statistical properties change over time. Those properties change with time of day, with the passing of weather fronts, and with the seasons. Most methods for simulating long periods of wind speed data use separate models for the non-stationary variations over longer periods (e.g. hours to months) and the stationary variations over shorter periods (e.g. seconds to minutes).

Previous authors have proposed a variety of methods for simulating non-stationary wind speed time series longer than a few hours [2]. The simulation methods divide the variations into high-frequency (periods less than approximately 15 minutes) and low-frequency (periods greater than 15 minutes) ranges. One method, which we will refer to as the "spectral method", joins together separate spectral models for the high- and low-frequency ranges in the frequency domain [3], [4] and generates time series using the Veers method [5]. The other class of methods, that we will refer to as the "parametric method", models the high-frequency range using a spectral model and the low-frequency range using a probability distribution [6]-[8]. Short periods (~10 minutes) of high-frequency data are generated using the Veers method, blended together, and then superimposed on low-frequency time series data. Most authors blend together the short time series of high-frequency data using a window function such as the Hann function that reduces leakage of energy outside the range of simulated [6], [9] but one author concatenates together the high-frequency time series without any windowing because discontinuities are smaller than the largest sample-to-sample variations in the blocks of simulated wind speed [7].

Both methods of modeling the low-frequency, non-stationary variations in wind speed are inadequate for certain types of power system planning and simulation because their simulations are not indexed to time of day and time of year. For example, the spectral and parametric methods can generate long time series that contain a certain level of wind speed variance with a given probability, but those methods cannot model what time of day or time of year that level of variance is likely to occur. Electrical power demand is a relatively predictable function of time of day and time of year, so wind simulations must correctly model wind properties as a function of time. Nielsen addresses this problem in a non-stationary simulation of a wind front passage by specifying the statistical properties of wind turbulence at certain reference states, using Veers method to simulate stationary turbulence at those reference states, and then interpolating between the stationary simulations with Bezier curves fit to the reference states [10].

Our work addresses and solves the problem of correctly placing events in time by creating "hybrid" wind speed time series that combine measured low-frequency wind speed data with simulated high-frequency data. This hybrid method is similar to the parametric methods described above, especially Nielsen [10], but the hybrid method uses low-frequency measured wind speed data instead of the low-frequency data generated by parametric methods, and low-pass filtering of the measured data instead of windowing or interpolation. Low-frequency measured wind data are available from meteorological stations and meteorological towers at wind farms. Low-frequency wind speed data are also available from meso-scale simulations, but users should be very careful to understand the limitations of particular meso-scale models and the spatial and time resolutions of the data they generate.

Our work also improves on the procedure used in the parametric methods by filtering the low-frequency data to remove noise that leaks into the high-frequency region. This filtering fixes the problem of spurious low-frequency content in the Power Spectral Density (PSD) of data generated by McFarlane's method [6].

We demonstrate that this hybrid method creates wind time series that closely match the high-frequency and low-frequency characteristics of measured wind data and that the results of wind turbine simulations run with our hybrid wind closely match the results of turbine simulations run with measured wind data.

3.2 Hybrid Method for Generating Wind Data

We propose a hybrid method to generate long periods (days to years) of wind speed time series data by combining measured wind speed statistics sampled at low rates with simulated wind turbulence sampled at high rates. Measured statistics capture the non-stationary properties of real wind and simulated turbulence interpolates between the measured data. The hybrid method simulates short periods of turbulence using measured mean wind speed (and variance, if available) as a parameter, then superimposes the simulated turbulence on measured mean wind speed.

We define T as the total length of the period covered by the input data (in seconds); the total length of the output data is also T because the hybrid method interpolates the measured data. The sampling interval of the low-rate measured statistics is $T_{sample,\ input} = (f_{sample,input})^{-1}$ (we use $T_{sample,input} = 600$ seconds, $f_{sample,\ input} = 1.7 \times 10^{-3}$ Hz). The sampling frequency of the output data is f_{output} (we use $f_{output} = 1$ Hz).

A hybrid wind speed time series $u(t)$ of length T with output sampling frequency f_{output} is created by the following steps, illustrated in Figure 3.1:

A. Statistics of wind speed data are calculated over long intervals. In this paper, the wind speed mean and variance are measured with a sampling interval of $T_{sample,input} = 600$ seconds.

B. A block of zero-mean, high-frequency turbulence is simulated for every *two* points of measured data ($2T_{sample,input}$) using a spectral model and the Veers method [5]. Blocks of turbulence are concatenated together without blending, overlapping, or windowing.

C. The measured mean wind speed is re-sampled to the desired sampling rate f_{output} and smoothed by a low-pass filter.

D. The simulated turbulence is added to the smoothed mean to create the hybrid wind speed time series.

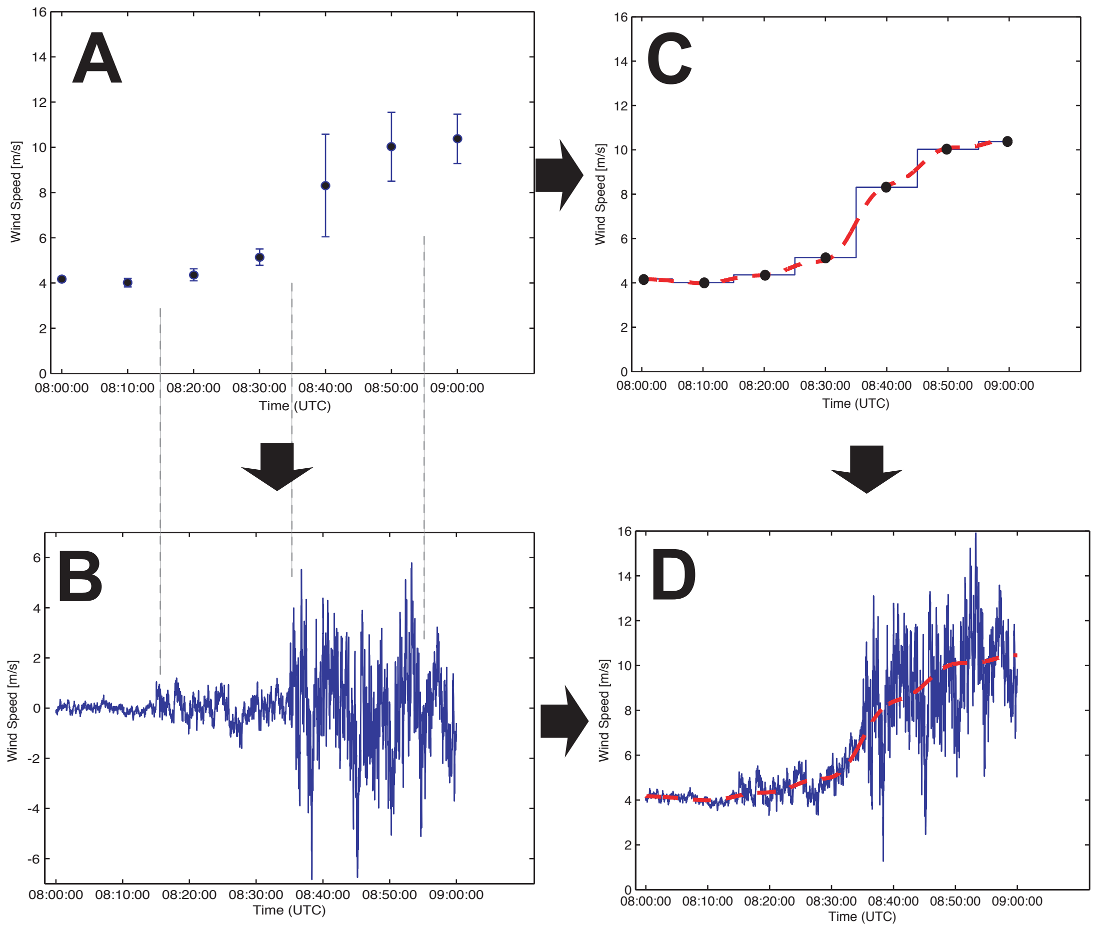

Figure 3.1: Procedure for generating wind speed time series from a hybrid of measured and simulated data. (A) Wind speed mean and variance measured for a long period Tinput are used as parameters to generate zero-mean turbulence in (B). The mean wind speeds in (A) are re-sampled at a higher rate foutput and smoothed by a low-pass filter in (C). The hybrid wind speed time series in (D) is the sum of (B) and (C).

3.2.1 Slowly-varying Measured Wind Speed (C)

The basis of a hybrid wind time series is mean wind speed measured at sampling intervals of $T_{sample,\ input}$. Low-rate mean wind speed captures slow changes such as diurnal and seasonal phenomena and the passing of weather fronts. Meteorological stations for wind resource assessment or weather prediction record the mean (and sometimes variance) of wind speed for periods of a few minutes. In this research, we use measured 10-minute mean $U_{0,p}$ and variance $\sigma^2_{u,p}$, where p is an index of the 10-minute period (Figure 3.1A).

We wish to create a time series of wind speeds of length T with a sampling rate of f_{output}. We re-sample the low-rate mean data to a sampling rate of f_{output} by repeating each measured mean $U_{0,p}$ at intervals f_{output} for a period of $T_{sample, input}$ (Figure 3.1C). Increasing the sampling rate from $f_{sample,input}$ to f_{output} does not add any new information, but it adds high-frequency noise. According to the sampling theorem, the maximum frequency signal that can be resolved by data sampled at $f_{sample,input}$ is $f_{\mathrm{Nyq},input} = (2T_{sample,input})^{-1}$ (the Nyquist frequency) [11]; all the content for frequencies higher than $f_{\mathrm{Nyq},input}$ is introduced noise. We remove the noise using a 3rd-order low-pass Butterworth filter with a cutoff frequency of $f_{cutoff} = f_{\mathrm{Nyq},input} = (2T_{sample,input})^{-1}$, where the gain of the filter is 1. The low-pass filter is implemented in the frequency domain by applying the Fourier transform to the data, convolving the transformed data with the filter, and then applying the inverse Fourier transform. To avoid wrap-around effects from the Fourier transform, we de-trend the data by subtracting the best-fit line before applying the Fourier transform and then adding that best-fit line after applying the inverse Fourier transform.

3.2.2 High-rate Turbulence (B)

The hybrid method simulates high-rate turbulence to interpolate between measured mean wind speed values, shown in Figure 3.1B. For every two measured mean wind speeds $U_{0,p}$ and $U_{0,p+1}$, we generate a zero-mean turbulence time series of length $2T_{sample, input}$. To model the non-stationary properties of real wind, the variance of each simulated turbulence time series is a function of the corresponding measured mean wind speed (and variance, if available). We model wind turbulence with two variations of the Kaimal spectrum: the form given in Kaimal's original paper that models variance as a function of surface roughness length z_0 [12], and the form given in the IEC 61400-1 standard that takes wind speed variance as an explicit input [13].

Wind turbulence is simulated by a method developed by Shinozuka [14] and extended by Veers [5]. The Veers method simulates wind turbulence by taking the Fourier transform of a turbulence spectrum. The procedure for simulating wind turbulence by Veers method is described in detail in many other sources [15] and summarized here:

1. Define a 1-sided spectrum for the wind turbulence $S(f)$
2. Discretize the spectrum for the desired output period and sample rate: $S[m] = S(f)\, f$
3. Scale the discretized spectrum and apply random phase angles: $\mathbf{V}[m] = \sqrt{\tfrac{1}{2}\eta\, S[m]}\, e^{i\phi[m]}$
4. Construct a two-sided spectrum $\mathbf{V}_{2\,side}$
5. Calculate the turbulence time series: $\mathbf{u} = \left|\mathrm{FFT}(V_{2\,side})\right|$

If the wind speed variance σ^2_u is known, the one-sided Kaimal spectral model specified in the IEC 61400-1 standard [13] can be used:

$$S(f) = \sigma_u^2 \frac{4(\frac{L_1}{U_0})}{\left(1 + 6(\frac{L_1}{U_0}) f\right)^{5/3}} \tag{3.1}$$

If the wind speed variance is not known but the surface roughness length z_0 is known (or can be estimated), the one-sided Kaimal spectral model proposed by Kaimal [12] can be used:

$$S(f) = u_*^2 \frac{105(\frac{z}{U_0})}{\left(1 + 33(\frac{z}{U_0}) f\right)^{5/3}} \tag{3.2}$$

where

σ_u = 10-minute standard deviation of longitudinal wind speed [m/s]

U_0 = 10-minute mean of longitudinal wind speed [m/s]

$$u_* = \frac{\kappa\, U_0}{\ln(\frac{z}{z_0})}$$

$L_1 = 8.1 * \Lambda_1$

$$\Lambda_1 = \begin{cases} 0.7z & z \le 60m \\ 42 & z > 60m \end{cases}$$

κ = 0.4 = von Kármán constant

z = turbine hub height [m]

z_0 = surface roughness length [m]

f = frequency [Hz]

The duration of each simulated interval of high-rate turbulence must be $2T_{sample,input}$ in order to generate frequency content up to $f_{Nyq,input}$, the highest frequency that the input data can resolve according to the Sampling Theorem [11]. Each simulated period will contain $N = 2T_{sample,\ input}f_{output}$ points; if N is not an integer, we round it up to the nearest even integer.

Each simulated time series corresponds to two low-rate measurements, so we must combine the measured means $U_{0,p}$ and $U_{0,p+1}$ and measured variances $\sigma^2_{u,p}$ and $\sigma^2_{u,p+1}$ according to the following formulas:

$$U_{0,p\cup p+1} = \frac{U_{0,p} + U_{0,p+1}}{2} \tag{3.3}$$

$$\sigma^2_{u,p\cup p+1} = \frac{\left(\frac{N}{2}-1\right)\sigma^2_{u,p} + \left(\frac{N}{2}-1\right)\sigma^2_{u,p+1}}{N-2} \tag{3.4}$$

where equation (3.4) is the formula for the pooled variance of two equally-sized samples of N/2 points each [16].

We discretize the continuous one-sided Kaimal spectrum $S(f)$ in equation (3.1) or (3.2) at discrete frequencies $f_m = m\Delta f$:

$$\mathbf{S}[m] = S(f_m)\Delta f \qquad m = \{0, 1, ..., M-1\} \tag{3.5}$$

There are $M = 1 + N/2$ unique frequencies in the one-sided spectrum, where $N = 2T_{sample,\ input}f_{output}$. We require that N be an even integer, so M will be an odd integer based on the definition above. We force $S[0] = 0$ because the steady-state ("DC") value of the simulated data is zero and we are simulating a zero-mean process.

We scale the magnitude of the discretized spectrum according to the following formula to create **V**, a vector of Fourier coefficients for a 1-sided spectrum:

$$\mathbf{V}[m] = \sqrt{\tfrac{1}{2}\eta\,\mathbf{S}[m]}\,e^{i\phi[m]} \tag{3.6}$$

The term $e^{i\phi[m]}$ creates random phases in **V** that make the output of Veers method random. The phases $e^{i\phi[m]}$ are complex numbers and $S[m]$ are real numbers, so $\mathbf{V}[m]$ are complex numbers. The phase angles $\phi[m]$ are drawn from a uniform random distribution over the range [0 2π]. Nearly all simulations that use the Shinozuka/Veers method use uniform randomly-distributed phase angles. Shinozuka proves that a simulated time series will be ergodic if uniform randomly-distributed phase angles are used [15]. In our analysis of measured wind speed data sampled at 5 – 52 Hz, we found that the differences between adjacent phase angles can be described by a von Mises distribution [17] and that the fit of the von Mises distribution improves for higher sampling frequencies. However, we find that it is statistically impossible to distinguish between uniform and von Mises distributions for the sampling frequencies used in our paper (~1 Hz). The dispersion of the von Mises distribution of the phase differences, analogous to the standard deviation in a normal distribution, is so low at this sampling frequency that statistical tests cannot establish that a von Mises distribution fits the data.

The factor of ½ in equation (3.6) is necessary because we will create a two-sided spectrum from **V**, but the spectra in equations (3.1) and (3.2) are one-sided spectra. The factor of ½ should be omitted if a two-sided spectrum is used. We introduce η to normalize $S[m]$ to compensate for the variance lost when $S(f)$ is discretized.

The factor η accounts for the difference between the desired variance $\sigma^2_{\text{desired}}$ and the actual variance σ^2_{actual} of data simulated with the discretized spectrum in equation (3.5). We define η as:

$$\eta = \frac{\sigma^2_{desired}}{\int_{\Delta f - \frac{1}{2}\Delta f}^{\Delta f + \frac{1}{2}\Delta f} S(f)df} \tag{3.7}$$

In theory, the variance σ^2 of wind turbulence simulated from a one-sided spectrum is given by equation (3.8) and approximated by (3.9), assuming that *M* is large:

$$\sigma^2 = \int_0^\infty S(f)df \tag{3.8}$$

$$\approx \sum_{m=0}^{M} \mathbf{S}[m] \tag{3.9}$$

In practice, the actual variance of the simulated wind turbulence is smaller than predicted in (3.8) and (3.9) because $S[0] = 0$ and *M* is not infinite. This is a problem because variance is a parameter in the spectrum in equation (3.1) and we want the variance of the simulated turbulence output to equal that parameter.

We show in Figure 3.2 that the actual variance of the simulated turbulence output is well-predicted by the following formula:

$$\sigma^2_{actual} \approx \sum_{m=1}^{M} \mathbf{S}[m] \approx \int_{\Delta f - \frac{1}{2}\Delta f}^{f_{Nyq} - \frac{1}{2}\Delta f} S(f)df \tag{3.10}$$

where the integration limits in (3.10) are determined by the method for discretizing the continuous spectrum, best illustrated by Figure 1 in a paper by Yang [18]. The integral of the continuous spectrum in a small region around f_m is approximated by a rectangle of height $S[m]$ and width Δf:

$$\mathbf{S}[m]\Delta f \approx \int_{f_m - \frac{1}{2}\Delta f}^{f_m + \frac{1}{2}\Delta f} S(f)df \tag{3.11}$$

Figure 3.2 shows that discretizing the turbulence spectrum causes a loss of variance in the simulated turbulence. We simulated 400 – 1600 seconds of turbulence at sampling frequencies from 0.2 – 20 Hz using Veers method and the Kaimal spectrum in equation (3.1). The actual variance of simulated turbulence deviates significantly from the desired variance ($\sigma^2_{desired} = 1$); the actual variance only approaches the desired variance asymptotically with increasing sampling frequency ($f_{output} \to \infty$) and increasing sample period ($T \to \infty$). In this paper, we use a sampling frequency of 5 Hz and a sampling period of 1200 sec; that means the variance of each period of simulated turbulence is approximately 8% lower than the measured variance used as a parameter in the simulation.

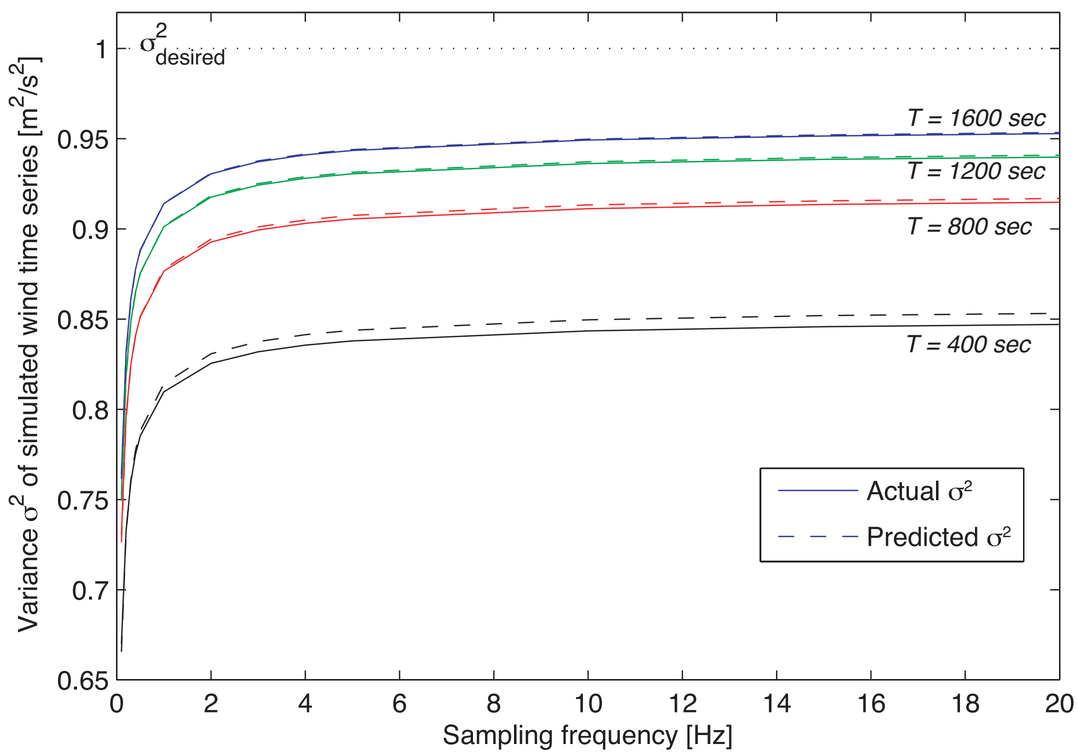

Figure 3.2: This figure plots the actual variance of turbulence simulated with the Kaimal spectrum in equation (3.1)and a variance parameter σ2desired = 1 against the sampling frequency of the simulation. Different curves plot simulations of different lengths. The actual variance is plotted as solid lines and the variance predicted by equation (3.10) is plotted as dotted lines. The turbulence is simulated with Veers method, the Kaimal spectrum from equation (3.1), U = 10 m/s, σ2 = 1 m2/s2, and z = 65.

We correct for that loss of variance using equation (3.10). Equation (3.10), plotted as dotted lines, closely predicts the actual variance of simulated turbulence, plotted as solid lines, without running a simulation. We use that prediction to calculate η in equation (3.7), and use η in equation

(3.6) to scale the spectrum so the variance of the simulated turbulence measured the desired variance.

We use the following pattern to create a two-sided spectrum of N points:

$$V_{2side} = \left[0,\ \mathbf{V}[2],\ \mathbf{V}[3],\ \ldots,\ \mathbf{V}[M-1],\ \left|\mathbf{V}[m]\right|,\ \mathbf{V}^*[M-1],\ \ldots,\ \mathbf{V}^*[2]\right] \tag{3.12}$$

where the negative frequencies are represented in the second half of $\mathbf{V}_{2\,side}$, each $\mathbf{V}_{2\,side}[n]$ is complex-valued except $\mathbf{V}_{2\,side}[N/2]$, and the first element $\mathbf{V}_{2\,side}[1]$ is forced to zero because we are creating a zero-mean simulation. To produce a time series of real-valued wind speeds, the $\mathbf{V}_{2\,side}$ must be conjugate symmetric, i.e. $\mathbf{V}_{2side}[n] = \mathbf{V}^*_{2side}[\mathrm{mod}(N-n+1,\quad N)+1]$, where the * operator represents complex conjugation. Note that the magnitudes of the one-sided spectra in equations (3.1) or (3.2) are multiplied by ½ in equation (3.6) in anticipation of creating the two-sided spectrum in equation (3.12).

We calculate the turbulence time series output $\mathbf{u}$ using the Fast Fourier Transform (FFT):

$$\mathbf{u} = \left|\mathrm{FFT}(\mathbf{V}_{2\,side})\right| \tag{3.13}$$

where the FFT is defined following Press [11] as:

$$\mathbf{u}[n] = \sum_{k=1}^{N} \mathbf{V}_{2side}[k]e^{i2\pi(n-1)(n-1)/N} \qquad n = \{1, \ldots, N\} \tag{3.14}$$

In theory it is not necessary to take the absolute value of the FFT in equation (3.13) because the conjugate-symmetric two-sided spectrum we constructed in equation (3.12) ensures the output of the FFT will be real-valued. In practice, the limited numerical precision of computers may cause the output $\mathbf{u}[n]$ to have small imaginary values.

Confusingly, different sources define the FFT and its inverse in opposite ways. Press [11] gives the definition of the FFT in equation (3.14), but Bracewell [19] and Newland [20] define that as the inverse FFT. The Matlab software uses the definition in equation (3.14) except for a minus sign in the exponential term; Mathematica accepts a parameter for the choice of definitions.

3.2.3 Combining Empircal and Simulated Data (D)

We create the hybrid wind speed time series by concatenating the blocks of simulated zero-mean turbulence and superimposing them on the filtered measured mean data (Figure 3.1D). We find that windowing the periods of simulated turbulence suggested by some authors [6], [9] is not necessary. We do not encounter the problem of excessive spectral content at low frequencies noted by McFarlane [6] because our method does not overlap consecutive blocks of simulated high-frequency data and because we low-pass filter the measured data.

3.2.4 Extension to Three Dimensions

We do not consider the general three-dimensional case of the Veers method here; good explanations can be found in papers by Veers [21] and Sørensen [4], but we will briefly summarize how to extend the one-dimensional case described above. A simulated 3-D wind field consists of parallel, coherent 1-D wind speed time series. A coherence matrix γ is introduced in equation (3.6), so the discretized spectrum $\mathbf{S}[m]$ must be a square matrix. Because $\mathbf{S}[m]$ is a square matrix, the square root operation must be replaced by the Cholesky decomposition or similar decomposition that yields a lower-triangular matrix. Similarly, the random phases in the $e^{j\phi[m]}$ term of equation (3.6) must be replaced by a square matrix with complex random phase angles on the diagonal and zeros elsewhere.

3.2.5 Application Notes

The general method we present here can be used to generate high-frequency wind speed time-series data. However, certain applications require details we have not discussed above.

Power production: The large rotors on multi-megawatt wind turbines filter most high-frequency turbulence, but make the power output of those turbines sensitive to the significant wind speed differences across the rotor induced by shear. Wagner has shown that calculating the power performance of a wind turbine from only hub-height wind speed measurements introduces significant uncertainties [22]; related research by Antoniou has shown hub-height measurements introduce similar uncertainties in power curve and wind resource calculation [23]. Wagner proposes several methods to calculate an "equivalent" wind speed that better correlates with power output [22]. Dolan proposes an alternative formula to calculate an equivalent wind speed based on a wind shear function [24]. These methods calculate an equivalent wind speed from wind speeds measured at several heights within the area of the turbine rotor. Our hybrid method can be used to generate wind speed times series at multiple heights, but the results will be sensitive to the models of wind shear and vertical coherence used. We also recommend simulating the low-pass filtering effect of the large rotor with the $H_{v,0}(s)$ filter proposed by Sørensen [25].

Power quality/Flicker: Power quality and flicker analyses deal with power variations at frequencies higher than approximately 1 Hz [26]. The large rotor of multi-megawatt wind turbines filters most wind fluctuations at frequencies higher than 10^{-1} Hz [27], but wind shear and the aerodynamic effect of blades passing the tower introduces noise at three times the rotation frequency ("3p"). We recommend applying the $H_{v,0}(s)$ and $H_{v,3}(s)$ filters proposed by Sørensen [25] to simulate the low-pass filtering effect of the large rotor and the 3p effect of wind shear and blades passing the tower.

3.3 Validation

We validate the method for creating hybrid wind speed data described above by comparing the data it generates to wind speed data measured at three sites in the U.S. The hybrid method was created to support simulations of wind power variability on time scales relevant to grid frequency regulation, so we focus on validating the characteristics of the hybrid method that are most important for that application. First we compare the characteristics of wind speed variation, especially the Power Spectral Density (PSD). Then we use that wind speed data to drive a simulated wind turbine to create wind power data. We compare the energy production and ramp rate characteristics of the wind power over different time scales.

The procedure for creating the data used to validate the hybrid wind method is:

1. Collect measured wind speed data from field measurements (see Table 3.1) and decimate data to 5 Hz. The measured 5 Hz data are the "Measured" data set
2. Calculate 10-minute statistics (mean and standard deviation) from measured wind data in step 1.The measured 10-minute mean wind speeds (resampled to 5 Hz) are the "Measured, 10-min avg" data set
3. Generate 5 Hz hybrid wind speed data
    a. Hybrid data created with equation (3.1), which takes wind speed standard deviation as an input, are the "Hybrid, σ" data set
    b. Hybrid data created with equation (3.2), which takes estimated surface roughness length as an input, are the "Hybrid, z_0" data set
4. Simulate time series of the power output of a 2-MW wind turbine, using the wind speed time series generated in Step 3.

3.3.1 Validation Data

To validate our hybrid method of creating long wind speed time series, we used publically-available wind speed data from three experiments conducted by the U.S. National Center for Atmospheric Research (NCAR): CASES99 (Cooperative Atmosphere-Surface Exchange Study) [28], FLOSSII (Fluxes Over Snow Surfaces, Phase II) [29], and ATST (Advanced Technology Solar Telescope site survey) [30], [31], summarized in Table 3.1. We decimate these data to 5 Hz by applying an 8th order low-pass Chebyshev Type I filter and then down-sampling the data by selecting every rth point, where r is the sampling frequency of the data set divided by 5 Hz [32]. We calculate the along-wind horizontal (longitudinal) wind speed from the decimated data. The large rotor on modern wind turbines acts as a low-pass filter to attenuate phenomena faster than approximately 0.5 Hz [27], so we choose a sampling rate of 5 Hz to ensure we capture all significant power variations.

Table 3.1: Properties of data sets from three U.S. National Center for Atmospheric Research (NCAR) experiments used to validate the hybrid wind model.

Data Set Name	Location	Measurement Height	Sampling Frequency	Surface Roughness Length z_0 (estimated)	Dates Sampled
CASES99	Leon, KS	55 m	20 Hz	0.03 m	6 – 30 Oct., 1999
FLOSSII	North Park, CO	30 m	60 Hz	0.03 m	20 – 31 Nov., 2002 15 – 29 Dec., 2002
ATST	Big Bear Lake, CA	25 m	30 Hz	0.003 m	7 May – 14 June, 2004

We group the data into contiguous blocks that share common atmospheric stability properties. First we calculate the stability criterion value $1/L$ for each 1-hour period, where L is the Obukhov length from Businger [33] calculated according to equation (3.15) below. Next we determine the Pasquill atmospheric stability class [34] corresponding to the calculated value of $1/L$ using a nomogram given by Golder [35], assuming the roughness lengths z_0 given in Table 3.1. Finally, we create each block of data by selecting the contiguous data with the same stability class: stable (Pasquill A, B, C), neutral (Pasquill D), or unstable (Pasquill E, F) and require that each block of data be a minimum of 2 hours long and have a mean wind speed greater than 4 m/s. The distribution of the data in the stability classes is shown in Table 3.2.

$$L = \frac{u_*^3 \overline{T}}{\kappa g \overline{w' T_v'}} \tag{3.15}$$

where

$u_* = \left(\overline{u'w'}^2 + \overline{v'w'}^2 \right)^{1/4}$ = friction velocity (definition from Weber [35])

u = longitudinal (along-wind) velocity [m/s]

v = latitudinal (across-wind) velocity [m/s]

w = vertical wind velocity [m/s]

T = absolute temperature [K]

T_v = virtual temperature [ºC]

κ = 0.4 = von Kármán constant

g = 9.8 m/s^2 = acceleration of gravity

$\overline{a'b'}$ = covariance of two variables a and b

Table 3.2: Distribution of the measured wind speed data in different atmospheric stability classes

Data Set	Stable Data [hours]	Neutral Data [hours]	Unstable Data [hours]
CASES99	148	177	10
FLOSSII	111	150	0
ATST	46	87	111

3.3.2 Wind Speed Time Series

Figure 3.3 qualitatively compares wind speed time series generated with our hybrid method to a measured wind speed time series. The two hybrid wind speed data sets ("Hybrid, σ" and "Hybrid, z_0") are generated by calculating the 10-minute mean and variance of the measured time series, then superimposing simulated high-frequency turbulence on the 10-minute mean data. For comparison, the "Measured, 10-min avg." plot shows the kind of measured data commonly captured from meteorological masts that would be used as the basis for generating hybrid wind data.

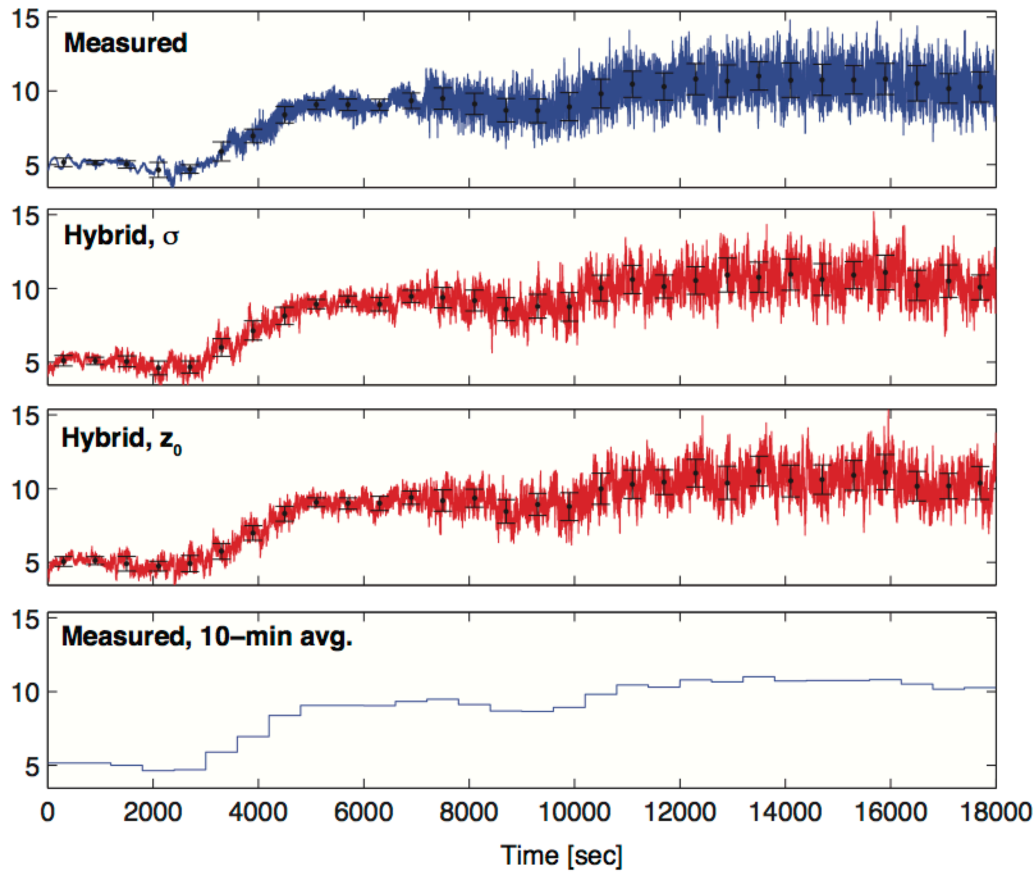

Figure 3.3: A comparison of measured wind speed data ("Measured"), hybrid wind speed data generated with empirical mean and variance statistics ("Hybrid, σ"), hybrid wind speed data generated with empirical mean statistics and estimated surface roughness length ("Hybrid, z0"), and empirical mean statistics ("Measured, 10-min avg."). These data are representative of the close match between hybrid wind speed data and measured data with similar statistical properties. These plots show 4 hours of data from the CASES99 experiment beginning at 20:00:00 October 28, 1999 (stable atmospheric conditions). The hybrid and "Measured, 10-min avg." data are generated using 10-minute statistics derived from the "Measured" data.

The plots in Figure 3.3 demonstrate that the hybrid method generates realistic non-stationary wind speed data. We calculate the 10-minute means and variances of a five-hour period of empirical wind speed data, labeled "Measured", that has a significant increase in mean wind speed beginning at t = 3000 seconds and a significant increase in wind speed variance beginning at t = 7000 seconds. Wind speed with the data simulated with the "Hybrid, σ" method, which takes mean and variance as inputs, captures the increase in mean wind speed and the increase in variance. Wind speed with the data simulated with the "Hybrid, z_0" method, which takes only the mean as an input, also captures the increase in mean wind speed and the increase in variance.

3.3.3 Wind Speed Turbulence Spectra

We compare the PSD (Power Spectral Density) of hybrid wind speed time series to the PSD of measured wind speed time series from the CASES99 experiment and plot the results in Figure 3.4. We calculate the PSD according to the following formula:

$$S_{2side}(f) = T\left|\mathrm{FFT}^{-1}(\mathbf{u})\right|^2 \tag{3.16}$$

where T is the duration of the data in second and the inverse Fourier Transform is defined by Press [11] as:

$$\mathbf{V}_{2side}[k] = \frac{1}{N}\sum_{n=1}^{N}\mathbf{u}[n]e^{-i2\pi(n-1)(k-1)/N} \qquad k = \{1, \ldots, N\} \tag{3.17}$$

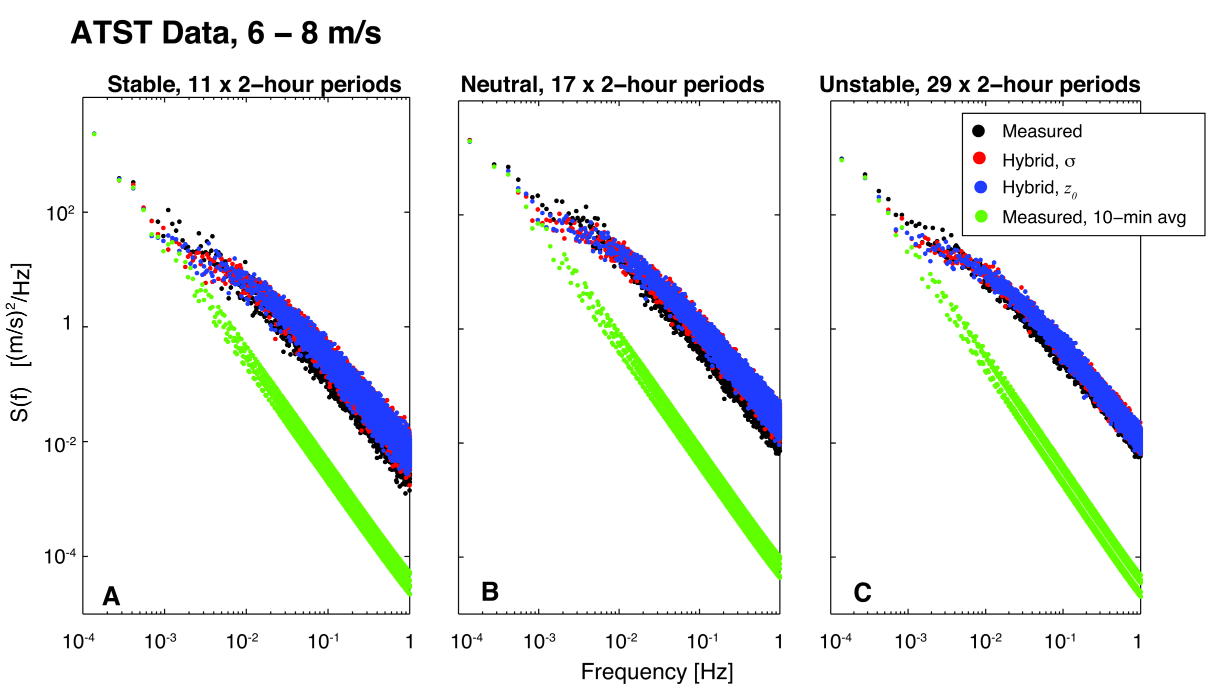

Figure 3.4: A comparison of Power Spectral Densities (PSD) of measured wind data, both variants of hybrid wind speed data, and measured 10-minute average data from the ATST field site for 6 – 8 m/s mean wind speed. Each PSD is the segment average of the PSDs all 2-hour segments of data in the specified mean wind speed range (see description in text). Data from stable conditions (0.01 < 1/L < 0.15) are plotted in (A), neutral conditions (-0.03 < 1/L < 0.01) are plotted in (B), and unstable conditions (-0.15 1/L < -0.03) in (C). We plot the spectral only to 2 Hz because we decimate (low-pass filter and down-sample) the measured data to 5 Hz, but the low-pass filtering attenuates the spectra of the measured data above 2 Hz.

Each PSD plotted in Figure 3.4 is the average of all the PSDs of 2-hour periods with the mean wind speed between 6 and 8 m/s. This averaging, called "segment averaging" in Press, Section 13.4

[11] reduces the variance of the PSD. The number of periods averaged is given in the title of each plot. We plot the spectra for mean wind speeds 6 – 8 m/s because that range consistently contains the most data across the three experimental sites. We plot the spectra of four different data sets: "Measured" is ATST field data decimated to 5 Hz, "Hybrid, σ" is hybrid data created with the Kaimal spectral model in equation (3.1), "Hybrid, z_0" is hybrid data created with the Kaimal spectral model in equation (3.2), and "Measured, 10-min avg" is 10-minute means of the ATST field data, re-sampled to 5 Hz by repeating each value. We include the "Measured, 10-min avg" data to show the results if 10-minute average data is re-sampled to a higher frequency without adding high-frequency turbulence. The spectrum of the "Measured, 10-min avg" data diverges from the spectrum of the "Measured" data for two reasons. First, calculating the 10-minute average of the "Measured" data acts as a low-pass filter that attenuates the spectral power beginning at approximately 10^{-3} Hz. Second, re-sampling 10-minute average data to create the "Measured, 10-min avg" data introduces noise at frequencies $f > 1.7 \times 10^{-3}$ Hz with spectral power that decreases as f^2.

Figure 3.4 demonstrates the advantage of the hybrid method: it adds the turbulence not found in the 10-minute average data (plotted in green). The spectra of the hybrid wind data in Figure 3.4 closely match the spectra of the measured ATST wind data in stable, neutral, and unstable atmospheric conditions. The spectra of wind speed data generated with both hybrid variants is almost indistinguishable from the spectra of the measured data at all frequencies. These results are representative of the results for other range of mean wind speed and for data from the CASES99 and FLOSSII experiments with one exception: the hybrid wind under-predicts the magnitude of turbulence for frequencies in the range of 1×10^{-3} – 3×10^{-3} Hz when compared to data from the CASES99 test site during stable atmospheric conditions (not shown). That range of frequencies is where measured data are joined with simulated turbulence to form hybrid wind, which suggests that the low-pass filter applied in Step C of the hybrid method may not be steep enough. However, this under-prediction is not evident in neutral and unstable CASES99 data or in any of the ATST and FLOSSII data.

3.3.4 Wind Turbine Simulation Model

All wind power data used in this paper are created by simulation of a single 2-MW wind turbine in Matlab/Simulink. The turbine is pitch-regulated, variable-speed model with an 80-m rotor, modeled using the Wind Turbine Blockset, v3.0 developed by Aalborg University [36]. This simulation model is not a static power curve; it models the dynamics of rotor acceleration and pitch and torque regulation. It does not model electrical transients or the 3p blade-passing frequency. We use the turbine design parameters, control scheme, control parameters, and first-order generator model recommended by the Danish Technical University (DTU) [37]. We incorporate a rotor-wind filter $H_{v,0}(s)$ proposed by Sørensen [25] into the wind turbine model to simulate the filtering effect of a large rotor on turbulence that is not spatially homogeneous, but we do not account for the effect of vertical wind shear across the rotor disk.

Each simulation takes wind speed sampled at 5 Hz as its input and generates real power sampled at 5 Hz as its output. We initialize each simulation by duplicating the initial wind speed value for 1000 seconds at the beginning of wind speed data set; this padding allows initial transients of the simulation model to settle out. We remove the corresponding first 1000 seconds of the output power data. As described in Section 3.1, each input data set consists of at least 2 contiguous hours of wind speed data in one stability regime (stable, neutral, or unstable) with a mean wind speed greater than 4 m/s.

3.3.5 Validation of Power Production

We compare the energy and power produced by one 2-MW wind turbine with 40-meter blades (described in Section 3.3.4) fed with both the measured and hybrid wind speed time series and plot the results in Figure 3.5. Comparing simulated wind power takes into account the filtering effect of a large wind turbine on wind speed fluctuations and the dynamic response of a modern turbine to those fluctuations. We do not compare simulated wind power to wind power measured from actual wind turbines because of the difficulties in controlling the output of actual turbines for wind direction, wakes, terrain, mechanical and electrical losses, power limits, and ramp rate limits. Future work should analyze met-mast and wind power data to give a more thorough comparison of the hybrid method to the output of an actual wind turbine.

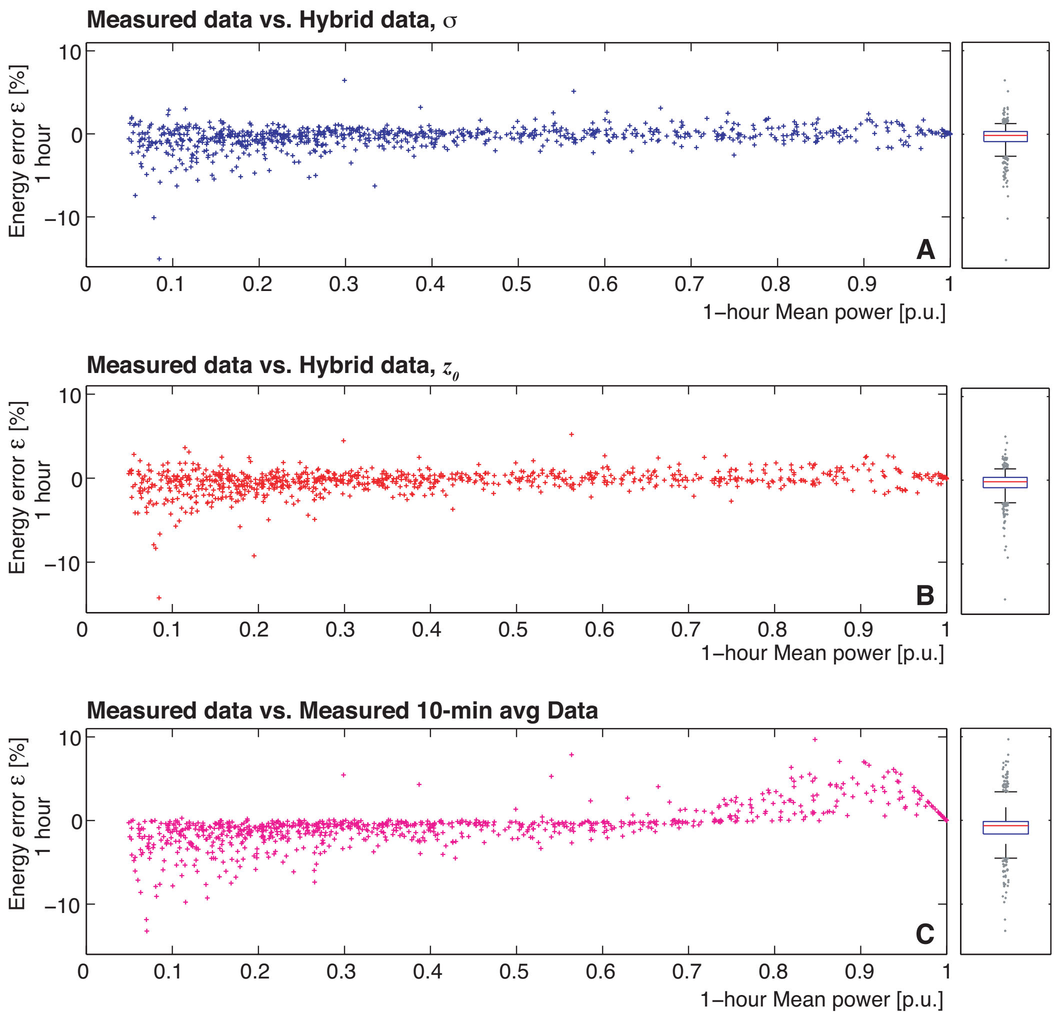

Figure 3.5: The plots on the left show percent difference in energy production ε between a turbine simulated with empirical wind data and hybrid wind data, plotted against per-unit (p.u.) mean power. (A) compares measured data to hybrid data created with equation (3.1), (B) compares measured data to hybrid data created with equation (3.2), and (C) compares measured data to 10-minute average measured data. The boxplots on the right plot the mean (center line), 25th and 75th percentile values (bottom and top of box), and the 5th and 95th percentiles (bottom and top "whiskers") of the same data [40].

Figure 3.5 shows a comparison between the energy generated by a 2-MW wind turbine driven by the measured wind data described in Table 3.1 and the corresponding hybrid wind data. Each sub-plot shows the percent error in energy generation in 1-hour periods plotted against the mean power for that 1-hour period, measured in the *per-unit* (p.u.) system. We use the per-unit system to express turbine power output as a fraction of the maximum power output (2 MW in our paper). Figure 3.5A compares hybrid wind data generated using equation (3.1), which takes wind speed standard deviation as a parameter. Figure 3.5B compares hybrid wind data generated using equation (3.2), which takes surface roughness length as a parameter. Figure 3.5C compares measures 10-minute average wind data to show the results if the hybrid method is not used to fill in high-frequency turbulence.

We define the 1-hour percent energy generation error ε in hour k as:

$$\varepsilon(k) = \frac{E_{meas}(k) - E_{hyb}(k)}{E_{meas}(k)} \qquad (3.18)$$

where $E_{meas}(k)$ is the energy generated by the simulated wind turbine driven by measured wind data in hour k and $E_{hyb}(k)$ is the energy generated with hybrid wind data in hour k.

Figure 3.5 shows both variants of hybrid wind (Figure 3.5A and B) have smaller errors in energy production than the 10-minute average data (Figure 3.5C) they are based on. The mean error for hybrid data created with both methods (A and B) is -0.4%; the mean error for the 10-minute average data (C) is -0.8%. Hybrid data also gives significantly less variance in the errors: 90% of the hybrid errors fall between -2.7% and +1.4%, whereas 90% of the errors for the 10-minute average data fall between -4.5% and 3.4%. Using the hybrid method to add high-frequency turbulence to low-frequency measured data significantly reduces the magnitude and range of error in energy production. The hybrid method also reduces the trend of energy error increasing as a function of mean power: Figure 3.5C shows that using 10-minute average data over-predicts energy production when the average power is low and under-predicts energy when the average power is high. Data created with the hybrid method do not show such a strong trend.

3.3.5.1 Power Ramp Rate

Figure 3.6 and Figure 3.7 show comparisons of the ramp rates of power generated by a 2-MW wind turbine driven by the measured wind data described in Table 3.1 to the corresponding hybrid wind data. Validation of the ramp rates is important to confirm that the hybrid method accurately models the variations on different time scales. Figure 3.6 shows a comparison of the distribution of sizes of ramp events and Figure 3.7 compares the size of extreme ramp events.

We use the definition that the ramp rate is the change in mean power from one period to the next: $P_{ramp}(n) = P_{mean}(n+1) - P_{mean}(n)$ [38]. The ramp rates are binned by the mean power of the starting period $P_{mean}(n)$. We analyze ramp rates over three different time scales: 10 minutes, 1 minute, and 10 seconds. The 10-minute ramp rates correspond to phenomena in the "load-following" time scale, 1-minute ramp rates correspond to phenomena in the "frequency-regulation" time scale, and the 10-second ramp rates correspond to "flicker" phenomena.

The duration curves in Figure 3.6 plot the percentile values of ramp rates. Ramp events are grouped together in bins by initial power $P_{mean}(n)$; Figure 3.6 shows the duration curves for 10-minute, 1-minute, and 10-second ramp events with an initial power of 0.6 to 0.7 per-unit (p.u.). This figure is similar to comparisons of measured and simulated wind power ramp rates given by Brower for validation of the Eastern Wind Integration and Transmission Study, but we plot a cumulative distribution function (CDF) where Brower plots a probability density function (PDF) [39].

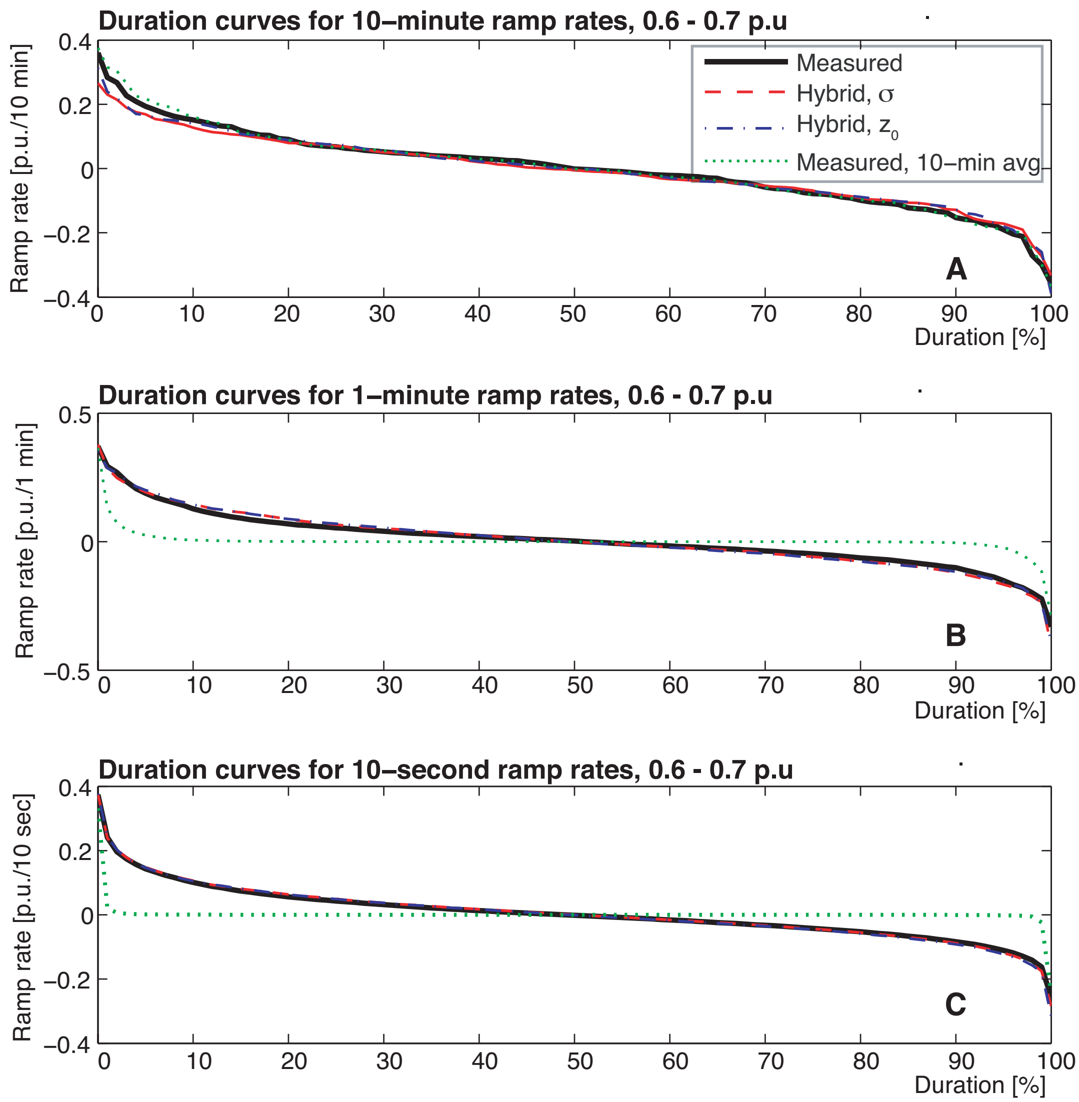

Figure 3.6: A comparison of the distribution (percentiles) of power ramp rates for a simulated turbine driven by measured wind data. All plots show changes in power starting in the range 0.6 – 0.7 per-unit (p.u.); (A) shows the distribution of 10-minute ramp rates, (B) the distribution of 1-minute ramp rates, and (C) the distribution of 10-second ramp rates. The hybrid data are nearly indistinguishable from the measured data, especially for 1-minute and 10-second ramp rates.

Figure 3.6 shows that the hybrid methods are slightly worse at modeling 10-minute ramp rates than 10-minute average measured data (A), but much better at modeling 1-minute and 10-second ramp rates (B and C). For 10-minute ramp rates starting from the 0.6 – 0.7 p.u. power range (Figure 3.6A), the mean-square error (MSE) between the measured data and the 10-minute average measured data is 8.7×10^{-5} p.u./10-min, significantly smaller than MSEs for the two hybrid data sets: 3.3×10^{-4} p.u./10-min and 2.2×10^{-4} p.u./10-min. For 1-minute ramp rates (Figure 3.6B), the MSE for the hybrid data sets is 1.9×10^{-4} p.u./1-min but the MSE for the 10-minute average measured data is more than an order of magnitude larger: 5.9×10^{-5} p.u./1-min. For 10-second ramp rates (Figure 3.6C), the MSEs for the hybrid data sets are 3.0×10^{-5} and 6.7×10^{-5} p.u./10-sec but the MSE for the 10-minute average measured data is two orders of magnitude larger: 4.9×10^{-3} p.u./10-sec. These results are typical of those in all other initial power ranges.

The power ramp rates based on hybrid wind data match very closely to the power ramp rates based on measured wind over time scales from 10 minutes to 10 seconds. The good match between hybrid and measured ramp rates on these time scales shows that the simulated turbulence introduced by the hybrid method models the characteristics of actual wind turbulence well. It is somewhat surprising that the hybrid wind predicts 10-minute power ramps that are smaller than than10-minute average measured data because the hybrid method adds zero-mean turbulence that should not affect the 10-minute ramp rate. We suspect that the under-prediction of 10-minute ramp rates by the hybrid method is an artifact of the low-pass filter used in creating the hybrid data. Figure 3.4 supports this hypothesis—the spectra of hybrid wind diverge slightly from the spectra of measured wind at approximately 1.1×10^{-3} Hz, which corresponds to a period of ~15 minutes.

Figure 3.7 plots the 1st percentile (most extreme down ramps) 10-minute, 1-minute, and 10-second ramp rates as a function of initial power $P_{\mathrm{mean}}(n)$. The data are grouped by initial power into 0.1 p.u. bins, so each plotted point is the 1st percentile ramp rate value for all the data in a particular bin. These plots are a cross-sectional slice of the plots in Figure 3.6, but varying the initial power instead of the percentile value. The 1st percentile ramp rates are significant because they put the greatest burden on other generators to compensate for the decrease in wind power.

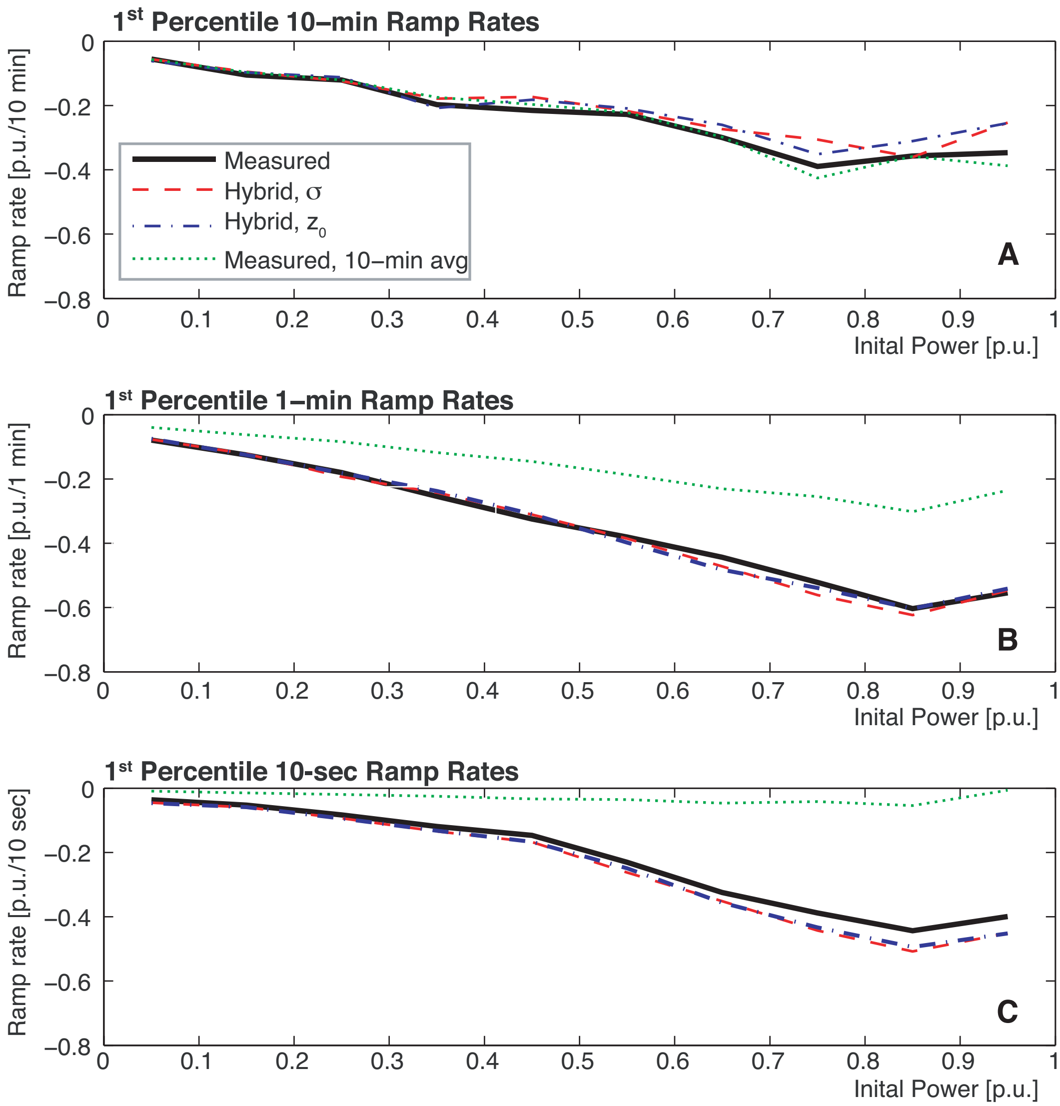

Figure 3.7: The extreme (1st percentile) power ramp rates for a simulated turbine driven by measured and hybrid wind data. Each plot shows the extreme power down ramp as a function of the initial power (power output at the start of ramping). (A) shows the distribution of extreme 10-minute ramp rates, (B) the distribution of extreme 1-minute ramp rates, and (C) the distribution of extreme 10-second ramp rates. The ramp rates of the hybrid data closely match the ramp rates of the measured data, but the hybrid data predicts more extreme 10-second ramp rates for initial power output in the range 0.7 – 1 p.u.

The data for extreme power ramp rates plotted in Figure 3.7 show a similar trend to the data in Figure 3.6: the hybrid data model power ramps over short periods (1-minute and 10-seconds) better than the 10-minute average data, but slightly worse for 10-minute ramping periods. For the 1st percentile 10-minute ramp rates (Figure 3.7A), the mean-square error (MSE) between the measured data and the 10-minute average measured data is 4.0 x 10^{-4} p.u./10-min, significantly smaller than the MSEs for the two hybrid data sets: 1.9 x 10^{-3} p.u./10-min and 1.5 x 10^{-3} p.u./10-min. For the 1st percentile 1-minute ramp rates (Figure 3.7B), the 10-minute average measured data has a MSE of 1.0 x 10^{-2} p.u./1-min, several orders of magnitude larger than the MSEs of the hybrid data: 8.2 x 10^{-5} and 6.9 x 10^{-5} p.u./1-min. Similarly for the 1st percentile 10-second ramp rates (Figure 3.7C), the 10-minute average measured data has a MSE of 1.4 x 10^{-2} p.u./1-min, which is two orders of magnitude larger than the MSEs of the hybrid data: 3.1 x 10^{-4} and 2.4 x 10^{-4} p.u./10-sec.

Similar to the ramp rate duration curves in Figure 3.6, the 1st percentile power ramp rates based on hybrid wind data match very closely to the power ramp rates based on measured wind over time scales from 10 minutes to 10 seconds. They do not match as well on a time scale of 10 minutes—we suspect that the under-prediction of 10-minute ramp rates by the hybrid method is an artifact of the low-pass filter used in creating the hybrid data. However, we are surprised that the hybrid data sets diverge significantly at higher initial powers. The hybrid method under-predicts extreme down ramp rates by 2.5% of the rated turbine power output (0.025 p.u.) for initial power 0.8 – 0.9 p.u., suggesting that the hybrid method generates too much turbulence at higher wind speeds.

3.3.6 Validation of Spinning Reserve Requirements

Figure 3.8 compares the power reserves needed for power generated by a 2-MW wind turbine driven by the measured wind data described in Table 3.1 and the corresponding hybrid wind data. Validation of the power reserve requirements is important to confirm that the hybrid method accurately models the variations on different time scales. We define the reserve requirement as the difference between mean power in one period and minimum power in the next: $P_{ramp}(n) = P_{mean}(n) - P_{min}(n+1)$ [38]. The reserve requirement values are binned by the mean power of the starting period $P_{mean}(n)$. As we did for the ramp rates, we analyze reserve requirements on 10-minute, 1-minute, and

10-second time scales. We analyze the 99th percentile reserve requirements because these represent the most extreme reserve requirements.

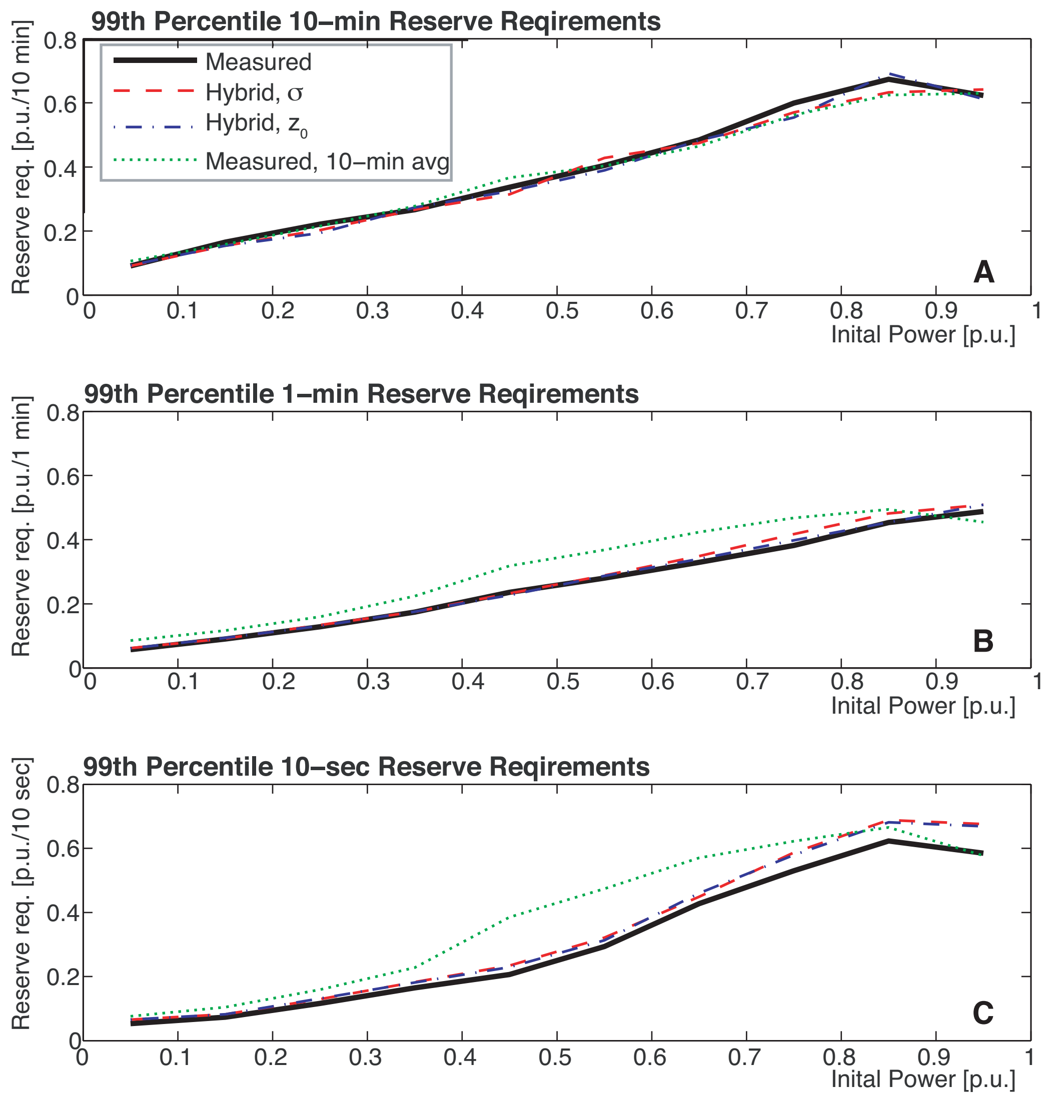

Figure 3.8: The extreme (99th percentile) reserve requirements for a simulated turbine driven by measured and hybrid wind data. Each plot shows the extreme reserve requirement as a function of the initial power (power output at the start of ramping). (A) shows the distribution of extreme 10-minute reserves, (B) the distribution of extreme 1-minute reserves, and (C) the distribution of extreme 10-second reserves. The reserve requirements of the hybrid data closely match the reserve requirements of the measured data, but the hybrid data predict more extreme 10-second reserve requirements for initial power output in the range 0.7 – 1 p.u.

The data for extreme power reserve requirements plotted in Figure 3.8 show that the hybrid method is consistently better at predicting reserve requirements than the 10-minute average measured data. For 10-minute reserve requirements (Figure 3.8A), the 10-minute average data are nearly as good as the hybrid data: it has a MSE of 4.5×10^{-4} p.u. compared to the MSEs of the hybrid data of 3.8×10^{-4} and 4.5×10^{-4} p.u. For 1-minute reserve requirements (Figure 3.8B), the hybrid method is significantly better: the MSE for 10-minute average data is 3.8×10^{-3} p.u., an order of magnitude worse than the MSEs for the hybrid data: 3.0×10^{-4} and 9.7×10^{-5} p.u. For 10-second reserve requirements (Figure 3.8C), the MSE for 10-minute average data is 2.6×10^{-3} p.u. and the MSEs for the hybrid data are an order of magnitude smaller: 4.6×10^{-4} and 3.9×10^{-4} p.u.

As with the extreme ramp rates in Figure 3.7, the hybrid data sets diverge significantly at higher initial powers. The hybrid method over-predicts extreme reserve requirements by 3% of rated turbine power output (0.03 p.u.) for initial power 0.8 – 0.9 p.u. This result again suggests that the hybrid method generates too much wind turbulence at higher wind speeds.

3.4 Conclusions

We demonstrate a method for creating long wind speed time series as a hybrid of measured and simulated wind speed. This method is meant to take advantage of wind speed data measured at low frequencies by meteorological stations and wind farm developers, and data simulated with appropriate spatial and temporal resolution by meso-scale weather models. The measured wind data capture non-stationary phenomena such as diurnal variations, the passing of weather systems, and seasonal variations, while our hybrid method simulates data to interpolate the fast turbulent variations that are needed to accurately model fast variations in wind power.

Our analysis shows that the wind speed time series created with our hybrid method accurately reproduce measured wind speed data from three different sites and in neutral, stable, and unstable atmospheres. We demonstrate that the total energy produced by a wind turbine simulated with hybrid wind is within -2.7%/+1.4% of the energy produced by the same turbine simulated with measured wind data for 90% of the tested period. We also demonstrate that the power ramp rates and spinning reserve requirements for a turbine simulated with hybrid wind data very closely match the results for a turbine simulated with measured wind data.

This method is well suited to studies of single wind turbine power fluctuations on the scale of seconds to minutes. It generates wind speed data time series sampled fast enough to simulate dynamic behavior of an individual wind turbine, such as pitch control, but retains their time-dependent characteristics such as diurnal variations, the passing of weather fronts, and seasonal variations.

3.5 Acknowledgements

This work was supported in part by the EPA STAR fellowship program, a grant from the Alfred P. Sloan Foundation and EPRI to the Carnegie Mellon Electricity Industry Center, and by the Doris Duke Charitable Foundation, the R.K. Mellon Foundation and the Heinz Endowments for support of the RenewElec program at Carnegie Mellon University. This research was also supported in part by the Climate and Energy Decision Making (CEDM) center. This Center has been created through a cooperative agreement between the National Science Foundation (SES-0949710) and Carnegie Mellon University.

3.6 References

[1] V. L. Nadolski, “Automated Surface Observing System (ASOS) User's Guide,” Mar. 1998.

[2] A. Kareem, “Numerical simulation of wind effects: a probabilistic perspective,” *Journal of Wind Engineering and Industrial Aerodynamics*, vol. 96, no. 10, pp. 1472–1497, 2008.

[3] C. Nichita, undefined author, undefined author, and undefined author, “Large band simulation of the wind speed for real time wind turbine simulators,” *IEEE Transactions on Energy Conversion*, vol. 17, no. 4, pp. 523–529, 2002.

[4] P. Sørensen, N. A. Cutululis, A. Vigueras-Rodríguez, H. Madsen, P. Pinson, L. E. Jensen, J. Hjerrild, and M. H. Donovan, “Modelling of power fluctuations from large offshore wind farms,” *Wind Energy*, vol. 11, no. 1, pp. 29–43, 2008.

[5] P. S. Veers, “Modeling Stochastic Wind Loads on Vertical Axis Wind Turbines,” *SAND83-1909*, p. 19, 1984.

[6] A. McFarlane, P. S. Veers, and L. Schluter, “Simulating high-frequency wind for long durations,” *13th AMSE WInd Energy Symposium (New Orleans, LA)*, 1994.

[7] N. D. Kelley and H. J. Sutherland, "Damage estimates from long-term structural analysis of a wind turbine in a US wind farm environment," presented at the 16th ASME Wind Energy Symposium, Reno, 1997.
[8] N. B. Negra, O. Holmstrøm, B. Bak-Jensen, and P. Sørensen, "Model of a Synthetic Wind Speed Time Series Generator," *Wind Energy*, vol. 11, pp. 193–209, 2008.
[9] D. O. Smallwood and T. L. Paez, "A frequency domain method for the generation of partially coherent normal stationary time domain signals," *Shock and Vibration*, vol. 1, no. 1, pp. 45–53, 1993.
[10] M. Nielsen, G. C. Larsen, and undefined author, "Simulation of inhomogeneous, non-stationary and non-Gaussian turbulent winds," *Journal of Physics: Conference Series*, vol. 75, p. 012060, 2007.
[11] W. H. Press, S. A. Teukolsky, W. T. Vetterling, and B. P. Flannery, *Numerical Recipes 3rd Edition: The Art of Scientific Computing*. 2007.
[12] J. Kaimal, J. Wyngaard, Y. Izumi, and O. Coté, "Spectral characteristics of surface-layer turbulence," *Quarterly Journal of the Royal Meteorological Society*, vol. 98, pp. 563–589, 1972.
[13] "IEC 61400-1: Wind Turbine Design Requirements (ed. 3.0)," *International Electrotechnical Commission*, pp. 22–31, Aug. 2005.
[14] M. Shinozuka, "Digital simulation of random processes and its applications," *Journal of Sound and Vibration*, vol. 25, no. 1, pp. 111–128, Nov. 1972.
[15] M. Shinozuka and G. Deodatis, "Simulation of stochastic processes by spectral representation," *Applied Mechanics Reviews*, vol. 44, no. 4, pp. 191–203, Jul. 1991.
[16] R. M. Bethea and R. R. Rhinehart, *Applied Engineering Statistics*. New York: Marcel Dekker Inc, 1991.
[17] N. Fisher, *Statisitcal Analysis of Circular Data*. New York: Cambridge University Press, 1993.
[18] J. N. Yang, "On the Normality and Accuracy of Simulated Random Processes," *Journal of Sound and Vibration*, vol. 26, no. 3, pp. 417–428, 1973.
[19] R. N. Bracewell, *The Fourier transform and its applications*. McGraw-Hill Science/Engineering/Math, 2000.
[20] D. E. Newland, *An Introduction to Random Vibrations and Spectral Analysis*, 1st ed. Longman Group (Far East), Limited, 1975.
[21] P. S. Veers, "Three-Dimensional Wind Simulation," *SAND88-0152*, p. 40, Mar. 1988.
[22] R. Wagner, I. Antoniou, S. Pedersen, M. Courtney, and H. E. Jørgensen, "The influence of the wind speed profile on wind turbine performance measurements," *Wind Energy*, vol. 12, no. 4, pp. 348–362, 2009.
[23] I. Antoniou, S. Pedersen, and P. Enevoldsen, "Wind shear and uncertainties in power curve measurement and wind resources," *Wind Engineering*, vol. 33, no. 5, pp. 449–468, 2009.
[24] D. S. L. Dolan and P. W. Lehn, "Simulation model of wind turbine 3p torque oscillations due to wind shear and tower shadow," *IEEE Transactions on Energy Conversion*, vol. 21, no. 3, pp. 717–724, 2006.
[25] P. Sørensen, A. D. Hansen, and P. Rosas, "Wind models for simulation of power fluctuations from wind farms," *Journal of Wind Engineering and Industrial Aerodynamics*, vol. 90, pp. 1381–1402, 2002.
[26] C. V. Moreno, H. A. Duarte, and J. U. Garcia, "Propagation of Flicker in Electric Power Networks Due to Wind Energy Conversion Systems," *IEEE Transactions on Energy Conversion*, vol. 17, no. 2, pp. 267–272, Jun. 2002.
[27] J. Apt, "The spectrum of power from wind turbines," *Journal of Power Sources*, vol. 169, no. 2, pp. 369–374, Jun. 2007.
[28] G. Poulos, W. Blumen, D. Fritts, J. Lundquist, J. Sun, S. Burns, C. Nappo, R. Banta, R.

Newsom, J. Cuxart, undefined author, undefined author, and undefined author, "CASES-99: A Comprehensive Investigation of the Stable Nocturnal Boundary Layer," *Bull. Amer. Meteor. Soc.*, vol. 83, no. 4, pp. 555–581, 2002.

[29] L. Mahrt and D. Vickers, "Boundary-layer adjustment over small-scale changes of surface heat flux," *Boundary-Layer Meteorology*, vol. 116, no. 2, pp. 313–330, 2005.

[30] G. Maclean and S. Oncley, "ATST Site Survey Report," *NCAR/Earth Observing Laboratory*. [Online]. Available: http://www.eol.ucar.edu/isf/projects/ATST/. [Accessed: 21-Apr-2010].

[31] H. Socas Navarro, J. Beckers, P. Brandt, J. Briggs, T. Brown, W. Brown, M. Collados, C. Denker, S. Fletcher, S. Hegwer, F. Hill, T. Horst, M. Komsa, J. Kuhn, A. Lecinski, H. Lin, S. Oncley, M. Penn, T. Rimmele, and K. Streander, "Solar Site Survey for the Advanced Technology Solar Telescope. I. Analysis of the Seeing Data," *Publications of the Astronomical Society of the Pacific*, vol. 117, no. 837, pp. 1296–1305, 2005.

[32] IEEE Acoustics Speech and Signal Processing Society--Digital Signal Procesing Committee, *Programs for digital signal processing*. New York: IEEE Press, 1979.

[33] undefined author, "A note on the Businger-Dyer profiles," *Boundary-Layer Meteorology*, vol. 42, no. 1, pp. 145–151, 1988.

[34] F. Pasquill, *Atmospheric diffusion: The Dispersion of Windborne Material from Industrial and other Sources*, 1st ed. London: Van Nostrand, 1962.

[35] D. Golder, "Relations among stability parameters in the surface layer," *Boundary-Layer Meteorology*, vol. 3, no. 1, pp. 47–58, Sep. 1972.

[36] F. Iov, A. D. Hansen, P. Sørensen, and F. Blaabjerg, "Wind Turbine Blockset in Matlab/Simulink," pp. 1–108, Feb. 2004.

[37] M. H. Hansen, A. D. Hansen, T. J. Larsen, S. Øye, P. Sørensen, and P. Fuglsang, "Control design for a pitch-regulated, variable speed wind turbine," Risø-R-1500(EN), Feb. 2005.

[38] P. Sørensen, N. A. Cutululis, A. Vigueras-Rodríguez, L. E. Jensen, J. Hjerrild, M. H. Donovan, and H. Madsen, "Power Fluctuations From Large Wind Farms," *IEEE Transactions on Power Systems*, vol. 22, no. 3, pp. 958–965, 2007.

[39] M. Brower, "Development of Eastern Regional Wind Resource and Wind Plant Output Datasets," National Renewable Energy Laboratory, Golden, CO, NREL/SR-550-46764, Dec. 2009.

Chapter 4: Quantifying the Hurricane Risk to Offshore Wind Turbines

Abstract

The U.S. Department of Energy has estimated that if the U.S. is to generate 20% of its electricity from wind, over 50 GW will be required from shallow offshore turbines. Hurricanes are a potential risk to these turbines. Turbine tower buckling has been observed in typhoons, but no offshore wind turbines have yet been built in the U.S. We present a probabilistic model to estimate the number of turbines that would be destroyed by hurricanes in an offshore wind farm. We apply this model to estimate the risk to offshore wind farms in four representative locations in the Atlantic and Gulf Coastal waters of the U.S. In the most vulnerable areas now being actively considered by developers, there is a 5% probability that more than 20% of the turbines in a wind farm will be destroyed in a 20-year period. Reasonable mitigation measures – increasing the design reference wind load, ensuring that the nacelle can be turned into rapidly changing winds, and building most wind plants in the areas with lower risk – can greatly enhance the probability that offshore wind can help to meet the United States' electricity needs.

This paper was published as S. Rose, P. Jaramillo, M. J. Small, I. Grossmann, and J. Apt, "Quantifying the hurricane risk to offshore wind turbines," *Proceedings of the National Academy of Science*, vol. 109, no. 9, pp. 3247–3252, Feb. 2012.

4.1 Corrections After Publication

The research in this chapter was published in the Proceedings of the National Academy of Science [1]. After it was published, Mark Powell and Steven Cocke of Florida State University wrote a letter to the editor pointing out one error and several flawed assumptions about hurricanes in the paper [2]. In this thesis, I present results corrected for the error described in point 1 below (confusing 1-min and 10-min average wind speeds) but I do not correct the results for the contentious assumptions listed in points 2 – 4 below. I also discovered typographical errors in equations 6 and 8 and the legend for figure S7 in the Supporting Information [3] that I have corrected in this thesis—they appear as equations (4.6) and (4.8) and Figure A-7.

The error and one of the flaws significantly reduce the calculated risks, which means we overstated the risks in our published paper. We addressed this in a response [4] that was published alongside their letter [2]. However, even the reduced risks are high enough to support the conclusion of this chapter of the thesis (and the published paper) that offshore wind turbines in hurricane prone areas need to be designed differently than current designs intended for northern Europe. For example, there still remains a 5% probability that more than 10 turbines will be destroyed during the lifetime of the farm off the coast of Galveston.

The letter from Powell and Cocke objected to four shortcomings in the published paper:

1. We incorrectly interpreted the maximum sustained wind speed reported for U.S. hurricanes as a 10-minute average. The U.S. National Hurricane Center records a 1-minute average. As a result, we overstated the maximum sustained wind speed by approximately 10% [5]. I recalculated the results for Galveston with this correction and plotted them as (B) in Figure 4.2.
2. Data from hurricanes after 1977 are considered more accurate because of improved reconnaissance aircraft measurements and data from hurricanes before 1900 are not

considered reliable for risk modeling. In the published paper, we fit a Generalized Extreme Value distribution to hurricanes as far back as 1851. While newer hurricane data is considered more reliable, I found the period of HURDAT hurricane intensity data does not significantly change the fitted distribution. A generalized extreme value (GEV) distribution fit to hurricane data from 1978 – 2008 is not statistically different from a GEV distribution fit to hurricane data from 1851 – 1977 at the 95% confidence level, according to a two-sample Kolmogorov-Smirnov test.

3. Hurricanes tend to weaken as they approach land [6], but we assumed in the published paper that the lifetime maximum intensity of a hurricane is representative of its intensity at landafall. I re-analyzed data from hurricanes in the Galveston region and confirmed that their average intensity at landfall was 65% of their peak intensity. However, the distribution of landfalling intensities of *all* hurricanes in the gulf of Mexico (Table 1, Rappaport et al. [6]) is statistically indistinguishable the distribution we use in the paper—peak intensities of only hurricanes in the Galveston region. Thus, the GEV distribution for Galveston does not change if we assume the landfalling intensity of a hurricane anywhere in the Gulf of Mexico is drawn from the same distribution instead of assuming that hurricanes passing through a region around Galveston maintain their peak intensity to landfall, as we previously assumed.
4. The area of a hurricane exposed to the maximum winds is significantly smaller than we assumed in the published paper. For example, Figure 4.1 plots the maximum sustained wind speed of each hurricane to strike Galveston County (directly or indirectly) at each point along the coast. The overall maximum sustained wind speed and track of each hurricane is taken from the HURDAT database and the radius of maximum winds (RMW) is calculated from the central pressure according to a relationship proposed by Powell et al. [7] If central pressure measurements are not available, the RMW is assumed to be 33 km, the median size

of Gulf hurricanes from figure 37 in Ho et al. [8]). The wind field is calculated with a model proposed by Holland et al. [9] Figure 4.1 shows that most hurricanes making landfall in Galveston County expose less than half the coastline to their maximum wind speeds.

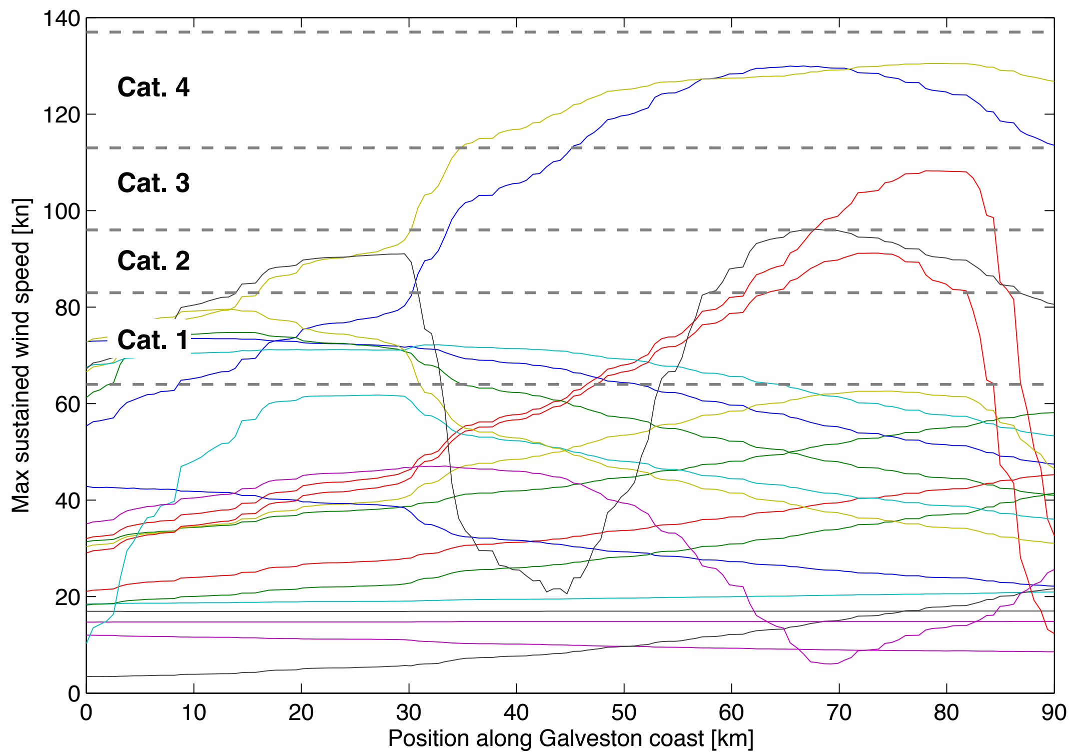

Figure 4.1: Wind profiles at landfall of all hurricanes making landfall in or near Galveston County, TX, 1900-2008.

Using the wind profiles from Figure 4.1, I re-calculated the results for a hypothetical wind farm located at 29.15°N, 94.66°W using the correct averaging period described above, and plotted the results as (C) in Figure 4.2. Those results are calculated from a Monte Carlo simulation of 200,000 years using a Poisson landfall rate of 9/107, a GEV fit of Gulf landfall maximum winds (Table 1, Rappaport et al. [6]), and a wind field for each hurricane randomly selected from the 9 Galveston landfalling hurricanes.

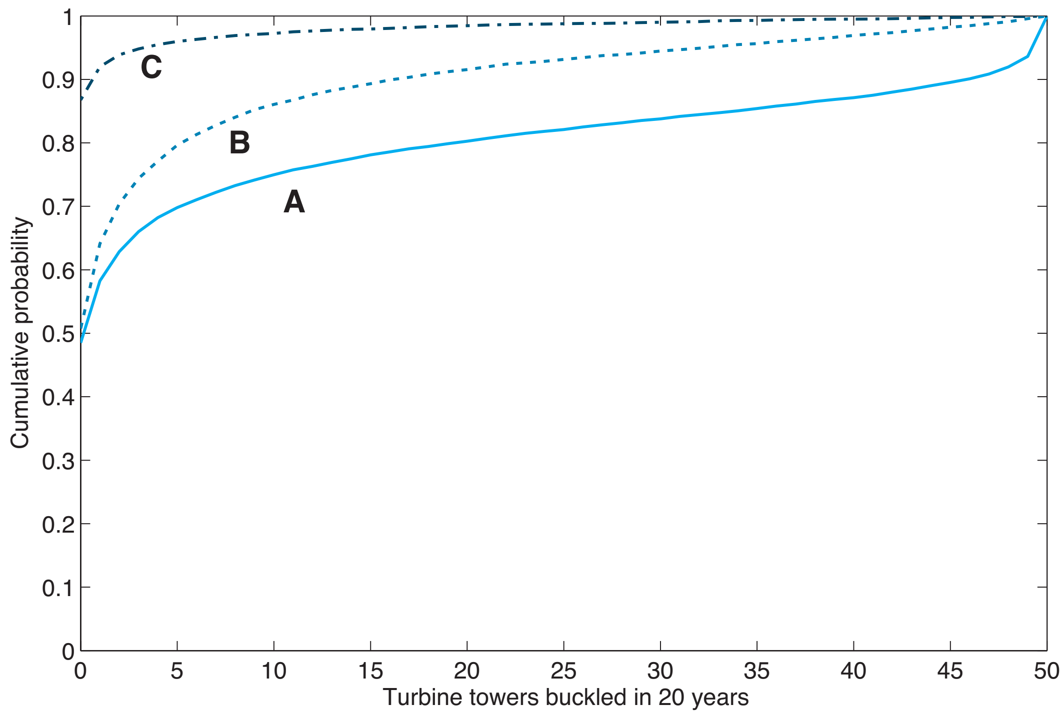

Figure 4.2: Cumulative distribution of the number of turbine towers in a 50-turbine wind at 29.15ºN, 94.66ºW buckled in 20 years if buckled towers are not replaced and there is no active yawing. The original results for Galveston published in Figure 2 of our paper are shown in (A). Results using the correction for 1 – average wind speeds are plotted in (B). Results using that correction and a wind field model are shown in (C).

4.2 Introduction

As a result of state renewable portfolio standards and federal tax incentives, there is growing interest and investment in renewable sources of electricity in the United States. Wind is the renewable resource with the largest installed-capacity growth in the last 5 years, with U.S. wind power capacity increasing from 8.7 GW in 2005 to 39.1 GW 2010 [10]. All of this development has occurred onshore. U.S. offshore wind resources may also prove to be a significant contribution to increasing the supply of renewable, low-carbon electricity. The National Renewable Energy Laboratory (NREL) estimates that offshore wind resources can be as high as four times the U.S. electricity generating capacity in 2010 [11]. Although this estimate does not take into account siting, stakeholder, and regulatory constraints, it indicates that U.S. offshore wind resources are significant. Though no offshore wind projects have been developed in the U.S., there are 20 offshore wind projects in the planning process (with an estimated capacity of 2 GW) [11]. The U.S. Department of Energy's 2008 report, *20% Wind by 2030* [12] envisions 54 GW of shallow offshore wind capacity to optimize delivered generation and transmission costs.

U.S. offshore resources are geographically distributed through the Atlantic, Pacific and Great Lake coasts. The most accessible shallow resources are located in the Atlantic and Gulf Coasts. Resources at depths shallower than 60 meters in the Atlantic coast, from Georgia to Maine, are estimated to be 920 GW; the estimate for these resources in the Gulf coast is 460 GW [11].

Offshore wind turbines in these areas will be at risk from Atlantic hurricanes. Between 1949 and 2006, 93 hurricanes struck the U.S. mainland according to the HURDAT database of the National Hurricane Center [13]. In this 58-year period, only 15 years did not incur insured hurricane-related losses [14]. The Texas region was affected by 35 hurricane events, while the southeast region (including the coasts of Florida, where no offshore resources have been estimated [11]) had 32 events.

Hurricane risks are quite variable, both geographically and temporally. Pielke et al. [15] note pronounced differences in the total hurricane damages (normalized to 2005) occurring each decade. Previous research has shown strong associations between North Atlantic hurricane activity and atmosphere-ocean variability on different timescales, including the multidecadal [16], [17]. Atlantic hurricane data show that hurricane seasons with very high activity levels occur with some regularity; for instance, since 1950, there have been 25 years with three or more intense hurricanes (Saffir-Simpson Category 3 or higher). There were two 2-year periods with 13 intense hurricanes: 1950-1951 and 2004-2005. 2004 and 2005 hurricanes were particularly damaging to the Florida and Gulf Coast regions (6 hurricanes made landfall in those areas in 2004 and 7 the following year).

These hurricanes resulted in critical damages to energy infrastructure. Hurricane Katrina (2005), for example, was reported to have damaged 21 oil and gas producing platforms and completely destroyed 44 [18]. Numerous drilling rigs and hydrocarbon pipelines were also damaged. Similarly, hurricanes have damaged powers systems. Liu et al. [19] reported that in 2003 Dominion Power had over 58,000 instances of the activation of safety devices in the electrical system to isolate damages as a result of Hurricane Isabel. Although no offshore wind turbines have been built in the U.S., there is no reason to believe that this infrastructure would be exempt from hurricane damages.

In order to successfully develop sustainable offshore resources, the risk from hurricanes to offshore wind turbines should be analyzed and understood. Here we present a probabilistic model to estimate the number of turbines that would be destroyed by hurricanes in an offshore wind farm. We apply this model to estimate the risk to offshore wind farms in four representative locations in the Atlantic and Gulf Coastal waters of the U.S.: Galveston County, TX; Dare County, NC; Atlantic County, NJ; and Dukes County, MA. Leases have been signed for wind farms off the coasts of Galveston [20] and Dukes County [21]; projects off the coasts of New Jersey and North Carolina have been proposed [21].

4.3 Materials and Methods

We model the distribution of the number of wind turbine towers buckled by hurricanes for two cases: (1) turbines are not replaced for the life of the wind farm, and (2) turbines are replaced after each hurricane. For each case, we calculate the distributions using two methods: an analytical probability distribution presented here and a Monte Carlo simulation discussed in Appendix A. The method is summarized in the flow chart shown in Figure 4.3.

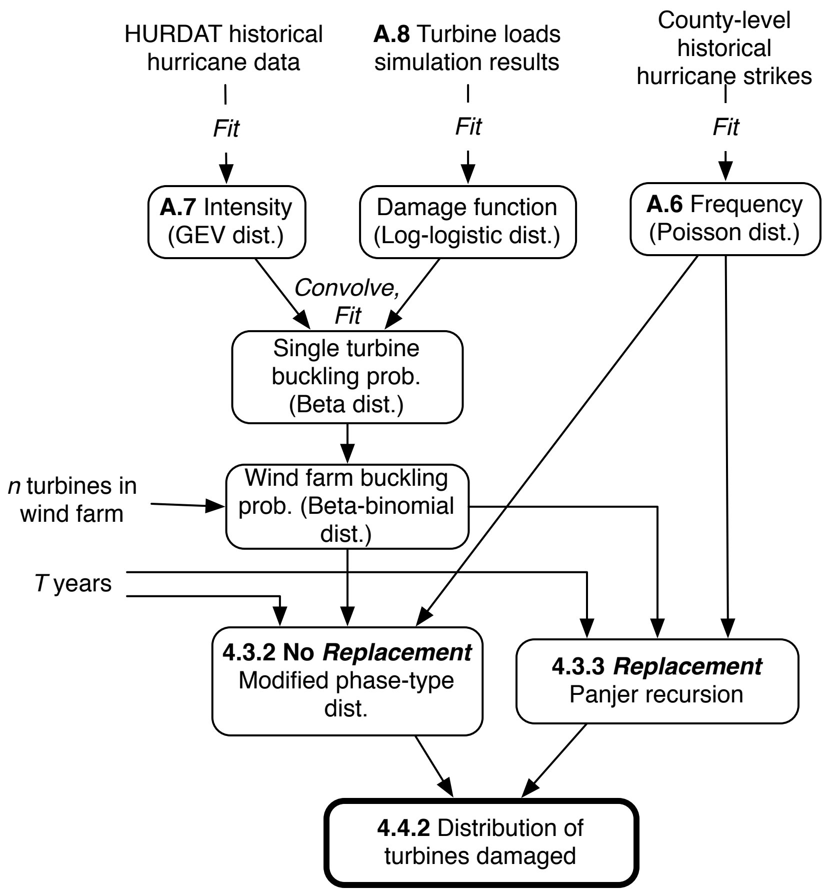

Figure 4.3: Flow chart for calculating the hurricane risk to offshore wind farms using historical hurricanes.

All the analyses presented here model a wind farm of 50 NREL 5-MW wind turbines [22] for 20 years. The turbines are shut down with their blades feathered to 90º because hurricane wind speeds are much higher than the maximum operating limit of wind turbines. We believe our results under-estimate the probability of loss because we model only buckling of the tower base but ignore damage to other components. Our results may also under-estimate the probability of tower buckling because we analyze the onshore version of the NREL 5-MW turbine, which has a rigid foundation structure and is not subjected to wave loads; Jha et al. [23] develop a more detailed model the NREL 5-MW turbine that includes foundation compliance and wave loads.

4.3.1 Assumptions

The risk model we develop in this chapter is based on several assumptions. The broadest assumption is that future hurricane activity will be similar to recorded hurricane activity in the period 1851 - 2008. Records of hurricane activity over that period are not uniformly reliable-- earlier are considered less complete (i.e. not all hurricanes were observed or recorded) and less accurate (e.g. poor measurements). This period also will not predict the effects of future climate change.

1. **Rate of Hurricane Occurrence:** We assume the rate of hurricanes striking a wind farm with their maximum intensity will be similar to the average rate of landfalling hurricanes in that county from 1900 – 2007. The historical record of landfalling hurricanes in that period is considered reliable. However, Powell and Cocke point out that the area exposed to maximum winds in a hurricane is smaller than many U.S. coastal counties [2]. Furthermore, we include "indirect" hurricane strikes from the historical record when we calculate that rate of hurricane occurrence, so we likely over-estimate the rate of hurricanes striking a wind farm.
2. **Hurricane Intensity:** We assume that the intensities (maximum 1-min average wind speed) of hurricanes at landfall will be similar to the maximum intensities of hurricanes within a few hundred miles of the U.S. coast (regions given in Table 4.2) from 1851 – 2008. This is a weak assumption for two reasons. First, Powell and Cocke point out that hurricanes tend to weaken from their maximum intensities as they move close to shore [2], so this assumption results in an over-estimation of intensities. Second, there is good evidence that historical record missed tropical cyclones until the advent of satellite imaging in the mid-20th century {Landsea:2007vh} and the intensity estimates for tropical cyclones early in the historical record are quite uncertain.

3. **Damage function:** We assume that the simulated wind loads on the turbine and the resulting stresses are representative of a real turbine designed for IEC Class 1B conditions. This is a reasonable assumption, though we believe we under-estimate the buckling probability because we do not model foundation compliance or wave slam loads (both discussed in Section A.8.1). The software used to simulate the turbine stresses is continuously improved and updated by NREL and used by many academic researchers and some turbine manufacturers. The software used to simulate the turbulent wind field is widely used for simulating typical turbulence, but we were not able to assess whether turbulence in a tropical cyclone has "typical" properties.

4.3.2 Analytical Distribution: Turbine Towers Buckled without Replacement

We model $Y_{\text{no rep}}$, the number of turbine towers that buckle in T years without replacement as a modified Phase-Type distribution with six parameters: $Y_{\text{no rep}} \sim \text{PH}(\lambda, \mu, \sigma, \xi, \alpha, \beta)$, where λ is the hurricane occurrence rate; μ, σ and ξ are the three parameters of the Generalized Extreme Value (GEV) distribution for event maximum wind speed; and α and β are the two parameters of the log-logistic wind speed-turbine buckling probability relationship. We use a Phase-type distribution because it models a series of events (storms) that occur randomly with a certain rate, and each buckles an integer number of turbine towers; it gives the distribution of time until all towers have been buckled. Figure 4.6 plots the results calculated with this method.

Hurricane occurrence is modeled as a Poisson process with rate parameter λ fitted to historical hurricane data. The probability that H, the number of hurricanes that occur in T years, equals a particular value h is:

$$\Pr(H = h) = \frac{(\lambda T)^h}{h!} e^{-\lambda T} \tag{4.1}$$

The maximum 10-minute sustained wind speed of each hurricane at 10-meter height is modeled as a Generalized Extreme Value (GEV) distribution with a location parameter μ, a scale parameter σ, and a shape parameter ξ fitted to historical hurricane data. The probability density function for *W*, the maximum sustained wind speed, evaluated at particular value *w* is:

$$f_W(w) = \frac{1}{\sigma}\exp\left(-\left(1+\xi\frac{w-u}{\sigma}\right)^{-\frac{1}{\xi}}\right)\left(1+\xi\frac{w-u}{\sigma}\right)^{-1-\frac{1}{\xi}} \tag{4.2}$$

The probability that a single wind turbine tower is buckled by a 10-minute sustained hub-height wind speed *u* is modeled using a Log-Logistic function with a scale parameter α and a shape parameter β. The parameters for turbines that can and cannot yaw to track wind direction are given in Table 4.1. These parameters are fit to probabilities of turbine tower buckling calculated by comparing the results of simulations of the 5-MW offshore wind turbine designed by the U.S. National Renewable Energy Laboratory [22] to the stochastic resistance to buckling proposed by Sørensen et al. [24] More extensive details are given in Appendix A.

Table 4.1: Parameters of log-logistic functions for probability of tower buckling.

	Turbine pointed into wind (Active Yawing)	Turbine pointed perpendicular to wind (Not Yawing)
Damage function parameters (log-logistic function)	α = 174, β = 19.3	α = 140, β = 18.6

The function is fitted to the results of simulations of stresses on a particular turbine design given a yaw direction relative to the wind, a wind turbulence intensity, and a sustained wind speed *u*, described in further detail in Appendix A. The Log-Logistic function is given by:

$$D(u) = \frac{\left(u/\alpha\right)^{\beta}}{1+\left(u/\alpha\right)^{\beta}} \tag{4.3}$$

The number of turbine towers buckled by a single hurricane in a wind farm of *n* turbines is modeled as a Beta Binomial distribution with parameters α_B and β_B. We derive the Beta Binomial distribution by fitting a Beta distribution with parameters α_B and β_B to the probability of buckling as a function of wind speed weighted by the probability of occurrence of each wind speed (a convolution of *D* and *W*) with a nonlinear least-squares fit. The wind speeds *W* are scaled to turbine hub height using the table of scaling values for hurricanes given by Franklin et al. [25] Fitting the distribution simplifies the model by replacing the convolution of *D* and *W*, which together have five parameters, with a Beta distribution that has only two parameters. The Beta distribution gives the distribution of buckling probabilities for a single turbine tower given a hurricane with random (GEV) maximum wind speed. The corresponding Beta Binomial distribution with the same parameter values α_B and β_B gives the probability that *X*, the number of turbine towers that buckle out of *n* total, equals a particular value *x*:

$$\Pr(X = x) = \binom{n}{x} \frac{\mathrm{B}(x+\alpha_B, n-x+\beta_B)}{\mathrm{B}(\alpha_B, \beta_B)} \tag{4.4}$$

where B( ) is the Beta function.

The cumulative distribution of the number of turbine towers buckled in *T* or fewer years without replacement, $Y_{no\ rep}$, is modeled as a modified Phase-Type distribution:

$$\Pr\left(Y_{no\ rep} \leq y \,\middle|\, \tau \leq T\right) = \boldsymbol{\pi} \exp\left(T\mathbf{T}(y, n)\right)\mathbf{e} \tag{4.5}$$

where $\boldsymbol{\pi}$ is a row vector of initial state probabilities, $\mathbf{T}$ is a matrix of jump intensities for the transitions between states, and $\mathbf{e}$ is a column vector of ones. A Phase-Type distribution gives the distribution of times $\boldsymbol{\tau}$ to reach the absorbing state of a Markov jump process [26], [27]. In this application, each jump (state transition) represents a hurricane occurrence, each state represents a unique number or turbines buckled, and the absorbing state is when all *n* turbine towers in the wind farm have buckled. We modify the Phase-Type distribution to calculate the distribution of the number of turbine towers buckled $Y_{no\ rep}$ in a fixed time T by iteratively redefining the absorbing state to include cases where less than n turbine towers are bucked, as shown in Figure 4.4.

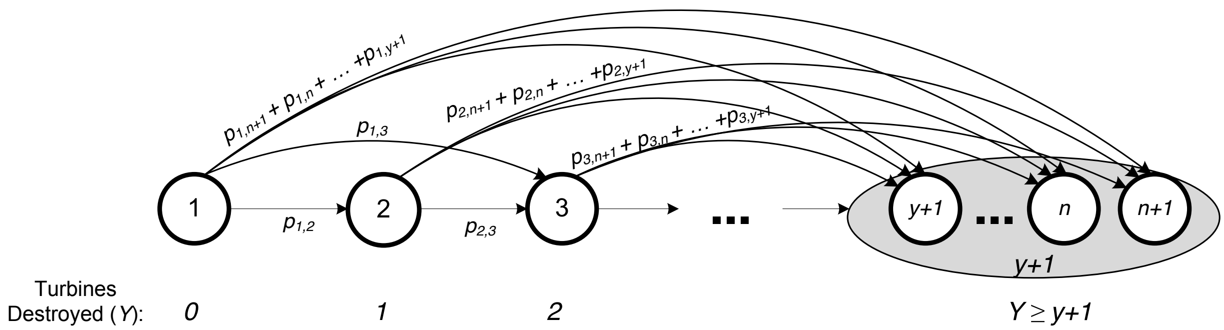

Figure 4.4: The Markov Chain used to calculate the probability that the number of turbine towers buckled is less than or equal to y. We define the absorbing state as all the states where $Y_{\text{no rep}} \geq y+1$.

This redefinition of the absorbing state makes the sizes of the vectors $\boldsymbol{\pi}$ and $\mathbf{e}$ a function of y and makes both the size and values of the matrix $\mathbf{T}$ a function of y. To calculate the probability that y or fewer turbine towers buckle, we define the absorbing state to include an integer number of turbine towers buckled from $y+1$ to n. There are $y+1$ total states; the $y+1^{\text{st}}$ state is the absorbing state. The term $\boldsymbol{\pi}$ in (4.5) is a $y+1$ element row vector of initial state probabilities; in this application $\boldsymbol{\pi} = [1\ 0\ \ldots\ 0]$ because the distribution begins in state 1 (no turbine towers buckled). The term $\mathbf{e}$ is a column vector of ones: $[1\ 1\ \ldots\ 1]^{\mathrm{T}}$. The term $\mathbf{T}$ is a $(y+1)$ X $(y+1)$ matrix of jump intensities, where the jump intensity $\mathbf{T}_{ij}(y,n)$ from the i^{th} state to the j^{th} state is the product of $\boldsymbol{\lambda}$, the rate of hurricane occurrence, and p_{ij}, the probability a hurricane causing a transition from state i to state j by buckling turbine towers. The off-diagonal elements of $\mathbf{T}(y,n)$ in the i^{th} row and j^{th} are calculated by:

$$T_{ij}(y,\ n) = \lambda\ \mathrm{BetaBinomial}\left(n-i+1,\ n-j+1;\ \alpha_B,\ \beta_B\right) \qquad j \geq i \tag{4.6}$$

$$\mathrm{T}_{ii}(y,n) = -\left(t_i(y,n) + \sum_{j>i} \mathrm{T}_{ij}(y,n) \right) \tag{4.7}$$

where **t** is the jump intensity for a hurricane that jumps directly to the absorbing state (i.e. destroys all remaining turbines):

$$t_i(y,n) = \lambda \sum_{m=0}^{n-y-1} \mathrm{BetaBinomial}((n-i+1), (n-i+1)-m; \alpha_B, \beta_B) \tag{4.8}$$

The off-diagonal elements of **T** do not sum to 1 along a row because some hurricanes do not cause a state transition (i.e. some hurricanes do not buckle any turbine towers).

4.3.3 Analytical Distribution: Turbine Towers Buckled with Replacement

We model Y_{rep}, the number of turbine towers that buckle in T years with replacement as a compound Poisson distribution with six parameters: $Y_{\mathrm{rep}} \sim$ Compound Possion(λ, μ, σ, ξ, α, β). We use a compound Poisson distribution because it models the distribution of the sum of independent identically-distributed events (hurricanes buckling wind turbines, in this case) that occur as a Poisson process. The compound Poisson distribution is a convolution of the Poisson distribution given in (4.1) for the number of hurricanes that occur in T years and the Beta Binomial distribution given in (4.4) for number of turbine towers buckled by each hurricane. No analytical expression exists for the PDF or CDF of a Compound Poisson distribution that contains a Beta Binomial distribution. We use Panjer's Recursion [28], [29], an iterative method, to approximate the PDF. The details are given in Appendix A.

4.3.4 Application to Specific Locations

The rate of hurricane occurrence parameter λ for the Poisson distribution given in (4.1) is calculated as the number of hurricanes to make landfall (direct and indirect strikes) in each county between 1900 and 2007 [30], divided by the length of the time period. The calculated values for the locations we investigate are given in Table 4.2. The parameters for the Generalized Extreme Value distribution given in (4.2) are fit to historical data for the maximum 10-minute sustained wind speed at 10-meter height for all hurricanes to pass through the geographic ranges of interest (described in the fourth column of Table 4.2) between 1851 and 2008.

Table 4.2: Distribution parameters for Poisson and GEV distributions.

	Rate of hurricane occurrence [events/year]	Max. sustained hurricane wind speed: GEV distribution [knots]	Geographic range of hurricanes modeled (lat/long)
Galveston County, TX	$\lambda = 0.19$	$\mu = 78.7$, $\sigma = 12.1$, $\xi = 0.251$	25.5°N–30°N 92°W–99°W
Dare County, NC	$\lambda = 0.21$	$\mu = 77.6$, $\sigma = 11.9$, $\xi = -0.0366$	32°–36.5°N 71°–81°W
Atlantic County, NJ	$\lambda = 0.047$	$\mu = 77.2$, $\sigma = 10.6$, $\xi = -0.0544$	36°–41°N 71°–77.5°W
Dukes County, MA	$\lambda = 0.075$	$\mu = 73.2$, $\sigma = 6.99$, $\xi = -0.139$	40.3°–42°N 66°–74.5°W

4.4 Results

4.4.1 Wind Farm Risk from a Single Hurricane

Wind turbines are vulnerable to hurricanes because the maximum wind speeds in those storms can exceed the design limits of wind turbines. Failure modes can include loss of blades and buckling of the supporting tower. In 2003, a wind farm of seven turbines in Okinawa, Japan was destroyed by typhoon Maemi [31] and several turbines in China were damaged by typhoon Dujuan [32]. Here we consider only tower buckling, since blades are relatively easy to replace (although their loss can cause other structural damage). To illustrate the risk to a wind farm from hurricane force wind speeds, we calculate the expected number of turbine towers that buckle in a 50-turbine wind farm as a function of maximum sustained (10-minute mean) wind speed, assuming that turbines cannot yaw during the hurricane to track the wind direction (we later consider the case in which the nacelle can be yawed rapidly enough to track the wind direction of the hurricane). Figure 4.5 plots the median, 5th

percentile, and 95th percentile of the number of turbine towers that buckle as a function of wind speed. The vertical dotted line shows the design reference wind speed for wind turbines in IEC Class 1 wind regimes, which includes the NREL 5-MW turbine we simulate, and nearly all offshore wind turbines currently in production. The IEC 61400-3 design standard for Class 1 wind regimes requires that a turbine survive a maximum 10-minute average wind speed with a 50-year return period of 50 m/s (97 knots) at hub height [33]; we scale this wind speed from 90-m height to 10-m height assuming power-law wind shear with an exponent of 0.077 [25] because hurricane wind speeds are given for 10-meter height.

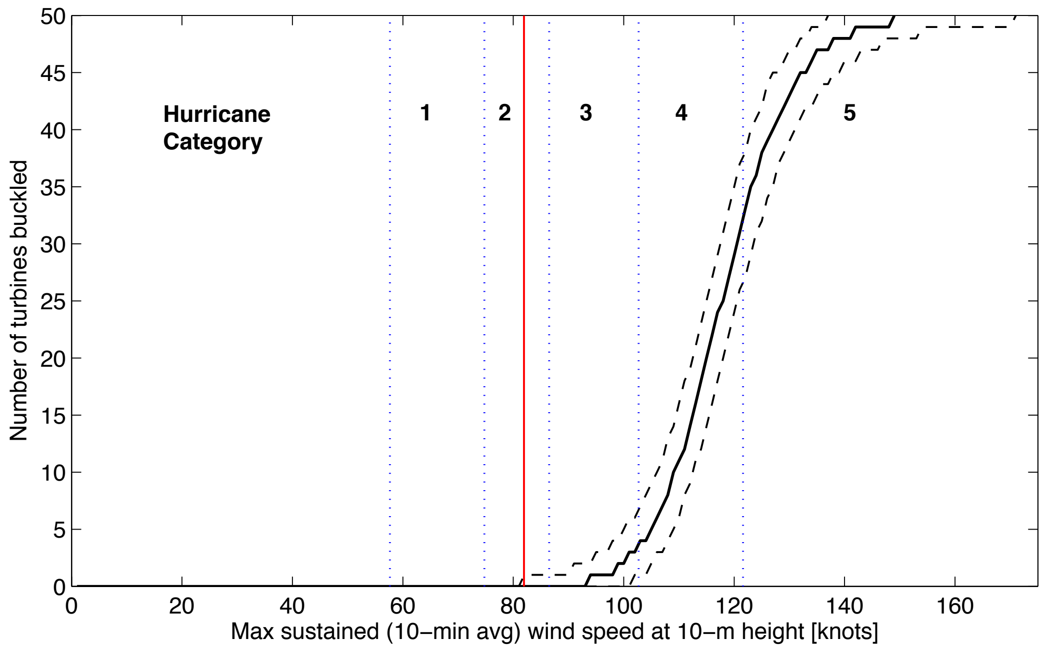

Figure 4.5: Cumulative distribution function of the expected number of turbine towers buckled by a single storm as a function of wind speed. This models a hurricane with a turbulence intensity of 9% in a 50-turbine wind farm of NREL 5-MW turbines (35) that cannot yaw to track the wind. The dashed lines plot the 5th and 95th percentile values and the solid vertical line shows V_{ref}, the design wind speed with a 50-year return period (15) scaled to 10-m height.

A Category 2 hurricane (wind speeds of 45 m/s or higher) will buckle up to 1% of the turbine towers in a wind farm. Hurricane Ike in 2008, for example, had a maximum sustained wind speed of 95 knots (49 m/s) at 10-meter height (Category 2) when it passed over the meteorological tower erected by the developers of the Galveston Offshore Wind project. If a 50-turbine wind farm had been located off the coast of Galveston when hurricane Ike struck, our model predicts that Hurricane Ike would have had a 5% probability of buckling 1 turbine tower.

Higher-category hurricanes will destroy a significant number of turbines; a Category 3 (wind speeds of 50 m/s or higher) will buckle up to 46% of the towers. The damage caused by Category 3, 4 and 5 hurricanes is important for offshore wind development in the U.S. because every state on the Gulf of Mexico coast and 9 of the 14 states on the Atlantic Coast have been struck by a Category 3 or higher hurricane between 1856 and 2008 [30].

4.4.2 Risk from Multiple Hurricanes

We calculate the cumulative distribution function (CDF) for the number of turbine towers that buckle in 20 years for wind farms at four different locations, assuming that buckled towers are not replaced after each storm. The distributions are modeled by a modified Phase-Type distribution described in the materials and methods section**.** Figure 4.6 shows the CDF for each location for two cases: turbines that can yaw to track wind direction (dashed line) and turbines that cannot yaw (solid line). The non-yawing case is a worst-case scenario, but it is realistic for two reasons. First, wind turbines typically do not have backup power for yaw motors and hurricanes often cause widespread power outages. Wind turbine design standards such as the IEC 61400-3 (Design Load Case 6.2) require turbine designers to assume a yaw misalignment up to ±180º if no yaw backup power is available, though designers can assume the turbine points directly into the wind if six hours of backup power is available for the yaw and control systems [33]. Second, wind direction in a hurricane may change faster than a wind turbine can yaw. The NREL 5-MW turbine we model is designed to yaw at 0.3º/sec, but Schroeder et al. show that the wind direction of Hurricane Bob in 1991 changed 30º in approximately 60 seconds (0.5º/sec), as measured 55 km away from the center of the storm [34]. The yawing case in Figure 4.6 illustrates how much the risk to a wind farm is reduced if the turbines can track the wind direction quickly and reliably as a hurricane passes.

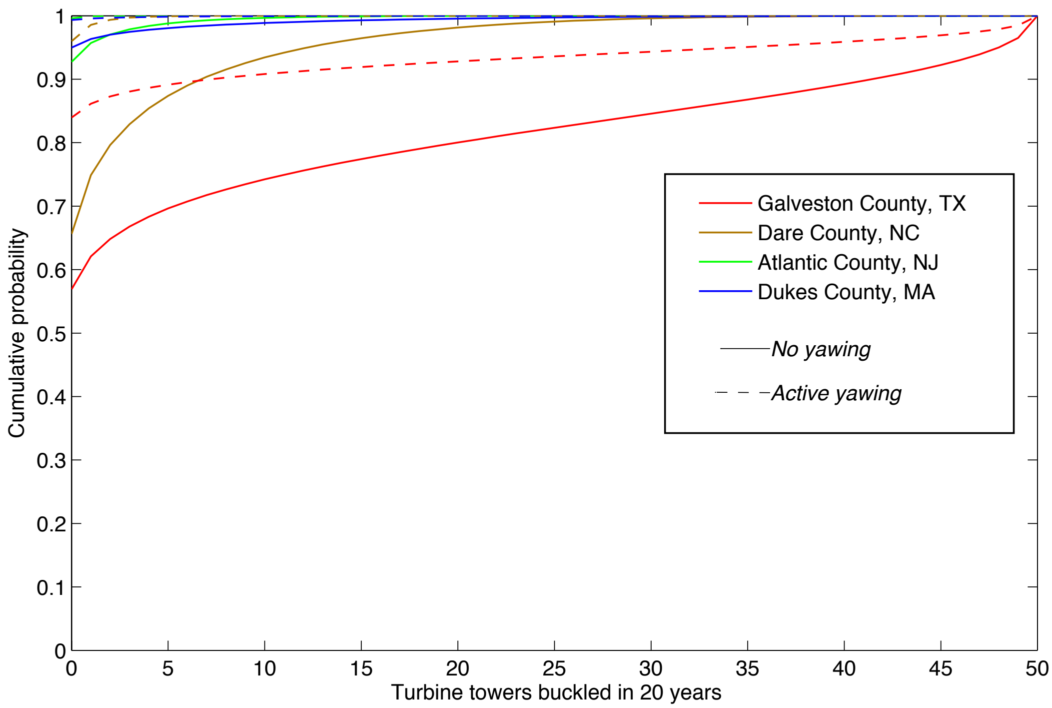

Figure 4.6: Cumulative distribution of the number of turbine towers in a 50-turbine wind farm buckled in 20 years if buckled towers are not replaced. Dashed lines plot the distribution for the case that turbines can yaw to track the wind direction, and solid lines plot the distribution for the case that turbines cannot yaw.

Galveston County is the riskiest location to build a wind farm of the four locations examined, followed by Dare County, NC. In contrast, Atlantic County, NJ and Dukes County, MA are significantly less risky. In Galveston County, there is a 43% probability that at least one tower will buckle in 20 years and a 18% probability that more than half will buckle if the turbines cannot yaw; if they are able to yaw, there is still a 16% probability that at least one tower will buckle and less than 6% probability that more than half will. These results for Galveston do not match line B in Figure 4.2, which are based on a GEV distribution fit to all landfalling hurricanes in the Gulf of Mexico, because these results are based on the GEV distribution given in Table 4.2, which is fit to only hurricanes that pass near Galveston. In Dare County, NC, there is a 34% probability that at least one tower will buckle in 20 years and a 1% probability that more than half will buckle if the turbines cannot yaw; if they are able to yaw, there is a 4% probability that at least one tower will buckle and much less than 1% probability that more than half will.

In Atlantic County, NJ there is a 7% probability that at least one tower will buckle in 20 years and less than 1% probability that more than half will buckle. In Dukes County, MA, there is a 5% probability that at least one tower will buckle in 20 years and less than 1% probability that more than half will buckle. If the turbines in Atlantic and Dukes counties are able to quickly yaw even when grid power is out, there is approximately a 99% probability that none will buckle in 20 years.

The results in Figure 4.6 assume the turbulence intensity of hurricanes is lognormally distributed with a mean of 9% and standard deviation of 1.5 %, where we define the turbulence intensity (TI) as the 10-minute standard deviation of wind speed divided by the 10-minute mean wind speed. The TI distribution is fitted to data from tropical cyclones over water, as discussed in Appendix A. The probability distributions in Figure 4.6 are sensitive to the chosen value of TI: higher turbulence intensities for a given mean wind speed means higher peak wind speeds, which increase the probability of a turbine tower buckling.

If turbines are replaced after each hurricane, the cumulative probabilities for fewer than 35 turbine towers buckling in 20 years is within two percentage points of the distributions without replacement shown in Figure 4.6. However, there is a possibility that more than 50 turbine towers will buckle in 20 years. For example, there is a 4% probability in Galveston County that more than 50 turbine towers will buckle if the turbines cannot yaw. The distributions with replacement are modeled as a compound Poisson distribution; the derivation of the distribution and a CDF plot of the results are given in Appendix A.

4.4.3 Distribution of Damage by Hurricane Intensity

The number of turbine towers that buckle in a wind farm during the farm's 20-year life is a function of the frequency of hurricane occurrence and the intensity of the hurricanes that occur. Higher-intensity storms buckle more turbine towers, but occur less frequently. To assess which categories of hurricanes cause the most expected damage, we use Monte Carlo simulation to calculate the expected value of the number of turbines that buckle in 20 years and the expected damage from each category of hurricane. The results are plotted in Figure 4.7. These results reflect damages averaged through 10,000 simulated 20-year periods. The results in any given 20-year period will be different, typically dominated by one or two hurricanes.

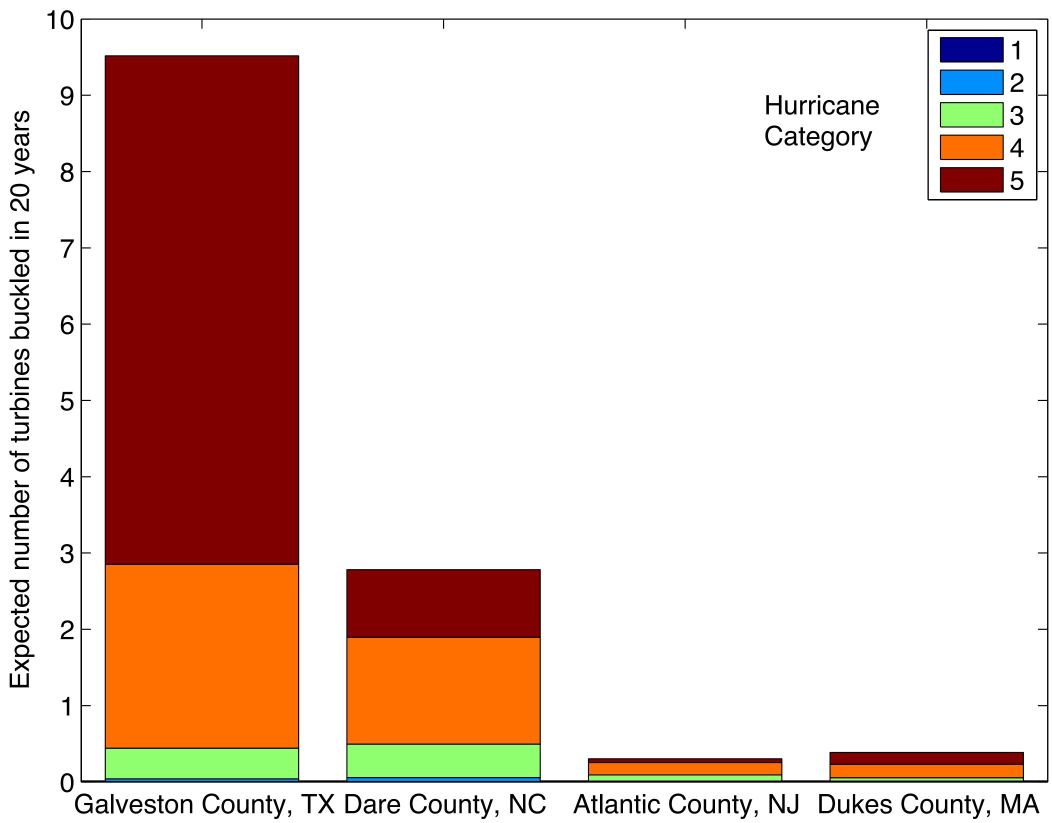

Figure 4.7: The expected number of turbine towers that buckle in a 50-turbine wind farm over 20 years for each location, subdivided by hurricane category.

Figure 4.7 indicates that Category 4 and 5 hurricanes are projected to cause most of the expected damage at each location: 95% in Galveston County, 82% in Dare County, 70% in Atlantic County, and 85% in Dukes County. However, no Category 4 and 5 hurricanes have made landfall in Dare, Atlantic, or Dukes counties since record keeping began in 1850. Analyses of U.S. hurricanes prior to 1850 report four landfalls in North Carolina that may have been category 4 (in 1815, 1827, 1842 and 1846) [35], [36] and one in 1821 that was likely either category 4 or 5 [36]. This historic record indicates that hurricanes of intensity 4 or higher should be possible in Dare County. Category 4 hurricanes also appear possible in Atlantic county with sufficiently warm sea-surface temperatures such as during late August. Hurricane model projections [35] indicate that the Great Colonial Hurricane of August 1635 most likely retained category 4 intensity until reaching southern New Jersey. However, storms of category 4 intensity in coastal Massachusetts may be physically impossible in present climate conditions. Generalized Extreme Value distributions (GEV) fit to the maximum sustained wind speeds of hurricanes in the regions around Dare, Atlantic, and Dukes counties predict probabilities of 4%, 2%, and 2%, respectively, that a hurricane making landfall in those counties will be Category 4 or 5.

We test the sensitivity of our results in Figure 4.6 and Figure 4.7 to the occurrence of category 4 and 5 hurricanes by repeating the Monte Carlo simulation of 10,000 20-year periods but excluding periods that contain a category 4 or 5 hurricane. This analysis excludes 16% of total simulations for Dare County, 2% for Atlantic County, and 2% for Dukes County. The results for Dare County are the most sensitive to the occurrence of high-category hurricanes: the expected number of turbine towers that buckle in 20 years decreases from 2.8 to 0.5, the probability of no turbine towers buckling increases from 61% to 72%, and the probability that less than half the turbine towers buckle increases from 97% to more than 99% when Category 4 and 5 hurricanes are excluded. The results for Atlantic and Dukes counties show a similar trend: the expected number of turbine towers that buckle falls from 0.35 to 0.08 in Atlantic County and from 0.43 to 0.06 in Dukes County. In both Atlantic and Dukes counties, the probabilities of none of the turbine towers and less than half the turbine towers buckling increase approximately one percentage point. Plots of the CDF of number of turbine towers bucked with higher-category hurricanes excluded are given in Appendix A.

4.5 Discussion

The 2008 DOE report [12] estimates that 54 GW of shallow offshore wind capacity will be required to bring the U.S. to 20% wind, and locates most of that capacity off the Gulf and East coasts. We find that hurricanes pose a significant risk to wind turbines off the U.S. Gulf and East coasts, even if they are designed to the most stringent current standard (IEC Class 1 winds). Now is an appropriate moment to consider mitigation strategies that can be incorporated to reduce risk to the grid and to operators, before large-scale offshore wind development is undertaken in the United States.

Engineered solutions can mitigate the risk of wind turbine damage as a result of hurricanes in the Eastern United States. Typically, wind turbines are designed based on engineering design codes for northern Europe and the North Sea, where nearly all the offshore and coastal wind turbines have been built. These codes specify maximum sustained wind speeds with a 50-year return period of 42.5 – 51.4 m/s (83 – 100 knots), lower than high intensity hurricanes [37]. Several authors have studied extreme winds in areas prone to tropical cyclones. Garciano et al. [38] propose increasing the 50-year design reference wind speed for the Philippines from 50 m/s to 58 m/s at hub height, Clausen et al. [39] propose 55 – 75 m/s (at 10-m height) for parts of the Philippines and southern Japan, and Ott proposes a model of extreme wind speeds in the western Pacific [40]. Some authors analyze the design codes in the context of tropical cyclones. A study by Jha et al., sponsored by a Joint Industry

Project that included two wind turbine manufacturers (GE Energy and Clipper Wind), compares the reliability levels of an offshore wind turbine designed to IEC 61400-3 and API RP-2A standards operating in several hurricane prone U.S. locations [23], [33], [41]. Clausen et al. [32] recommend increasing the design load safety factor, currently 1.35, to 1.7 in order to maintain the same level of reliability in tropical cyclone areas. They estimate increasing the safety factor will increase the cost of an onshore turbine 20 – 30%. The percentage cost increase to strengthen an offshore turbine, like the one we model in this paper, for tropical cyclones is likely to be smaller because a significant portion of the cost of offshore turbines is in the logistics of transporting, installing, and maintaining them.

We have also demonstrated that wind turbines that have external power available to yaw can have a substantially reduced risk of being destroyed. Installing lead-acid batteries to allow a turbine to yaw without external power would add $30,000 - $40,000 (2010 prices) to the price of a turbine and 1,400 – 2,400 kg to its weight, assuming 6 hours of backup power for yaw motors that draw 12 kW of power [42]. The yaw rate of the turbine we model is 0.3 degrees per second. Further work is needed to determine the yaw rate that is appropriate for hurricanes. Backup power, robust wind direction indicators, and active controls may be a low-cost way to reduce risk to the turbine.

A main concern with losing wind turbines during hurricanes is the implication this will have for grid reliability, and more work is needed on this issue. We hypothesize, however, that there is ample warning of hurricanes, and supplemental generation reserves can be brought on line to cover for the wind plants that will be shut down for the months to years that it may take to rebuild buckled towers. However, system operators must make it economical for the owners of such spare generation to stay in business even in years with no hurricane damage, and suitable capacity payment mechanisms will be required.

The probability of hurricane landfalls is not geographically uniform. Figure 4.8 plots the offshore wind resources within water shallower than 60 meters [11] and the annual rate of hurricane landfalls for states in the Eastern U.S. since 1900 [43]. Information for Florida, Alabama, and Mississippi is not included in Figure 4.8. Though these states have moderate to high hurricane occurrence rates (0.44, 0.14, and 0.10 year^{-1} respectively), there are no offshore wind resource estimates available for them. The specific results shown in this paper are thus not representative of all the risk of hurricanes to all possible offshore wind farm locations. It is clear, however, that analysis of the type presented here should be performed as part of the wind farm siting analysis.

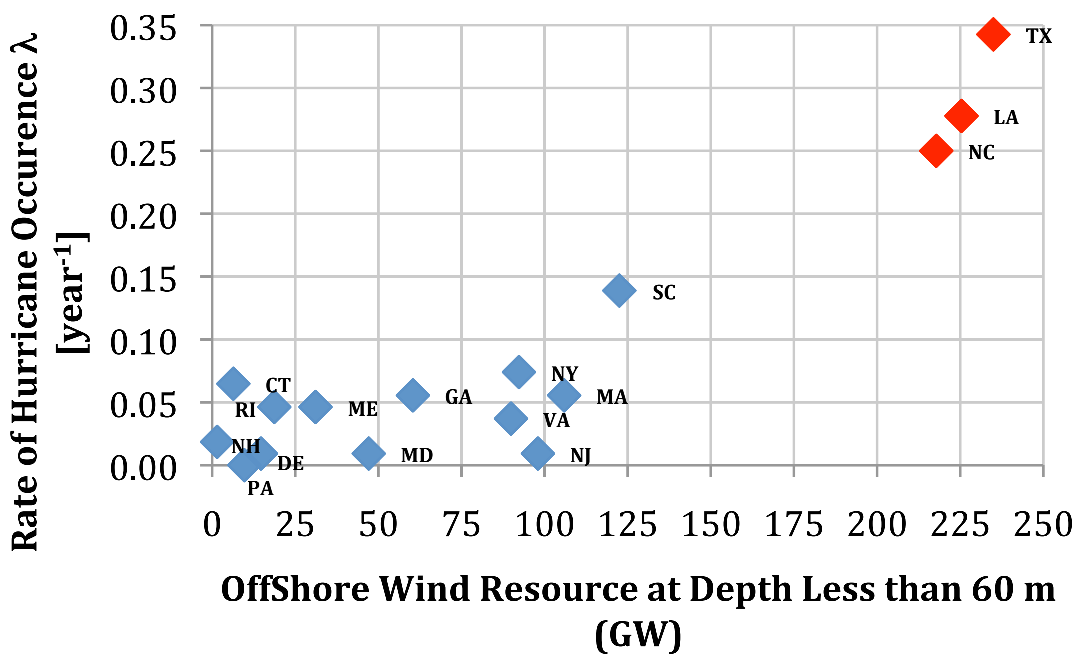

Figure 4.8: Resource vs. Hurricane Occurrence Rate λ [year^{-1}]. Texas, Louisiana, and North Carolina are shown in red because the annual rate of hurricane occurrence in those states is significantly higher than in the other states considered.

Our analysis also assumed that historic wind speeds and historic rates of hurricane occurrence are representative of future conditions. Historical conditions may be poor predictors if climate change were to affect hurricane intensity or frequency. Detection of climate change effects on hurricanes is complicated by the very high sensitivity of hurricanes to variations in atmosphere-ocean conditions on multiple timescales, including the multidecadal [44], and by the short period over which hurricane observations are considered reliable [44], [45]. Current high-resolution modeling studies project a relatively small increase in Atlantic hurricane intensity with increased global temperatures due to an increase in available thermal energy. Some of these models also identify a possible decrease in Atlantic hurricane frequency, which may be attributable to the stabilization of the upper atmosphere [46]. According to these projections, an increase in intensity due to climate change may not be noticeable for the next few decades [45]-[48]. In line with this, Pielke et al. [15] report that no trends in normalized damages can be detected. On the other hand, a recent observational study [49] finds that there has been an increase in the intensity of the most intense hurricanes. Wind farm developers will invest and operate under the current uncertainties on the future development of Atlantic hurricane activity. The method developed here will support the decision process of wind turbine investors in hurricane-prone areas. Sensitivity analysis on models like the one presented here can allow investors and regulators to see how distribution parameters affect the risk.

There is a very substantial risk that Category 3 and higher hurricanes can destroy a substantial fraction of the turbines in wind farms at some locations. By knowing the risks before building multiple GW of offshore wind plants, we can avoid precipitous policy decisions after the first big storm buckles a few turbine towers. Reasonable mitigation measures – increasing the design reference wind load, ensuring that the nacelle can be turned into the wind, and building most wind plants in the areas with lower risk – can greatly enhance the probability that offshore wind can help to meet the United States' electricity needs.

4.6 Acknowledgements

This work was supported in part by the EPA STAR fellowship program, a grant from the Alfred P. Sloan Foundation and EPRI to the Carnegie Mellon Electricity Industry Center, and by the Doris

Duke Charitable Foundation, the R.K. Mellon Foundation and the Heinz Endowments for support of the RenewElec program at Carnegie Mellon University. This research was also supported in part by the Climate and Energy Decision Making (CEDM) center. This Center has been created through a cooperative agreement between the National Science Foundation (SES-0949710) and Carnegie Mellon University.

4.7 References

[1] S. Rose, P. Jaramillo, M. J. Small, I. Grossmann, and J. Apt, "Quantifying the hurricane risk to offshore wind turbines," *Proceedings of the National Academy of Science*, vol. 109, no. 9, pp. 3247–3252, Feb. 2012.

[2] M. D. Powell and S. Cocke, "Hurricane wind fields needed to assess risk to offshore wind farms," *Proc Natl Acad Sci U S A*, vol. 109, no. 33, pp. E2192–E2192, Aug. 2012.

[3] S. Rose, "Correction for Rose et al., Quantifying the hurricane risk to offshore wind turbines.," *Proc Natl Acad Sci U S A*, vol. 109, no. 33, pp. 13464–13464, Aug. 2012.

[4] S. Rose, P. Jaramillo, M. J. Small, I. Grossmann, and J. Apt, "Reply to Powell and Cocke: On the probability of catastrophic damage to offshore wind farms from hurricanes in the US Gulf Coast," *Proc Natl Acad Sci U S A*, vol. 109, no. 33, pp. E2193–E2194, Aug. 2012.

[5] B. Harper, J. Kepert, and J. Ginger, "Guidelines for converting between various wind averaging periods in tropical cyclone conditions," World Meteorological Organization, Geneva, WMO/TD-1555, Aug. 2010.

[6] E. N. Rappaport, J. L. Franklin, A. B. Schumacher, M. DeMaria, L. K. Shay, and E. J. Gibney, "Tropical Cyclone Intensity Change before U.S. Gulf Coast Landfall," *Weather and Forecasting*, vol. 25, no. 5, pp. 1380–1396, Oct. 2010.

[7] M. D. Powell, G. Soukup, S. Cocke, N. Morisseau-Leroy, N. Dorst, and L. Axe, "Atmospheric Science Component: State of Florida Public Hurricane Model," May 2005.

[8] F. P. Ho, J. C. Su, K. L. Hanevich, R. J. Smith, and F. P. Richards, "NOAA Technical Report NWS 38: Hurricane Climatology for the Atlantic and Gulf Coasts of the United States," National Weather Service, Silver Spring, MD, NOAA Technical Report NWS 38, Apr. 1987.

[9] G. J. Holland, J. I. Belanger, and A. Fritz, "A Revised Model for Radial Profiles of Hurricane Winds," *Mon. Wea. Rev.*, vol. 138, no. 12, pp. 4393–4401, Dec. 2010.

[10] EIA, "Electric Power Annual 2010," U.S. Energy Information Administration, Nov. 2011.

[11] M. Schwartz, D. Heimiller, S. Haymes, and W. Musial, "Assessment of Offshore Wind Energy Resources for the United States," National Renewable Energy Laboratory, Golden, CO, NREL/TP-500-45889, Jun. 2010.

[12] DOE, "20% Wind Energy by 2030," U.S. Department of Energy, DOE/GO-102008-2567, Jul. 2008.

[13] E. S. Blake, E. N. Rappaport, and C. Landsea, "The deadliest, costliest, and most intense United States tropical cyclones from 1851 to 2006 (and other frequently requested hurricane facts)," NOAA/National Weather Service, National Centers for Environmental Prediction, National Hurricane Center, Miami, NWS TPC-5, Apr. 2007.

[14] S. A. Changnon, “Characteristics of severe Atlantic hurricanes in the United States: 1949–2006,” *Nat Hazards*, vol. 48, no. 3, pp. 329–337, 2009.
[15] R. A. Pielke, J. Gratz, C. W. Landsea, D. Collins, M. A. Saunders, and R. Musulin, “Normalized Hurricane Damage in the United States: 1900–2005,” *Natural Hazards Rev.*, vol. 9, no. 1, p. 29, 2008.
[16] C. Landsea, R. Pielke, A. Mestas-Nunez, and J. Knaff, “Atlantic basin hurricanes: Indices of climatic changes,” *Climatic Change*, vol. 42, no. 1, pp. 89–129, 1999.
[17] S. Goldenberg, C. Landsea, A. Mestas-Nunez, and W. GRAY, “The recent increase in Atlantic hurricane activity: Causes and implications,” *Science*, vol. 293, no. 5529, pp. 474–479, 2001.
[18] A. M. Cruz and E. Krausmann, “Damage to offshore oil and gas facilities following hurricanes Katrina and Rita: An overview,” *J Loss Prevent Proc*, vol. 21, no. 6, pp. 620–626, 2008.
[19] H. Liu, R. A. Davidson, D. V. Rosowsky, and J. R. Stedinger, “Negative Binomial Regression of Electric Power Outages in Hurricanes,” *Journal of Infrastructure Systems*, vol. 11, no. 4, p. 258, 2005.
[20] DOE, “Company Plans Large Wind Plant Offshore of Galveston, Texas,” *Energy Efficiency & Renewable Energy Network News*. [Online]. Available: http://apps1.eere.energy.gov/news/news_detail.cfm/news_id=9502. [Accessed: 02-Nov-2005].
[21] DOE, “Interior Department Signs First U.S. Offshore Wind Energy Lease,” *Energy Efficiency & Renewable Energy Network News*. [Online]. Available: http://apps1.eere.energy.gov/news/news_detail.cfm/news_id=16398. [Accessed: 13-Oct-2010].
[22] J. Jonkman, S. Butterfield, W. Musial, and G. Scott, “Definition of a 5-MW reference wind turbine for offshore system development,” National Renewable Energy Laboratory, Golden, CO, NREL/TP-500-38060, Feb. 2009.
[23] A. Jha, D. Dolar, W. Musial, and C. Smith, “On Hurricane Risk to Offshore Wind Turbines in US Waters,” presented at the Offshore Technology Conference, Houston, 2010, pp. 1–14.
[24] J. D. Sørensen and N. J. Tarp-Johansen, “Reliability-based optimization and optimal reliability level of offshore wind turbines,” *International Journal of Offshore and Polar Engineering*, vol. 15, no. 2, pp. 141–146, 2005.
[25] J. Franklin, M. Black, and K. Valde, “GPS Dropwindsonde Wind Profiles in Hurricanes and Their Operational Implications,” *Weather and Forecasting*, vol. 18, no. 1, pp. 32–44, 2003.
[26] M. F. Neuts, *Matrix-Geometric Solutions in Stochastic Models: An Algorithmic Approach*. Baltimore: Johns Hopkins University Press, 1981.
[27] M. Bladt, “A review on phase-type distributions and their use in risk theory,” *ASTIN Bulletin*, vol. 35, no. 1, pp. 145–161, 2005.
[28] H. Panjer, “Recursive evaluation of a family of compound distributions,” *ASTIN Bulletin*, vol. 12, no. 1, pp. 22–26, 1981.
[29] D. C. M. Dickson, “A Review of Panjer's Recursion Formula and Its Applications,” *British Actuarial Journal*, vol. 1, no. 1, pp. 107–124, 1995.
[30] National Hurricane Center, “County by county hurricane strikes 1900–2009,” National Hurricane Center, Coral Gables, FL, 2010.
[31] K. Takahara, T. Mekaru, F. Shinjo, T. Ishihara, A. Yamaguchi, and S. Matsuura, “Damages of wind turbine on Miyakojima Island by Typhoon Maemi in 2003,” *2004 European Wind Energy Conference and Exhibition*, 2004.

[32] N. E. Clausen, A. Candelaria, S. Gjerding, S. Hernando, P. Nørgård, S. Ott, and N. Tarp-Johansen, "Wind farms in regions exposed to tropical cyclones," *2007 European Wind Energy Conference and Exhibition*, 2007.
[33] IEC, "Wind turbines - Part 3: Design requirements for offshore wind turbines," 61400-3, Feb. 2009.
[34] J. L. Schroeder, D. A. Smith, and R. E. Peterson, "Variation of Turbulence Intensities and Integral Scales During the Passage of a Hurricane," *Journal of Wind Engineering and Industrial Aerodynamics*, vol. 77, pp. 65–72, 1998.
[35] B. R. Jarvinen, *Storm tides in twelve tropical cyclones (including four intense New England hurricanes).* Coral Gables, FL: National Hurricane Center, 2006.
[36] B. H. Bossak, "Early 19th Century U.S. Hurricanes: A GIS Tool And Climate Analys," Florida State University, Tallahassee, FL, 2003.
[37] K. Argyriadis, "Recommendations for Design of Offshore Wind Turbines (RECOFF), Section 2.1: External Conditions," 2003.
[38] L. E. O. Garciano and Takeshi Koike, "New Reference Wind Speed for Wind Turbines in Typhoon-Prone Areas in the Philippines," *Journal of Structural Engineering*, vol. 136, no. 4, pp. 463–467, 2010.
[39] N. E. Clausen, S. Ott, N. Tarp-Johansen, undefined author, undefined author, undefined author, and S. Hernando, "Design of Wind Turbines in an Area with Tropical Cyclones," presented at the 2006 European Wind Energy Conference and Exhibition, Athens, 2006.
[40] S. Ott, "Extreme winds in the western North Pacific," Nov. 2006.
[41] API, "Recommended Practice for Planning, Designing, and Constructing Fixed Offshore Platforms - Working Stress Design," Washington, D.C., RP-2A-WSD, Dec. 2000.
[42] J. Aabakken, "Power Technologies Energy Data Book, Fourth Edition," 2006.
[43] B. R. Jarvinen, C. J. Neumann, and M. A. S. Davis, "A Tropical Cyclone Data Tape for the North Atlantic Basin, 1886-1982: Contents, Limitations, and Uses," National Hurricane Center, Miami, FL, NOAA Technical Memorandum NWS NHC 22, Oct. 1988.
[44] I. Grossmann and M. G. Morgan, "Tropical cyclones, climate change, and scientific uncertainty: what do we know, what does it mean, and what should be done?," *Climatic Change*, vol. 108, no. 3, pp. 543–579, 2011.
[45] C. W. Landsea, B. A. Harper, K. Hoarau, and J. A. Knaff, "Can we detect trends in extreme tropical cyclones?," *Science*, vol. 313, no. 5786, pp. 452–454, 2006.
[46] T. R. Knutson, J. L. McBride, J. Chan, K. A. Emanuel, G. Holland, C. Landsea, I. Held, J. P. Kossin, A. K. Srivastava, and M. Sugi, "Tropical cyclones and climate change," *Nat Geosci*, vol. 3, no. 3, pp. 157–163, Feb. 2010.
[47] L. Bengtsson, K. I. Hodges, M. Esch, N. Keenlyside, L. Kornblueh, J.-J. Luo, and T. Yamagata, "How may tropical cyclones change in a warmer climate?," *Tellus A*, vol. 59, no. 4, pp. 539–561, 2007.
[48] M. A. Bender, T. R. Knutson, R. E. Tuleya, J. J. Sirutis, G. A. Vecchi, S. T. Garner, and I. M. Held, "Modeled Impact of Anthropogenic Warming on the Frequency of Intense Atlantic Hurricanes," *Science*, vol. 327, no. 5964, pp. 454–458, 2010.
[49] J. B. Elsner, J. P. Kossin, and T. H. Jagger, "The increasing intensity of the strongest tropical cyclones," *Nature*, vol. 455, no. 7209, pp. 92–95, 2008.

A Appendix

A.1 Risk From Multiple Hurricanes with Replacement

In the main body of the paper, Figure 4.6 present CDF plots for the number of turbines destroyed in 20 years if buckled turbine towers are not replaced. Here we present similar results for the case in which buckled towers are replaced after each storm. Figure A-1 plots the CDF for each location for two cases: turbines that can yaw to track wind direction (dashed lines) and turbines that cannot yaw (solid lines).

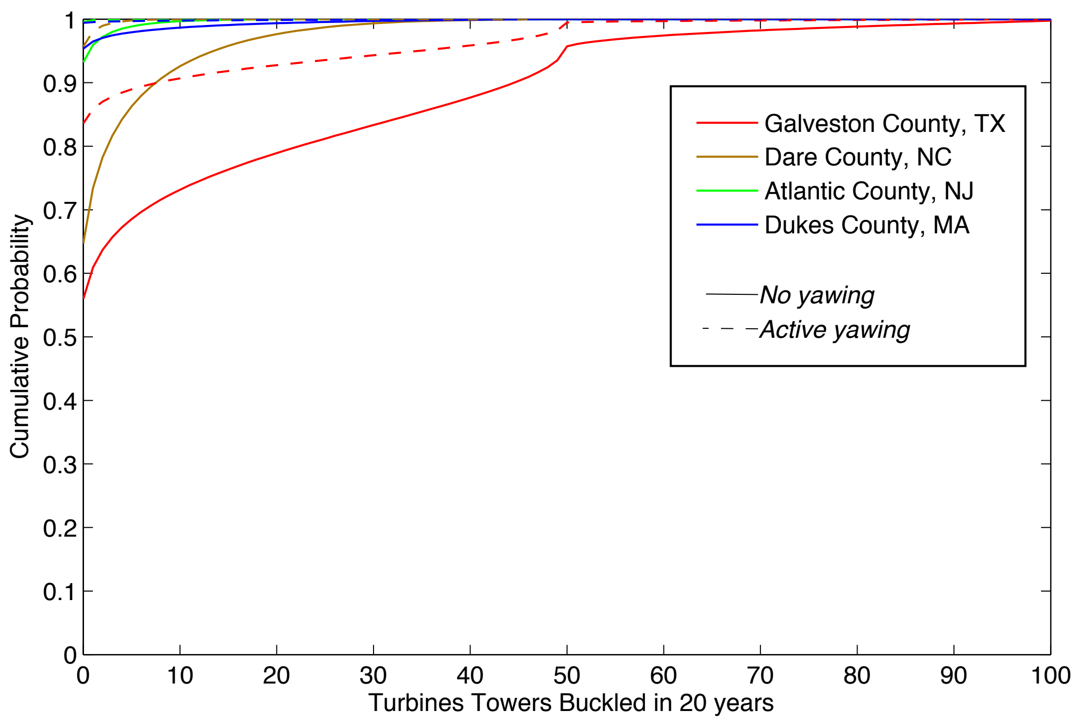

Figure A-1: Cumulative distribution of the number of towers in a 50-turbine wind farm buckled in 20 years if buckled toowers are replaced after each storm if they buckle. Dashed lines plot the distribution for the case that turbines can yaw to track the wind direction, and solid lines plot the distribution for the case that turbines cannot yaw.

In this scenario, buckled towers are replaced after each storm so there is no limit to the maximum number of towers that buckle. There is a 4% probability that more than 50 turbine towers will buckle in Galveston County and less than 1% probability that more than 50 will buckle in Dare County.

A.2 Risk From Multiple Hurricanes, Cat. 4 and 5 Hurricanes Excluded

To illustrate the effect of excluding category 4 and 5 hurricanes for Dare, Atlantic, and Dukes counties, we plot the CDF of the number of turbines damaged with and without those higher-category hurricanes. The results for the case that turbines cannot yaw to track the wind direction are shown in Figure A-2, where solid lines plot the results for all hurricanes and dotted lines plot the results excluding category 4 and 5 hurricanes. Similarly, the results for the case that turbines can actively yaw are shown in Figure A-3, where solid lines plot the results for all hurricanes and dotted lines plot the results excluding category 4 and 5 hurricanes.

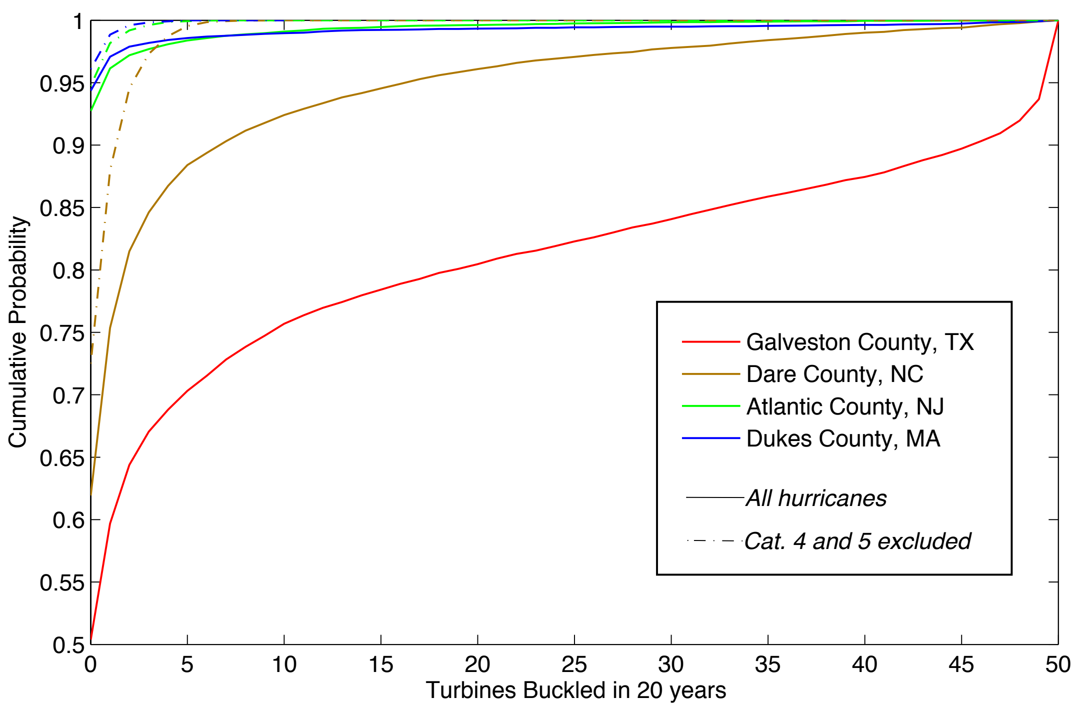

Figure A-2: CDF of the number of turbine towers buckled in 20 years without replacement; turbines cannot yaw to track the wind. Solid lines plot the distribution including all hurricanes, and dotted lines plot the distribution with category 4 and 5 hurricanes excluded.

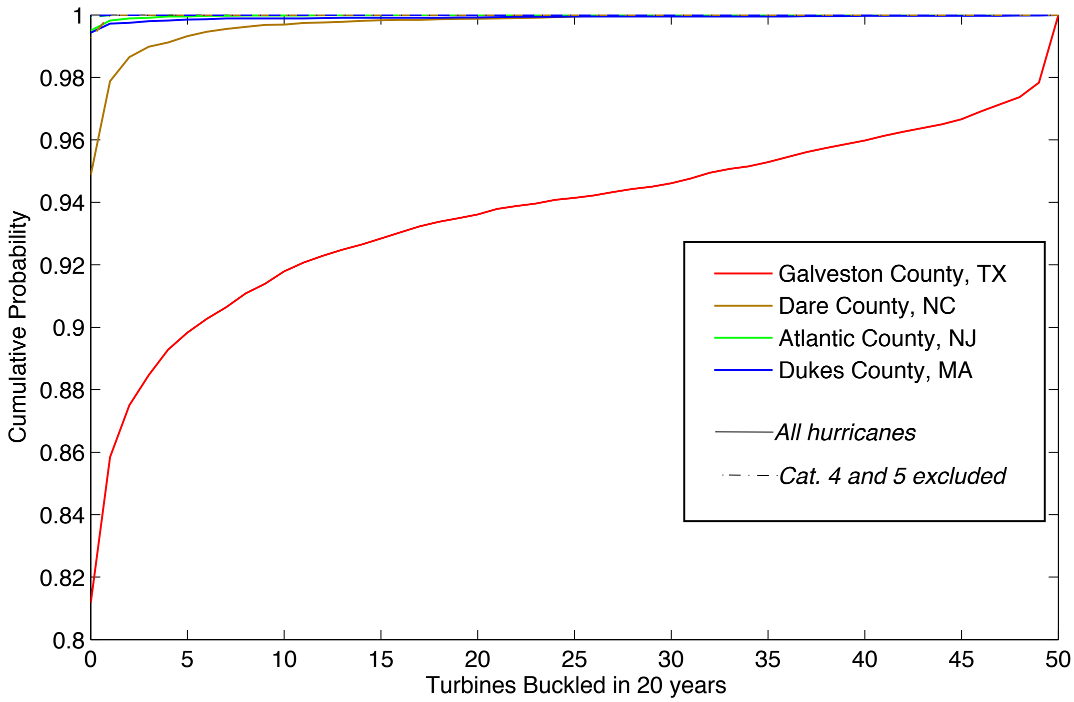

Figure A-3: CDF of the number of turbine towers buckled in 20 years without replacement; turbines can actively yaw to track the wind. Solid lines plot the distribution including all hurricanes, and dotted lines plot the distribution with category 4 and 5 hurricanes excluded.

A.3 Analytical Distribution: Turbine Towers Buckled with Replacement

As described in the main document, we use a Compound Poisson distribution to model Y_{rep}, the total number of turbine towers buckled in T years in a wind farm of n turbines if towers are immediately replaced after they are buckled by a hurricane. The Compound Poisson distribution is a function of six parameters: λT, μ, σ, ξ, α, and β.

$$Y_{\text{rep}} \sim \text{Compound Poisson}(\lambda T, \mu, \sigma, \xi, \alpha, \beta) \qquad \textbf{(A 1)}$$

No analytical expression exists for the PDF or CDF of a Compound Poisson distribution that contains a Beta Binomial distribution. We use Panjer's Recursion [1], [2], an iterative method, to compute the exact pdf:

$$\Pr(Y_{rep} = y) = g_y = \sum_{j=1}^{y} \left(a + \frac{bj}{y} \right) f_j g_{y-j} \qquad \textbf{(A 2)}$$

where

$$f_j = \begin{cases} \Pr(X_i = j) & j \le n \\ 0 & j > n \end{cases} \quad \textbf{(A 3)}$$

The value of f_j is zero for $j > n$ in equation (A 2) because the Beta Binomial distribution for the number of turbine towers buckled in the ith hurricane X_i is not defined for $x > n$, i.e. the number of towers buckled in one hurricane cannot be larger than the number of turbines in the wind farm.

Panjer defines a and b for a Poisson distribution [1]:

$$a = 0$$

$$b = \lambda T$$

The initial value of f is:

$$f_0 = \Pr(X_i = 0) = \binom{n}{0} \frac{\mathrm{B}(0 + \alpha_B, n - 0 + \beta_B)}{\mathrm{B}(\alpha_B, \beta_B)} = \frac{\mathrm{B}(\alpha_B, n + \beta_B)}{\mathrm{B}(\alpha_B, \beta_B)} \quad \textbf{(A 4)}$$

and the initial value g_0, from [3], gives the probability that no turbine towers are buckled by hurricanes in T years as the probability that no hurricanes occur ($H = 0$) plus the probability that a positive number of hurricanes occur but cause no damage:

$$\begin{aligned} g_0 &= \Pr(H = 0) + \Pr(Y = 0 | H > 0) \\ &= \frac{(\lambda T)^0}{0!} e^{-\lambda T} + \sum_{i=1}^{\infty} \Pr(X = 0) \Pr(H = i) \\ &= e^{-\lambda T} + \sum_{i=1}^{\infty} \left(\binom{n}{0} \frac{\mathrm{B}(0 + \alpha_B, n - 0 + \beta_B}{\mathrm{B}(\alpha_B, \beta_B)}) \right)^i \frac{(\lambda T)^i}{i!} e^{-\lambda T} \\ &= e^{-\lambda T} + \sum_{i=1}^{\infty} \left(\frac{\mathrm{B}(\alpha_B, n + \beta_B}{\mathrm{B}(\alpha_B, \beta_B}) \right)^i \frac{(\lambda T)^i}{i!} e^{-\lambda T} \end{aligned} \quad \textbf{(A 5)}$$

where $\mathrm{B}(\alpha, \beta)$ is the Beta function:

$$\mathrm{B}(\alpha_B, \beta_B) = \frac{\Gamma(\alpha_B)\Gamma(\beta_B)}{\Gamma(\alpha_B + \beta_B)} = \frac{(\alpha_B - 1)!\,(\beta_B - 1)!}{(\alpha_B + \beta_B - 1)!} \quad \textbf{(A 6)}$$

and $\Gamma()$ is the Gamma function.

A.4 Monte Carlo Distribution: Turbine Towers Buckled with Replacement

To check the Compound Poisson distribution described above, we use Monte Carlo simulations to calculate Y_{rep}, the distribution of the total number of turbine towers buckled in T years in a wind farm of n turbines if towers are replaced after each hurricane. We simulate 10,000 20-year periods using the same distributions used in the Compound Poisson distribution: H for the frequency of hurricane occurrence, W for the maximum sustained wind speed, and D for the probability of buckling as a function of wind speed.

For each simulated 20-year period in a given location, we calculate the total number of towers that buckle according to the following procedure:

1. Draw number of hurricanes from Poisson distribution H described in Section A.6.
2. Draw maximum sustained wind speed for each hurricane from Generalized Extreme Value distribution W described in Section A.7.
3. Scale maximum sustained wind speed to hub height [4] and calculate probability of a single turbine tower buckling at that wind speed using the Log-Logistic damage function described in Section A.8.
4. Calculate the number of towers buckled in each hurricane using a Binomial distribution with the probability of buckling calculated in step 3 and n turbines.

A comparison of the distributions calculated with the compound Poisson distribution and the Monte Carlo simulation is shown in Figure A-4.

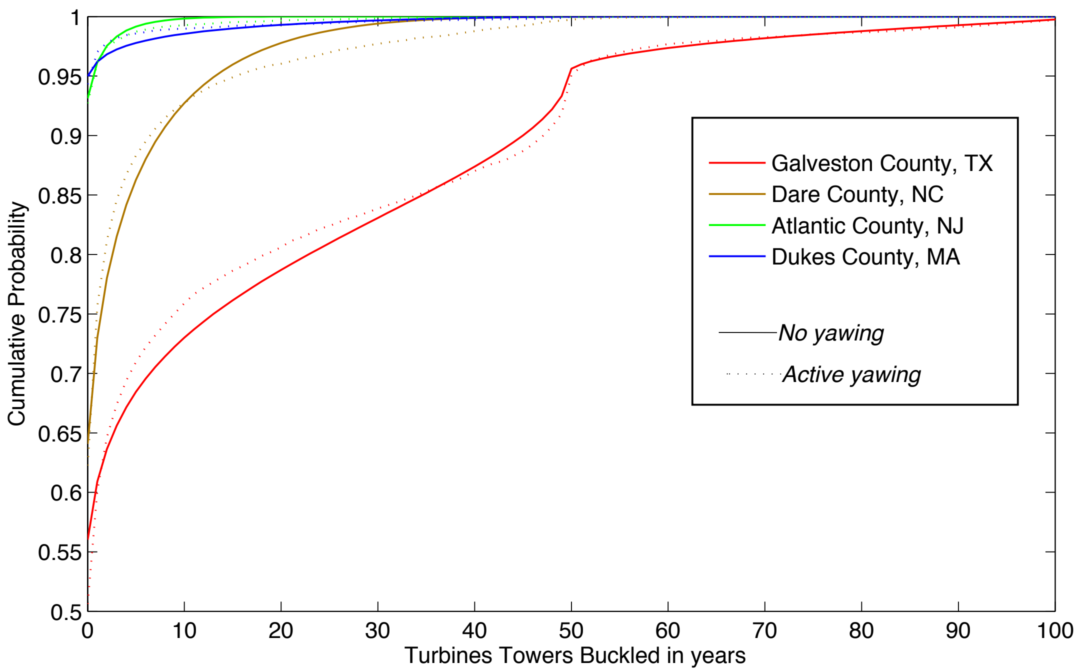

Figure A-4: A comparison of the cumulative probability distributions of number of turbine towers buckled in 20 years for the case where turbine towers are replaced after each storm if they buckle. Results calculated with Monte Carlo simulation are plotted as dashed lines and results calculated with a compound Poisson distribution are plotted as solid lines.

A.5 Monte Carlo Distribution: Turbine Towers Buckled without Replacement

To check the Phase-Type distribution described in the main paper, we use Monte Carlo simulations to calculate $Y_{\text{no rep}}$, the distribution of the total number of turbine towers buckled in T years in a wind farm of n turbines if turbines are not replaced after they are destroyed. We simulate 10,000 20-year periods using the same distributions used in the Phase-Type distribution: H for the frequency of hurricane occurrence, W for the maximum sustained wind speed, and D for the probability of buckling as a function of wind speed.

For each simulated 20-year period in a given location, we calculate the total number of turbine towers buckled according to the following procedure:

1. Draw number of hurricanes from Poisson distribution H described in Section A.6.
2. Draw maximum sustained wind speed for each hurricane from Generalized Extreme Value distribution W described in Section A.7.

3. Scale maximum sustained wind speed to hub height [4] and calculate probability of a single turbine tower buckling at that wind speed using the Log-Logistic damage function described in Section A.8.
4. Calculate the number of remaining turbines buckled in each hurricane using a Binomial distribution with the probability of buckling calculated in step 3 and the number of turbines remaining after all the previous hurricanes.

A comparison of the distributions calculated with the Phase-Type distribution given in the main paper and the Monte Carlo simulation described above is shown in Figure A-5.

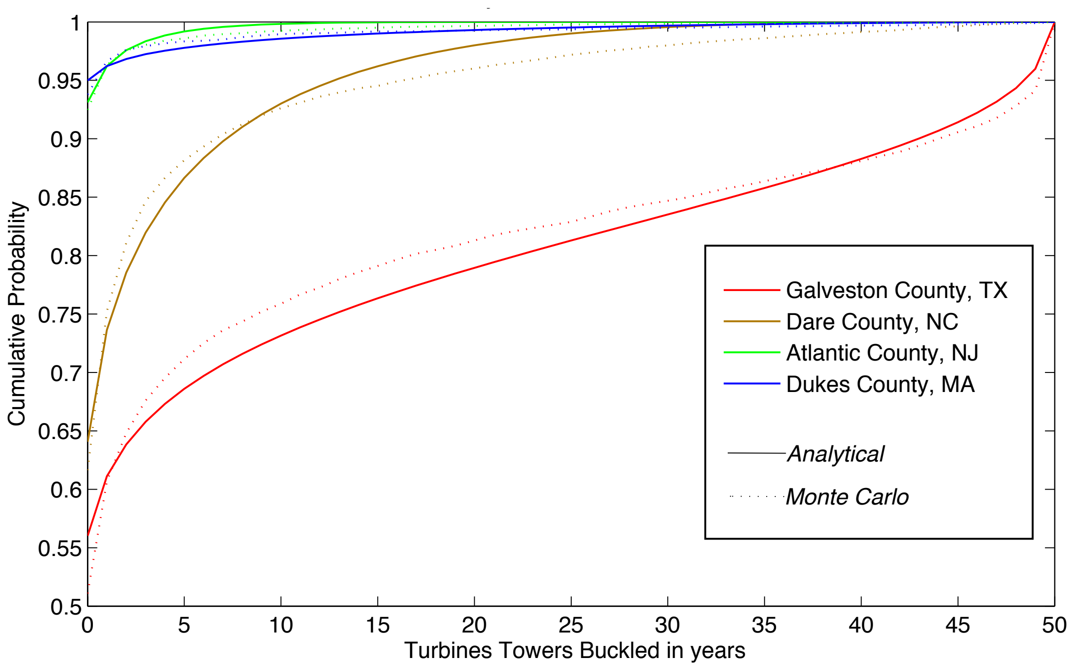

Figure A-5: A comparison of the cumulative probability distributions of number of turbine towers buckled in 20 years for the case where towers are not replaced if they buckle. Results calculated with Monte Carlo simulation are plotted as dashed lines and results calculated with a Phase-Type distribution are plotted as solid lines.

A.6 Hurricane Frequency (H)

We fit a Poisson distribution to the rate of hurricane occurrence in a particular county by dividing the number of hurricanes to make landfall in that county from 1900 to 2006 by the number of years [5]. Table 4.2 in the main paper lists the resulting rate of hurricane occurrence values λ for the four counties we examine. This method of calculating the rate of hurricane occurrence assumes that the rate is constant and equal to the average rate. However, previous research has shown strong associations between North Atlantic hurricane activity and atmosphere-ocean variability on different timescales, including the multidecadal [6], [7].

A.7 Hurricane Intensity (W)

We fit a Generalized Extreme Value distribution (GEV) to the maximum 10-minute sustained wind speed at 10-meter height of hurricanes that pass through a region around the counties we examine. Table 4.2 in the main paper gives the parameters of the fitted GEV distributions for each location and the latitude and longitude limits of the regions around those locations. Figure A-6 compares the empirical and fitted CDFs for the maximum sustained wind speed at each location.

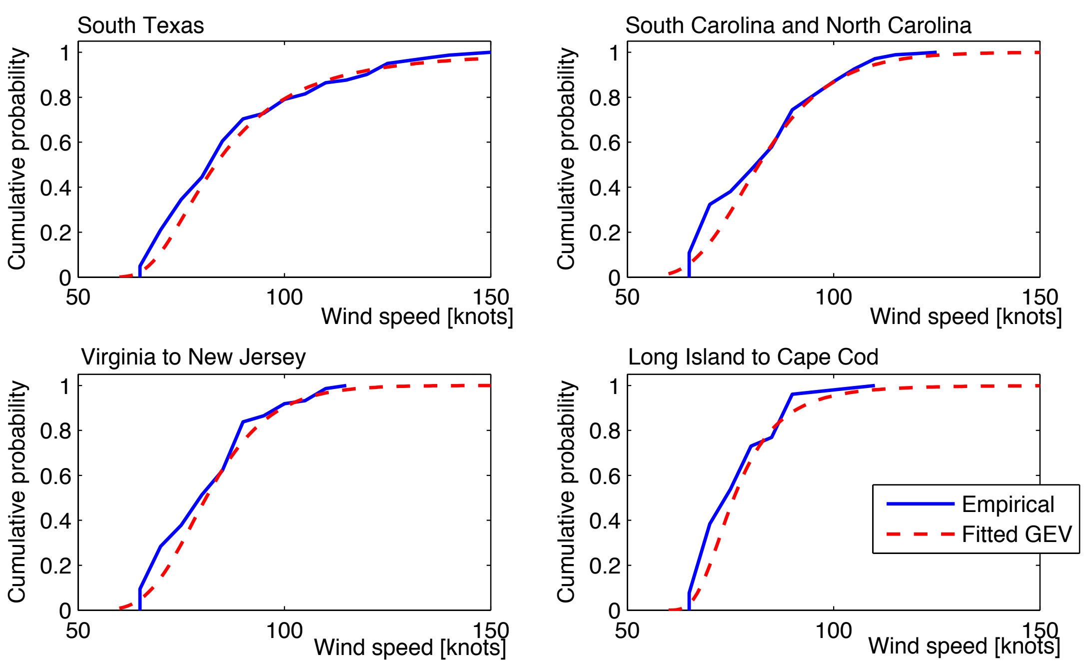

Figure A-6: Comparison of empirical CDFs for maximum hurricane wind speed in the regions we examine and the GEV distributions fitted to those data.

A.8 Wind Turbine Damage Function (D)

We fit a Log-Logistic distribution to the probability of a wind turbine tower buckling as a function of 10-minute sustained wind speed at hub height. The probability of the turbine tower buckling at a given wind speed is calculated by simulating tower bending moments of a 5-MW NREL turbine and comparing them to the stochastic resistance to buckling of the turbine tower. In our analysis, we model the 5-MW wind turbine design created by the U.S. National Renewable Energy Laboratory (NREL) for two load cases (active yawing and not yawing).

We calculate separate damage functions for the "active yawing" and "not yawing" load cases because those are the best- and worst-case wind load conditions for an idling wind turbine. The active-yawing case assumes the grid power is available to the turbine or the turbine has a backup power source for the yaw motors and control system; the not-yawing case assumes the turbine does not have a backup power source and grid power has been lost, a typical occurrence in hurricanes [8]. The current design standards for wind turbines given by the IEC [9] and Germanischer-Lloyd [10] require that an idling wind turbine be able to survive 10-minute sustained wind with 50-year recurrence period (load case 6.2). If backup power is not available for the yaw and control systems, the IEC standard requires the turbine must be able to survive a yaw misalignment of ±180º and the Germanischer-Lloyd standard specifies ±30º. The "active yawing" case we simulate assumes backup power for the yaw system, and the "not yawing" case assumes a yaw misalignment of 90º. The probability of buckling as a function of wind speed for the "active yawing" and "not yawing" cases are plotted in Figure A-7.

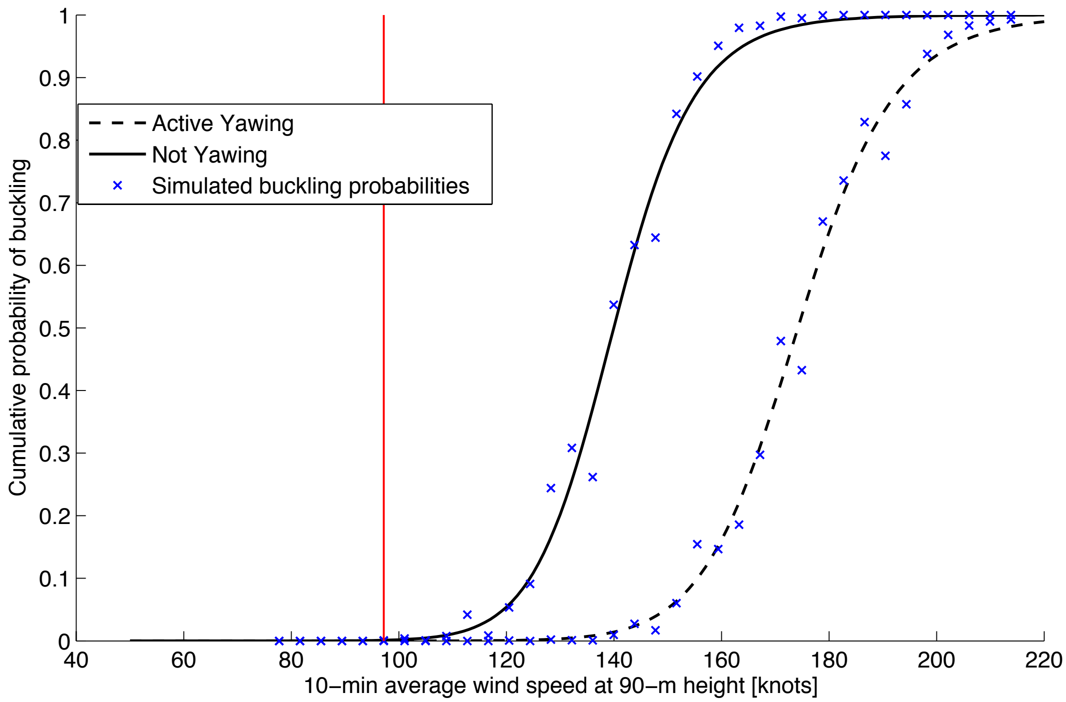

Figure A-7: Log-logistic functions fitted to probability of tower buckling as a function of wind speed. The vertical red line at 95 knots plots the 10-minute sustained wind speed with a 50-year return period used to design Class I wind turbines in the IEC 61400-3 standard.

A.8.1 Bending moment simulation

We calculate a range of maximum tower bending moments by simulating the mechanical loads on an NREL 5-MW turbine [11] for mean wind speeds from 40 to 110 m/s (78 – 214 knots) at hub height. We simulate 30 10-minute periods for each mean wind speed, with the turbulence intensity of each period drawn from a lognormal distribution with a mean of 9% and standard deviation of 1.5%. The turbine is shut down with blades feathered because the wind speed is higher than the operating limit.

The NREL 5-MW turbine we simulate is designed for offshore installation in an IEC Class 1B wind regime [12]. We simulate the configuration referred to by NREL as "onshore", which is identical to the "offshore" except that the "onshore" configuration assumes a rigid foundation and no ocean wave loads. The rigid foundation we use in our simulations is likely to give lower estimates of the maximum tower bending moment than a compliant "offshore" foundation design, according to simulations conducted by Bush et al. [13] Neglecting wave loads is also likely to give lower estimates of the maximum tower bending moment because wave loads contribute significantly to the tower bending moment, as shown by simulations conducted by Jha et al. [14] These two simplifications of the turbine model embodied in the "onshore" configuration likely underestimate tower bending moments and therefore underestimate the probabilities of tower buckling.

We use the TurbSim software, version 1.50 [15], to simulate a turbulent 3-dimensional wind field . We generate 30 10-minute wind speed time series for each mean wind speeds from 40 – 110 m/s (78 - 214 knots) in 2 m/s increments. The turbulence around each mean wind speed is generated from the Normal Turbulence Model (NTM) given in the IEC 61400-3 design standard [9]. For each simulation, we randomly draw a 10-minute turbulence intensity (TI) value from a lognormal distribution with a mean of 9% and a standard deviation of 1.5%. Turbulence intensity I is calculated as the quotient of the 10-minute mean wind speed u and the 10-minute standard deviation σ: $I = u_{10\ \mathrm{min}}/\sigma_{10\ \mathrm{min}}$. The lognormal distribution is fitted to TI values measured in hurricanes and tropical cyclones over water. The directly-measured TI values are given in Table A-1 and TI values calculated from directly-measured gust factors are given in Table A-2.

Table A-1: 10-minute turbulence intensities measured for hurricanes over water.

TI	Measured Height	Source
15%	10 m	[25] Table 6
11%	10 m	[16] Table 2
13%	19 m	[26] Fig. 1
17%	19 m	[26] Fig. 1

Table A-2: 10-minute turbulence intensities calculated from gust factors of hurricanes over water. Turbulence intensities are related to gust factor by the relation TI = (GF – 1)/α , where α = 2.44, an average of measured values from figure 7 in the paper by Yu et al. [16] Gust factors calculated from 60-minute periods are converted to 10-minute periods by dividing by 1.055, as recommended by Vickery et al. [17]

GF	Calculated TI (10-min)	Measurement height	Source	Notes
1.4	16%	10 m	[27] Table 2	
1.38	16%	10 m	[27] Table 2	
1.45	15%	10 m	[17] Table 4	60-min avg. period
1.32	10%	44 m	[17] Table 4	60-min avg. period
1.46	16%	10 m	[17] Table 4	60-min avg. period
1.36	12%	10 m	[17] Table 4	60-min avg. period
1.38	13%	10 m	[17] Table 4	60-min avg. period
1.48	17%	10 m	[17] Table 4	60-min avg. period

Turbulence intensity values are calculated from measured gust factor (GF) values according to the relationship TI = (GF – 1)/alpha, where α = 2.44 is averaged from several values given by Yu [16]. Gust factor values given by Vickery et al. use a 60-min averaging period; Vickery et al. recommend dividing the GF by 1.055 to calculate the 10-min value [17]. We scale the TI values to hub height h = 90 meters using the following relationship derived from equation 2.3.2-3 in the API RP-2A design standard:

$$\mathrm{TI}(h) = \mathrm{TI}(h_{ref}) \left(\frac{h}{h_{ref}} \right)^{-0.22} \tag{A 7}$$

Figure A-8 plots the TI values directly measured and derived from gust factor measurements in tropical cyclones, other TI values measured over water in extra-tropical storms, the tropical-cyclone TI values scaled to hub height, and the power-law from equation (A 7) used to scale them to hub height.

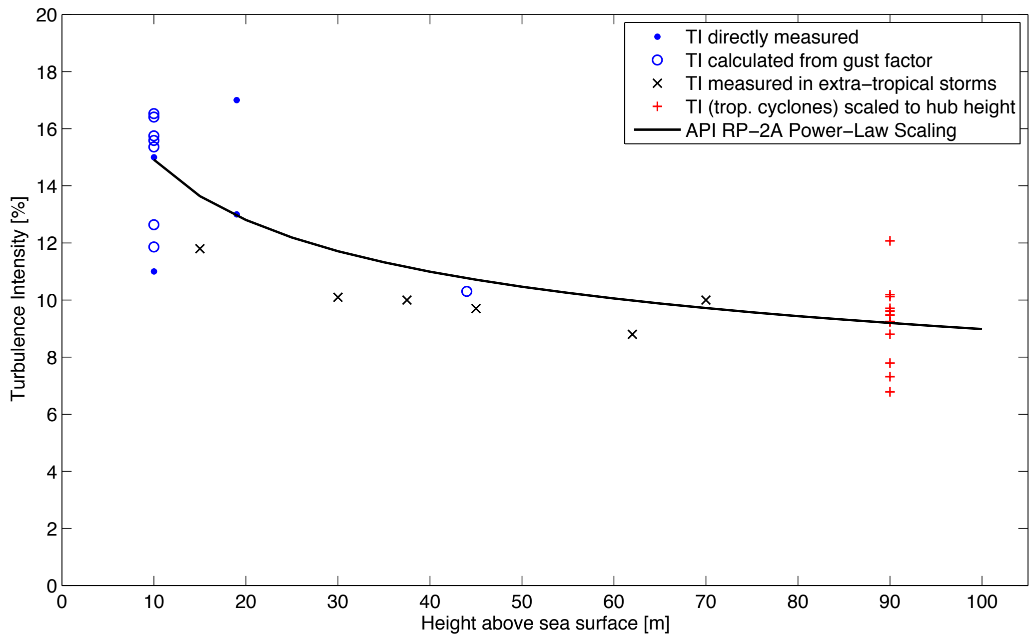

Figure A-8: Turbulence intensity (TI) in over-water tropical cyclones vs height. TI values from tropical cyclones are scaled to 90-meter height using a power-law relationship adapted from equation 2.3.2-3 in the API RP-2A-WSD standard. TI values measured in extra-tropical storms in the North Sea are also shown for comparison.

The bending moment on base of the turbine tower is dominated by three forces: aerodynamic force on the turbine blades, aerodynamic force on the nacelle, and aerodynamic force on the tower. We calculate the horizontal components (x and y) of the moments caused by those three forces for each 0.0125-second time step in a 10-minute simulation. We select the maximum vector sum of the moments after excluding the first 60-seconds of the simulation to remove transient oscillations caused by initial conditions of the simulation. The process is repeated for 30 simulations at each value of mean wind speed. Figure A-9 plots the magnitude of the average of maximum tower bending moments as a function of mean wind speed, with the contributions of wind loads on the blades, nacelle, and tower separated. Figure A-9A plots the moments for the "Active Yawing" load case, where the wind strikes the turbine head-on, and Figure A-9B plots the moments for the "Not Yawing" load case, where the wind strikes the turbine from the side.

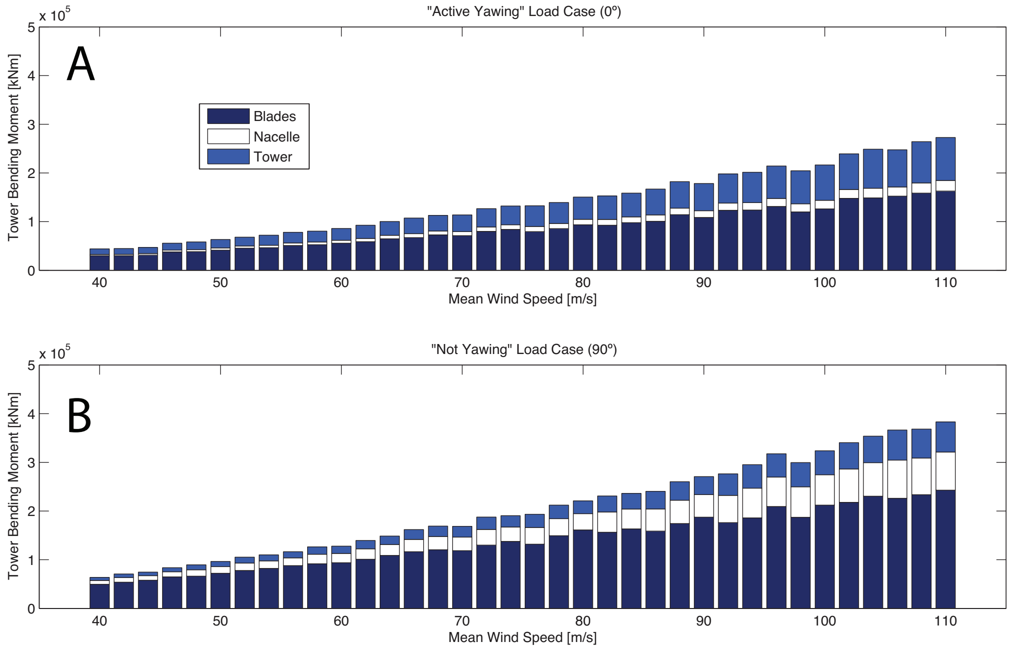

Figure A-9: Magnitude of bending moment on the tower base vs. 10-min mean wind speed. The "Blades" component of the moment is simulated using the NREL FAST software. The "Nacelle" component is calculated using [A8] the "Tower" component is calculated using [A10].

We simulate the moment caused by the aerodynamic force on the feathered blades using the NREL FAST software, version 7.00.01a-bjj [18]. The output signals for the x- and y-components of the bending moment at the tower base are labeled "TwrBsMxt" and "TwrBsMyt". The maximum moments in some simulations are anomalous, especially for the "Not Yawing" load case where the wind strikes the turbine from the side. We believe these outliers are the result of numerical convergence problems in the FAST software. We exclude the outliers by fitting a robust quadratic least-squares line with bi-square weights to the maximum moments as a function of mean wind speed and excluding maximum moments outside the ±50% range around the quadratic regression line, as shown in Figure A-10.

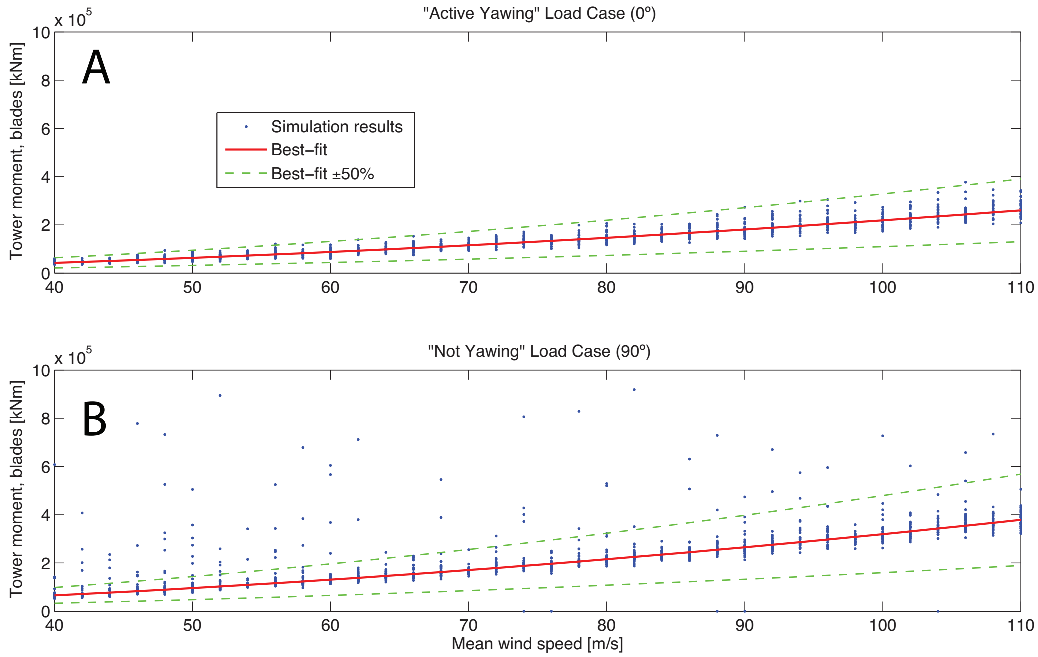

Figure A-10: The method for excluding anomalous simulation results for maximum tower bending moment. The red line is a robust linear best-fit to the data and the green dashed lines are 0.5 and 1.5 times the best-fit line. Data outside the green dashed lines are excluded.

FAST does not simulate wind loads on the nacelle or tower [19], [20], so we calculate the moment caused by the aerodynamic force on the nacelle using the following expression adapted from sections 5.2.1 and 5.3.1 of the DNV-RP-C205 design standard [21]:

$$\mathbf{M}_{nacelle} = \begin{cases} C_{front}(\frac{1}{2}\rho_a u_x^2)\, S_{front}\, h_{max}\, \hat{x} + C_{side}(\frac{1}{2}\rho_a u_y^2)\, S_{side}\, h_{max}\, \hat{y} & \text{Active yaw tracking} \\ C_{side}(\frac{1}{2}\rho_a u_x^2)\, S_{side}\, h_{max}\, \hat{x} + C_{front}(\frac{1}{2}\rho_a u_y^2)\, S_{front}\, h_{max}\, \hat{y} & \text{No yaw tracking} \end{cases} \quad \textbf{(A 8)}$$

where u_x and u_y are the horizontal components of wind speed parallel to and perpendicular to the long axis of the nacelle and $\hat{x}$ and $\hat{y}$ are the unit vectors in those directions. The surface area S and shape coefficient C of the nacelle are based on the nacelle dimensions of the comparable REpower 5M offshore turbine, which is 6 meters wide, 6 meters tall, and 18 meters long [22]. The shape factors are taken from Table 5-5 in the DNV-RP-C205 design standard [21]. The parameter values are given in Table A-3.

Table A-3: Parameters of wind load on the nacelle

Parameter	Value	Description
ρ_a	1.21 kg/m3	density of dry air at 20°C
h_{max}	90 m	tower height
c_{front}	0.7	shape coefficient, nacelle front
c_{side}	1.2	shape coefficient, nacelle side
s_{front}	36 m2	nacelle surface area, front
s_{side}	108 m2	nacelle surface area, side

The bending moment caused by wind load on the tower is more complicated because the wind acts across the whole length of the tower and because the diameter of the tower decreases with height. We model the diameter of the tower D as a function of height h as a linear function:

$$D(h) = D_{base} + \left(\frac{D_{top} - D_{base}}{h_{max}}\right)\ h \qquad \text{(A 9)}$$

where D_{base} is the tower diameter at its base, D_{top} is the diameter at the top, and h_{max} is the height of the top of the tower. The shape coefficient for the tower, a long cylinder, is C_{tower} = 0.5 from Figure 6-6 in the DNV-RP-C205 design standard [21]. Assuming a uniform wind speed across the whole length of the tower, the bending moment from the wind load on the tower is:

$$\begin{aligned} M_{tower} &= C_{tower}\ (\frac{1}{2}\rho_a u^2) \int_0^{h_{max}} \left(D_{bottom} + \frac{D_{top} - D_{bottom}}{h_{max}}\right)\ h\ dh \\ &= \frac{1}{6} C_{tower}\ (\frac{1}{2}\rho_a u^2)\ h_{max}^2\ (D_{bottom} + 2D_{top}) \end{aligned} \qquad \text{(A 10)}$$

The contribution of the wind load on the tower is significant, especially at higher wind speeds, as shown in Figure A-9.

A.8.2 Calculation of Buckling Probability

Given the magnitude *M* of the maximum tower bending moments calculated above, we calculate the probability of a turbine tower buckling by comparing the magnitude of the simulated bending moments to a random variable for the resistance of a tower to buckling. For each load case ("Active Yawing" or "Not Yawing") and mean wind speed *u*, we create 5,000 bending moment values by repeatedly sampling the simulation results with equal probability. If no anomalous values were excluded, there are 30 simulation values to sample from; there are fewer if some were excluded.

We calculate 5000 resistance to buckling values M_{cr} according to equation (A 11), the resistance to buckling of a thin-walled cylinder, by randomly sampling the parameters from the distributions given in Table A-4 [23]:

$$M_{cr} = \tfrac{1}{6}\left(1 - 0.84\frac{D}{t}\frac{X_{y,ss}F_y}{X_{E,ss}E}\right)\left(D^3 - (D-2t)^3\right)X_{y,ss}X_{cr}F_y \qquad \textbf{(A 11)}$$

Table A-4: Parameters of resistance to buckling at the base of a NREL 5-MW turbine tower. LN = log-normal distribution, COV = coefficient of variance. Adapted from Søresnen et al. [23]

Variable	Description	Distribution type	Expected value	COV
D_{base}	tower diameter (base)	-	6 m	-
D_{top}	tower diameter (top)	-	3.87 m	-
t	tower thickness (base)	-	0.027 m	-
E	Young's modulus	-	210 GPa	-
F_y	yield stress	LN	1	0.05
$X_{y,ss}$	model uncertainties due to scale effects: yield stress	LN	1	0.05
$X_{E,ss}$	model uncertainties due to scale effects: Young's modulus	LN	1	0.02
X_{cr}	critical load capacity	LN	1	0.10

The damage function D at a given 10-minute mean wind speed for a given load case ("Active Yawing" or "Not Yawing") is calculated by comparing all the sampled bending moment values to the sampled resistance-to-buckling values to find the probability of buckling for each 10-minute mean wind speed u:

$$D(u) = \Pr\left(M_{cr} \leq M(u)\right) \qquad \textbf{(A 12)}$$

We generalize the results calculated in equation (A 12) by fitting a log-logistic function to the data. The form of the log-logistic function is given by equation (4.3) in the body of the paper.

The distribution of number of turbine towers buckled in a hurricane is modeled in (4.4) by a beta-binomial distribution. The beta-binomial distribution gives a binomial distribution for the number of turbine towers buckled in a single hurricane, where all turbines have the same probability of buckling. The assumption that all turbines have the same buckling probability implies a strong correlation between the buckling of the towers in the wind farm. Our results are not sensitive to this assumption of strong correlation. Figure A-11 compares the distribution of the number of turbine towers buckled in a single hurricane for two different models of correlation between tower buckling. The model labeled “Identical turbines” in Figure A-11 is the model we use in our paper, where the number of towers buckled is binomial distributed and all turbines have the same probability of buckling. We compare that model to a model that implies a weaker correlation between turbines, labeled “Distribution of turbine properties”. In that distribution, each turbine is exposed to different wind conditions with turbulence intensities drawn from a lognormal distribution and each tower has a different resistance to buckling calculated with (A 11). The results in Figure A-11 are calculated for a mean wind speed of 70 m/s (136 knots) but results for other mean wind speeds show similarly-good matches between the distributions.

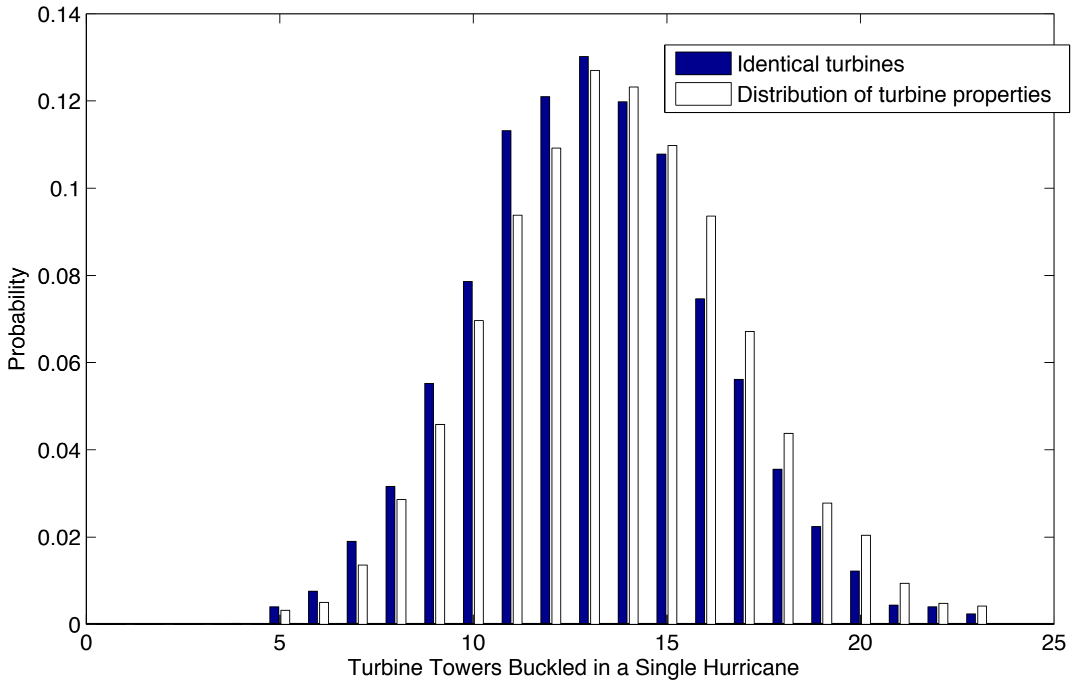

Figure A-11: Distribution of number of turbine towers buckled in a single hurricane a mean wind speed of 70 m/s (136 knots). Blue bars plot results for the case used in our paper, where buckling probabilities are identical for all turbines. White bars plot results for the case where the resistance to buckling of each tower is drawn randomly from the distribution given in (A 11).

A.9 Nomenclature

T = time period to investigate

n = number of turbines in the wind farm

u = 10-min average hub height wind speed

λ = rate parameter for occurrence of hurricanes

μ = location parameter for distribution of wind speed in a hurricane

σ = scale parameter for distribution of wind speed in a hurricane

ξ = shape parameter for distribution of wind speed in a hurricane

α = scale parameter for the log-logistic distribution of the probability of a turbine tower buckling at a 10-min average wind speed u

β = shape parameter for the log-logistic distribution of the probability of a turbine tower buckling at a 10-min average wind speed u

α_B, β_B = parameters of the beta-binomial distribution for the distribution of turbine towers buckled in a single hurricane (parameters are derived by fitting a beta distribution to the damage function weighted by the probability of occurrence of wind speed)

W = random variable for the maximum sustained (10-min) wind speed of a hurricane

w = a wind speed drawn from W

D = random variable for the probability of turbine damage for a given wind speed w

X = random variable for the number of turbines damaged in one hurricane

x = a number of damaged turbines drawn from X

H = random variable for the number of hurricanes in Y-years

h = a number of hurricanes drawn from H

Y_{rep} = random variable for the number of turbines damaged in T-years with replacement

$Y_{no\ rep}$ = random variable for the number of turbines damaged in T-years, no replacement

y = a number of turbines damaged drawn from Y

a = constant for alternative description of the Poisson distribution used in Panjer recursion from [24]

b = constant for alternative description of the Poisson distribution used in Panjer recursion from [24]

$\boldsymbol{\tau}$ = the time to destroy all turbines (or reach an absorbing state) if turbines are not replaced

z = number of Monte Carlo simulations

$\mathbf{T}$ = transition matrix for phase-type distributions (state transition intensities). The values T_{ij} are the probabilities of transition from state i to state j. There are n + 1 states, where the n + 1 state is the absorbing state

t = vector of intensities of state transitions directly to the absorbing state

π = starting probabilities for each state

k = number of turbines in absorbing state

m = an index for summation

C = shape coefficient

ρ_a = density of dry air at 20°C

u = wind speed

S = surface area

A.10 References

[1] H. Panjer, "Recursive evaluation of a family of compound distributions," *ASTIN Bulletin*, vol. 12, no. 1, pp. 22–26, 1981.

[2] D. C. M. Dickson, "A Review of Panjer's Recursion Formula and Its Applications," *British Actuarial Journal*, vol. 1, no. 1, pp. 107–124, 1995.

[3] T. Mikosch, *Non-Life Insurance Mathematics: An Introduction with the Poisson Process*, 2nd ed. Berlin: Springer-Verlag, 2009.

[4] J. Franklin, M. Black, and K. Valde, "GPS Dropwindsonde Wind Profiles in Hurricanes and Their Operational Implications," *Weather and Forecasting*, vol. 18, no. 1, pp. 32–44, 2003.

[5] National Hurricane Center, "County by county hurricane strikes 1900–2009," National Hurricane Center, Coral Gables, FL, 2010.

[6] C. Landsea, R. Pielke, A. Mestas-Nunez, and J. Knaff, "Atlantic basin hurricanes: Indices of climatic changes," *Climatic Change*, vol. 42, no. 1, pp. 89–129, 1999.

[7] S. Goldenberg, C. Landsea, A. Mestas-Nunez, and W. GRAY, "The recent increase in Atlantic hurricane activity: Causes and implications," *Science*, vol. 293, no. 5529, pp. 474–479, 2001.

[8] Y. Liu and C. Singh, "A Methodology for Evaluation of Hurricane Impact on Composite Power System Reliability," *IEEE Transactions on Power Systems*, vol. 26, no. 1, pp. 145–152, 2007.

[9] IEC, "Wind turbines - Part 3: Design requirements for offshore wind turbines," 61400-3, Feb. 2009.

[10] GL, "Guideline for the Certification of Offshore Wind Turbines Edition 2005," Jun. 2005.

[11] J. Jonkman, S. Butterfield, W. Musial, and G. Scott, "Definition of a 5-MW reference wind turbine for offshore system development," National Renewable Energy Laboratory, Golden, CO, NREL/TP-500-38060, Feb. 2009.

[12] J. M. Jonkman and M. L. Buhl, "Loads Analysis of a Floating Offshore Wind Turbine Using Fully Coupled Simulation: Preprint," presented at the WINDPOWER 2007, Los Angeles, 2007.

[13] E. Bush and L. Manuel, "Foundation Models for Offshore Wind Turbines," presented at

the 47th Aerospace Sciences Meeting, Orlando, 2009, pp. 1–7.
[14] A. Jha, D. Dolar, W. Musial, and C. Smith, “On Hurricane Risk to Offshore Wind Turbines in US Waters,” presented at the Offshore Technology Conference, Houston, 2010, pp. 1–14.
[15] B. J. Jonkman, “TurbSim User's Guide: Version 1.50,” NREL/TP-500-46198, Sep. 2009.
[16] B. Yu and A. Gan Chowdhury, “Gust Factors and Turbulence Intensities for the Tropical Cyclone Environment,” *Journal of Applied Meteorology and Climatology*, vol. 48, no. 3, pp. 534–552, Mar. 2009.
[17] P. J. Vickery and P. F. Skerlj, “Hurricane gust factors revisited,” *Journal of Structural Engineering*, vol. 131, no. 5, pp. 825–832, 2005.
[18] J. M. Jonkman and M. L. J. Buhl, “FAST User's Guide,” National Renewable Energy Laboratory, Golden, CO, Aug. 2005.
[19] J. Jonkman, “Normal aerodynamic forces on the tower,” *wind.nrel.gov/forum/wind/*, 05-Jul-2011. [Online]. Available: https://wind.nrel.gov/forum/wind/viewtopic.php?f=16&t=493. [Accessed: 04-Nov-2011].
[20] MMI, “Comparative Study of OWTG Standards,” MMI Engineering, Oakland, California, MMW528, Mar. 2009.
[21] DNV, “Recommended Practice DNV-RP-C205,” DNV-RP-C205, Oct. 2010.
[22] E. de Vries, “REpower Systems: Less is More Offshore,” *RenewableEnergyWorld.com*, 28-Apr-2009. [Online]. Available: http://www.renewableenergyworld.com/rea/news/article/2009/04/repower-systems-less-is-more-offshore. [Accessed: 25-Oct-2011].
[23] J. D. Sørensen and N. J. Tarp-Johansen, “Reliability-based optimization and optimal reliability level of offshore wind turbines,” *International Journal of Offshore and Polar Engineering*, vol. 15, no. 2, pp. 141–146, 2005.
[24] B. Sundt and W. S. Jewell, “Further Results on Recursive Evaluation of Compound Distributions,” *ASTIN Bulletin*, vol. 12, no. 1, pp. 27–39, 1981.
[25] B. M. Paulsen and J. L. Schroeder, “An examination of Tropical and Extratropical Gust Factors and the associated wind speed histograms,” *Journal of Applied Meteorology*, vol. 44, pp. 270–280, Feb. 2005.
[26] J. L. Schroeder, D. A. Smith, and R. E. Peterson, “Variation of Turbulence Intensities and Integral Scales During the Passage of a Hurricane,” *Journal of Wind Engineering and Industrial Aerodynamics*, vol. 77, pp. 65–72, 1998.
[27] B. Wang, F. Hu, and X. Cheng, “Wind gust and turbulence statistics of typhoons in South China,” *Acta Meteorologica Sinica*, vol. 25, no. 1, pp. 113–127, Feb. 2011.

Chapter 5: QUANTIFYING THE HURRICANE CATASTROPHE RISK TO OFFSHORE WIND POWER

Abstract

The U.S. Department of Energy has estimated that over 50 GW of offshore wind power will be required for the United States to generate 20% of its electricity from wind. Developers are actively planning offshore wind farms along the U.S. Atlantic and Gulf coasts and several leases have been signed for offshore sites. These planned projects are in areas that are sometimes struck by hurricanes. We present a method to estimate the catastrophe risk to offshore wind power using simulated hurricanes. Using this method, we estimate the fraction of offshore wind power simultaneously offline and the cumulative damage in a region. In Texas, the most vulnerable region we studied, 11% of offshore wind power could be offline simultaneously due to hurricane damage with a 100-year return period and 5% could be destroyed in any 10-year period. We also estimate the risks to single wind farms in four representative locations; we find the risks are significant but lower than those estimated in previously published results. Much of the hurricane risk to offshore wind turbines can be mitigated by designing turbines for higher maximum wind speeds, ensuring that turbine nacelles can turn quickly to track the wind direction even when grid power is lost, and building in areas with lower risk.

This paper, written with Mitch Small, Paulina Jaramillo, and Jay Apt, was submitted to *Risk Analysis* in December 2012.

5.1 Background

As a result of state renewable portfolio standards and federal tax incentives, there is growing interest and investment in renewable sources of electricity in the United States. Wind is the renewable resource with the largest installed-capacity growth in the last 5 years, with U.S. wind power capacity increasing from 8.7 GW in 2005 to 47 GW in 2011 [1]. All of this development has occurred onshore. U.S. offshore wind resources may also prove to be a significant contribution to increasing the supply of renewable, low-carbon electricity. The National Renewable Energy Laboratory (NREL) estimates that offshore wind resources can be as high as four times the 2010 U.S. electricity generating capacity [2]. Although this estimate does not take into account siting, stakeholder, and regulatory constraints, it indicates that U.S. offshore wind resources are significant. No offshore wind projects have been developed in the United States, but there are 10 offshore wind projects in the planning process (with an estimated capacity of 3.8 GW) [1] and more proposed [3]. The U.S. Department of Energy's 2008 report, *20% Wind by 2030* envisions 54 GW of shallow offshore wind capacity to optimize delivered generation and transmission costs [4].

The U.S. has good wind resources along the Atlantic, Pacific, and Great Lake coasts. Many areas along the Atlantic Coast and Gulf Coast are particularly attractive because they have high average wind speeds, are in relatively shallow water, and are close to major population centers. Unconstrained resources at depths shallower than 30 m in the Atlantic coast, from Georgia to Maine, are estimated to be 345 GW; the estimate for these resources in the Gulf of Mexico (Texas and Louisiana) is 198 GW [2]. For comparison, the 2010 net summer generation capacity for the entire U.S. was 1,039 GW [5].

Offshore wind turbines in these areas will be at risk from Atlantic hurricanes. Between 1949 and 2006, 93 hurricanes struck the U.S. mainland according to the HURDAT (Hurricane Database) database of the National Hurricane Center [6]. Only 15 years in this 58-year period did not incur insured hurricane-related losses [7]. Wind turbines are vulnerable to hurricanes because the maximum wind speeds in those storms can exceed the design limits of wind turbines. In 2003, a wind farm of seven utility-scale turbines in Okinawa, Japan, was destroyed by typhoon Maemi, which had an estimated maximum sustained wind speed of 60 m/s [8] (equivalent to a Category 4 hurricane), and several turbines in China were damaged by typhoon Dujuan [9].

It is rare but not unprecedented for a single natural disaster to damage multiple conventional power plants. Hurricane Katrina flooded critical pumps and controllers at one power plant, and damaged cooling tower shrouds and fans at several others [10]. Hurricane Sandy in 2012 may have damaged several gas turbine power plants in New Jersey [11]. The Tohoku earthquake and tsunami in March 2011 caused significant damage to the Fukushima Daiichi and Daini power stations; four reactors at Fukushima Daiichi, totaling 2,719 MW of capacity, were permanently shut down [12]. The earthquake and tsunami also damaged several large coal power plants: 6,050 MW of capacity were offline after the earthquake, 4,250 MW were still offline in July 2011, and 2,000 MW (the Haramachi Power Station) were expected to be offline until the summer of 2013 [13], [14]. Interestingly, the Kamisu semi-offshore wind farm was struck by a 5-meter tsunami during the Tohoku earthquake but resumed operation three days later when the local electrical grid was re-established [15].

Hurricane effects on offshore wind power may be more similar to damage to the electrical transmission system than damage to conventional power plants. Like the components of the transmission system, offshore wind turbines are geographically dispersed and operate independently. Severe weather events, such as hurricanes [10] and ice storms [16], sometimes damage individual transmission components, which in turn can cause blackouts. However, repairing damage to offshore wind turbines will likely take much longer and require more specialized equipment than repairing damages to the transmission system. Many transmission system components are commodities and are often stockpiled before hurricane seasons, but most wind turbine components are built-to-order and offshore wind turbine repairs require specialized ships and cranes.

Previous work by Rose et al. estimated the hurricane risk to a single wind farm over its lifetime using compound probability distributions fitted to one hundred years of historical hurricane records [17]. That study likely over-estimates the risk to a wind farm because it assumes that any hurricane making landfall in a county affects the entire coastline of that county with its maximum winds, but the area of maximum winds is typically smaller than a coastal county in the U.S [18]. Furthermore, that method did not consider hurricane tracks, so it could not assess the correlated risk to nearby wind farms. The new work we present here calculates the correlated risk to all wind farms in a region by analyzing thousands of simulated hurricanes and accounting for the wind field of each hurricane.

The research presented in this paper follows a catastrophe modeling approach [19]. We construct a hazard model that describes the frequency of occurrence, intensity, and location of hurricanes that make landfall in the continental U.S. We also create an inventory of wind turbines at risk by placing simulated turbines in offshore locations likely to be developed. Finally, we model the vulnerability of the wind turbines to hurricane winds.

5.2 Method

We calculate the distribution of wind power offline due to hurricane damage by simulating fifty 5,000-year periods of hurricane activity along the U.S. coast (a total of $2.5x10^5$ years). Each hurricane is generated by a statistical-deterministic model developed by Emanuel et al. [20] We calculate the wind field of each hurricane to determine the wind speed at each turbine location, and use a probabilistic damage function to determine whether each turbine buckles. The method is summarized in the flow chart shown in Figure 5.1.

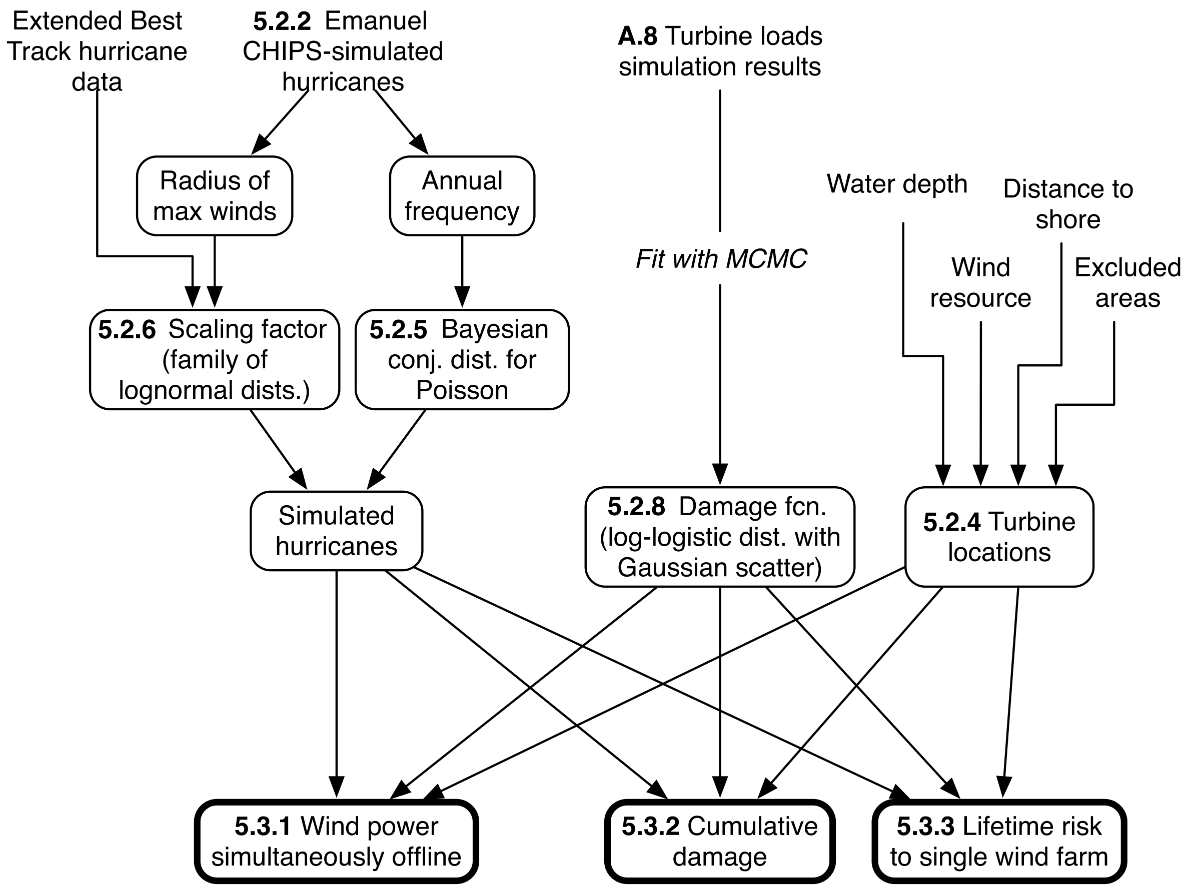

Figure 5.1: Flow chart for calculating the hurricane risk to offshore wind farms using simulated hurricanes.

This method differs from the one developed by Rose et al. [17] because that previous method calculated hurricane rates of occurrence and intensities by fitting probability distributions to historical hurricanes and did not model the wind field. After towers buckle, we assume it takes several years to rebuild them in case several hurricanes strike the same area in a short period (for example, seven hurricanes made landfall in Florida in 2004-5, with two each year striking the same area). Using simulated hurricanes allows us to base our risk calculations on much longer periods of hurricane activity than are available in historical records, which reduces the uncertainty of our estimates. However, we explicitly model uncertainties in hurricane size and rate of occurrence, and the turbine damage function.

5.2.1 Assumptions

The risk model we develop in this chapter is based on several assumptions. The broadest assumption is that future hurricane activity will be similar to the hurricanes simulated based on climatological conditions from 1979 – 2011; we discuss the details of this assumption below. That limited period may not capture trends or long-term cycles in hurricane activity, and will not predict the effects of future climate change.

1. **Rate of Hurricane Occurrence:** We assume the annual rate of hurricanes making landfall in the continental U.S. follows a 33-year cycle and the rate in each year of the cycle is similar to the rate in of landfall of hurricanes simulated with the corresponding year's climatological conditions. The rate of occurrence of the simulated hurricanes is sensitive to the rate at which proto-hurricanes form in the Atlantic Basin, a parameter that Emanuel et al. estimate from tropical cyclones from 1981 – 2000 [21]. The rate of occurrence is also sensitive to "steering effects" that may cause hurricanes to strike the U.S. more or less frequently than their absolute numbers would indicate; assumptions governing the hurricane tracks are discussed below. Finally, this assumption will also not capture longer-term trends or cycles in hurricane activity, though the evidence for either of those in historical hurricane records is ambiguous.
2. **Hurricane Intensity:** We assume the intensities (maximum 1-min average wind speed) of hurricanes will be similar to the intensities of the simulated hurricanes. This is a good assumption as long as future sea surface temperatures (SST), which are the main driver of hurricane intensity, are similar to the SSTs in 1979 – 2011 period that we used for our simulations. The 1979 – 2011 climatological data we used for our simulations encompasses at least one El Niño/La Niña cycle but it may not capture longer climatological cycles.

3. **Hurricane size:** We assume that the distribution of the radius of maximum winds (RMW) of hurricanes will be similar to the distribution of RMW of hurricanes measured from 1988 – 2011. It is difficult to determine whether the distribution of hurricane RMW from that period is typical because records of RMW before that period are spotty and are usually not measured directly. We believe that the RMWs of the simulated hurricanes, which are calculated from the simulated intensity [22], are as consistent because they are based on a physics model. However, the RMWs calculated with that model are consistently smaller than historical hurricanes and therefore not reliable without correction.
4. **Hurricane Tracks:** We assume that future hurricane tracks will be similar to tracks of the simulated hurricanes in a statistical sense. The tracks are generated by a stochastic method that depends on the tracks of historical tropical cyclones after 1970 [20], which we estimate is approximately 400 named storms for the Atlantic Basin from 1970 - 2005. This means that the simulated hurricane tracks are unlikely to model phenomena that occurred infrequently or not at all during that period, such as changes in the Gulf Stream or higher-altitude winds that influence hurricane track.
5. **Damage function:** We assume that the simulated wind loads on the turbine and the resulting stresses are representative of a real turbine designed for IEC Class 1B conditions. This is a reasonable assumption, though we believe we under-estimate the buckling probability because we do not model foundation compliance or wave slam loads (both discussed in Section A.8.1). The software used to simulate the turbine stresses is continuously improved and updated by NREL and used by many academic researchers and some turbine manufacturers. The software used to simulate the turbulent wind field is widely used for simulating typical turbulence, but we were not able to assess whether turbulence in a tropical cyclone has "typical" properties.

5.2.2 Simulated Hurricanes

The historical record of hurricanes in the U.S. is insufficient to confidently estimate the risk of intense hurricanes. For this reason, we estimate the risk using hurricanes simulated with the method of Emanuel et al. that generates hurricanes with statistical properties that agree with the historical record [20]. Emanuel's method simulates hurricanes by first randomly seeding weak vortices randomly in space and time [21]. Those vortices follow a track stochastically determined by ambient winds, and their intensity evolves along that track as a deterministic function of wind and ocean conditions known as the Coupled Hurricane Intensity Prediction System (CHIPS); some vortices grow into hurricanes but most dissipate [23].

We generate 300 tropical cyclones that make landfall in the continental U.S. based on climatological conditions for each year from 1979-2011, for a total of 9,900 storms. This range of years covers periods of low hurricane activity in the continental U.S. (e.g. 1981-2, 2000-1) and periods of high activity (e.g. 1985, 2004-2005) [6] as well as several El Niño/La Niña cycles. The 3,285 storms that reach hurricane intensity within 200 km of the continental U.S. are the pool of hurricanes we draw randomly from when we create long time series of hurricane activity. For each hurricane, we calculate the maximum 1-minute sustained wind speed at each offshore wind turbine location using the wind profile proposed by Holland et al. [24] The wind profile depends on the radius of maximum wind r_{max}. We scale the CHIPS-calculated r_{max} value for each hurricane by a lognormal-distributed random variable (described in Section 5.2.6 below) to make the distribution of radii similar to the distribution of radii of historical hurricanes. The maximum sustained wind speed we calculate for each hurricane is the sum of the circular wind speed, a fraction of the of the wind speed at 850 hPa height, and a latitude-dependent fraction of the hurricane's translation speed [25].

5.2.3 Historical Hurricanes

We use the historical data for north Atlantic hurricanes to check the results calculated with the simulated hurricanes above. The historical record we use consists of the Extended Best Track data set for 1988-2011[26] combined with the HURDAT data set for 1900-1987[6]. The Extended Best Track data includes estimates of the radius of maximum wind r_{max} for each hurricane but HURDAT does not, so we estimate missing r_{max} values from minimum central pressure, if available, using the following formula given by Powell et al. [27] in (5.1):

$$r_{max} = \frac{1}{1.852} \exp(2.0633 + 0.0182\Delta_p - 0.00019008\Delta_p^2 + 0.0007336\phi^2 + \epsilon) \qquad (5.1)$$

where the factor of 1/1.852 converts from nautical miles to km, Δ_p is the difference between ambient pressure (1,013 hPa) and minimum central pressure, ϕ is latitude, and ε is a normally-distributed error term with mean of 0 and standard deviation of 0.3. When pressure is not available, we assume a radius of maximum wind of 33 km, the historical median for landfalling hurricanes in the continental US given by Ho et al. [28]

5.2.4 Wind Farm Placement

We place offshore wind turbines in all feasible locations along the U.S. East Coast and Gulf Coast (Figure 5.2). We define "feasible locations" as locations with suitable wind resource between 8 and 93 km (5 – 50 nautical miles) from shore with water shallower than 30 m, similar to the definition used in the Eastern Wind Integration and Transmission Study (EWITS) [29]. We follow the definition of "suitable wind resource" used in EWITS: average annual wind speed at 80 m sufficient for a typical IEC Class II turbine to have a capacity factor of at least 32% (approximately 7.4 m/s at 90-m height). The wind resource data are taken from maps created by the National Renewable Energy Laboratory (NREL), scaled from 90 m to 80 m height with a power law exponent of 1/7. We exclude marine sanctuaries, military practice areas, Navy aviation warning areas, shipping lanes, active oil and gas leases, and bays and inland waterways. References for the wind resource and exclusion area databases are given in Appendix B. The turbines are placed with a density of 5 MW/km2, equivalent to a spacing of approximately 8 rotor diameters between turbines for the NREL 5MW reference turbine; for comparison, turbines at the Horns Rev I wind farm west of Denmark are spaced 7 rotor diameters apart [30].

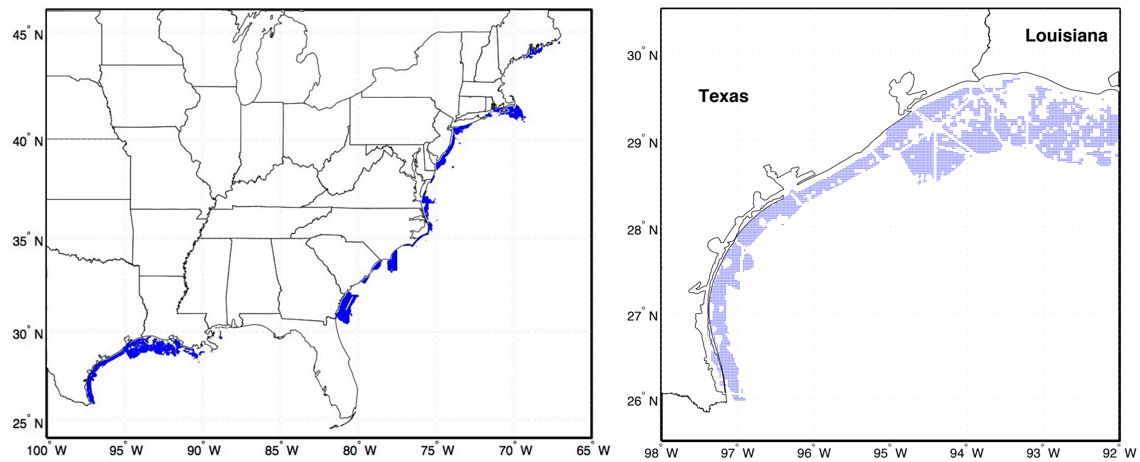

Figure 5.2: Wind turbine locations for the "Full Development" scenario. Mississippi, Alabama, and Florida are excluded because wind resource estimates are not available for those states. Detail of the wind turbine location map for Texas and western Louisiana, showing excluded areas such as shipping lanes and oil and gas leases.

The turbines are grouped into four regions in order to aggregate damages from individual hurricanes: Texas, the Southeast (Georgia, South Carolina, and North Carolina), the Mid-Atlantic (Virginia, Maryland, Delaware, New Jersey, and New York), and New England (Rhode Island, Massachusetts, New Hampshire, and Maine).

5.2.5 Rate of Hurricane Occurrence

The number of U.S.-landfalling hurricanes in our 5000-year simulations is drawn from a cyclic nonhomogeneous Poisson process. Emanuel's method [20], which generates the pool of simulated hurricanes (described above) also generates a Poisson rate parameter Λ_m for each of the 33 years of climatological conditions: m = [1979, 1980, … , 2011]. We cyclically repeat those 33 rate parameters so that there is a rate parameter corresponding to each of the 5000 years in the periods of hurricane activity we simulate: [Λ_{1979}, Λ_{1980}, … , Λ_{2011}, Λ_{1979}, Λ_{1980} , …]. To determine the number of hurricanes that make landfall in each year of the simulation, we draw from a Poisson distribution with the corresponding rate parameter.

The value of the rate parameter Λ_m is uncertain because it is calculated from a finite number of storms. We model this uncertainty as a Bayesian posterior distribution with an informationless prior. The posterior for the Poisson distribution is a gamma distribution with shape hyperparameter t_m and rate hyperparameter k_m: $\Lambda_m \sim \text{Gamma}(t_m, k_m)$. The hyperparameter k_m is the number of U.S.-landfalling hurricanes in the climatological conditions of year m. The hyperparameter t_m is number of years for k_m lanfalling hurricanes to occur; we calculate this as the number of storms seeded in the climatological conditions of year m divided by a universal constant that relates the storm seeding rates with global historical genesis rates [21]. To simulate the number of hurricanes in a year of a 5000-year simulation, we first draw a realization λ from the corresponding gamma-distributed random variable Λ_m, and then we draw the number of hurricanes from a Poisson distribution with the rate parameter λ.

5.2.6 Hurricane Size

The radius of maximum wind $r_{\max}$ of each simulated hurricane is calculated deterministically by the CHIPS model [31] from climatological conditions . However, we find those $r_{\max}$ values tend to be smaller and more narrowly distributed (Figure 5.3B) than the $r_{\max}$ values of comparable hurricanes in the historical record (Figure 5.3A). Therefore we scale the $r_{\max}$ values of the simulated hurricanes by a lognormal-distributed random variable S so that the distribution of their scaled $r_{\max}$ values (Figure 5.3C) better matches the distribution for historical hurricanes.

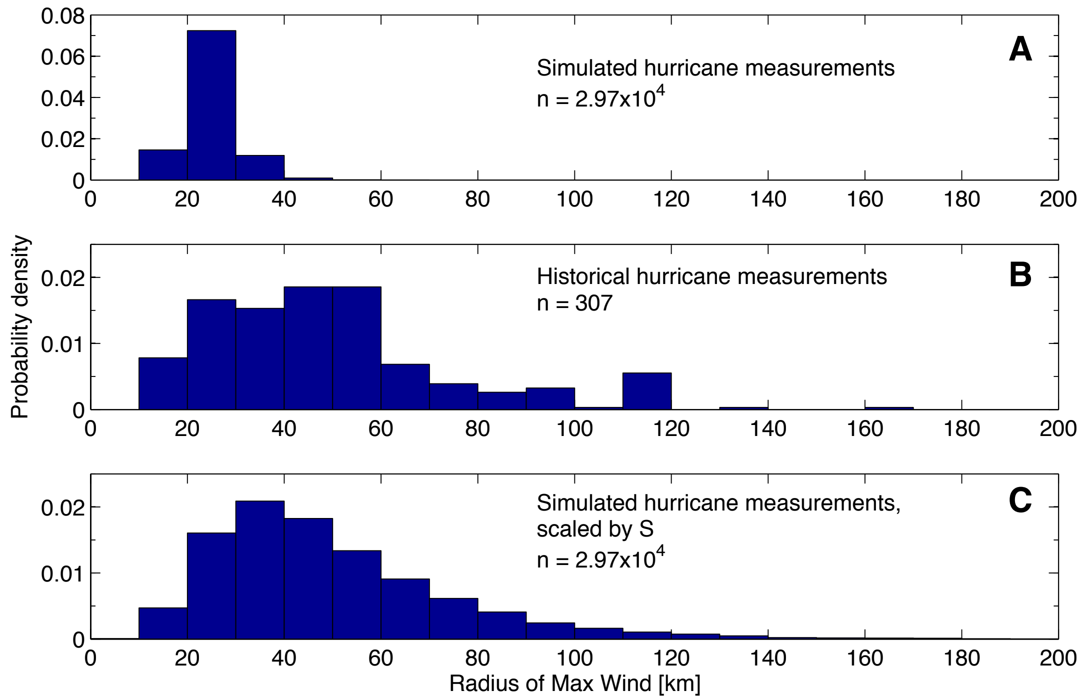

Figure 5.3: Histogram of radius of maximum winds for hurricanes within 200 km of the continental U.S. coast. The distribution of r_{max} in (C), has been scaled by a lognormal distribution described in Section 5.2.6 to match the distribution of r_{max} for historical hurricanes in (B) better than the r_{max} calculated by Emanuel's CHIPS model shown in (A).

We calculate the lognormally-distributed scaling factor $S = H/M$, where H is a lognormal distribution fit to r_{max} of historical hurricanes from the Extended Best Track data set for 1988-2010 [26] and M is a lognormal distribution fit to r_{max} of the simulated hurricanes described above. The distributions for both H and M are fitted to only hurricanes within 200 km of the continental U.S. coast.

The distributions H and M are uncertain because they are fitted to a finite number of hurricane size measurements. We model these uncertainties as Bayesian posterior distributions with informationless priors [32]. The posterior for the joint distribution of normal distribution parameters μ and θ (where the precision $\theta = 1/\sigma^2$) is a normal-gamma distribution with three hyperparameters calculated from sufficient statistics: α is the number of observations of r_{max}, β is the sum of the observed r_{max} values, and γ is the sum of the square of the observed r_{max} values. The marginal distribution for θ is shown in (5.2) and conditional distribution for μ given θ is shown in (5.3).

$$\theta \sim \text{Gamma}\left(\frac{\alpha\gamma - \beta^2}{2\alpha}, \frac{\alpha+1}{2}\right) \tag{5.2}$$

$$\mu|\theta \sim \text{Normal}\left(\frac{\beta}{\alpha}, \frac{1}{\alpha\theta}\right) \tag{5.3}$$

We use the posterior for a normal distribution because lognormal distributions use the same parameters as the corresponding normal distribution. The hyperparameter values for r_{max} measurements 2 hours apart for historical hurricanes within 200 km of the continental U.S. coast are: $\alpha_H = 479$, $\beta_H = 1.83\text{x}10^3$, $\gamma_H = 7.17\text{x}10^3$ and the hyperparameters for r_{max} measurements 2 hours apart for simulated hurricanes within 200 km of the continental U.S. coast are: $\alpha_M = 40337$, $\beta_M = 1.30\text{x}10^5$, $\gamma_M = 4.19\text{x}10^5$.

We limit the scaled radius of maximum winds to the range 18.5 - 98.9 km based on the observed 5th and 95th percentile values in the Extended Best Track data set for 1988-2010 within 200 km of the U.S. coast (409 observations for 41 hurricanes) [26]. These limits are comparable to the r_{max} values that meet quality control standards in the analysis by Willoughby et al. [33] and the limits on Powell's expression for r_{max} as a function of central pressure and latitude [27].

5.2.7 Model Validation for Hurricane Occurrence and Wind Speeds

In order to validate the simulated hurricane activity we use in this paper, we calculate the return period of tropical storms, hurricanes, and intense hurricanes at 45 locations along the Gulf and Atlantic coasts to compare to return periods calculated from historical hurricanes for the same locations by Keim et al. [34] and we calculate return periods for a range of wind speeds for New Orleans and Miami to compare to results presented by Emanuel and Jagger [35]. The results, which are presented in Appendix B, show that the model we develop here predicts return periods for intense hurricanes (≥ Category 3) similar to return periods calculated from the historical record.

5.2.8 Wind Turbine Damage Function

We calculate the probability of a single turbine tower buckling as a function of the maximum 10-minute sustained wind speed it experiences at hub height. This damage function is similar to that used by Rose et al. [17] but we modify it here by adding normally-distributed scatter around the log-logistic function to better represent the uncertainty in fitting the function to simulated turbine buckling data (Figure 5.4). The parameters of the damage function used here (given in Table 5.1) are calculated from simulations of the NREL 5-MW offshore reference turbine design [36]; we expect other turbine designs will have damage functions with similar forms but different parameters. This damage function does not account for wave loads or damage mechanisms other than tower buckling.

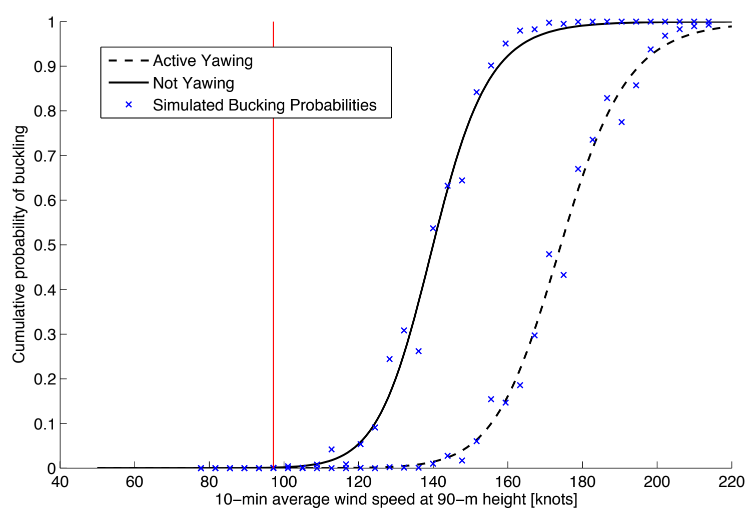

Figure 5.4: Log-logistic functions fitted to probability of tower buckling as a function of wind speed. The vertical red line at 95 knots is the 10-minute sustained wind speed with a 50-year return period used to design Class I wind turbines in the IEC 61400-3 standard.

The hurricane wind field model calculates 1-minute sustained wind speed but our damage function is based on 10-minute sustained wind speed; we divide the 1-minute speed by a factor of 1.11 to get 10-minute sustained speed, as suggested by Harper et al. [37]

The probability of a wind turbine tower buckling $D(u)$ as a function of 10-minute average hub-height wind speed u is calculated as a log-logistic function with normally-distributed scatter, described by equation (5.4) and equation (5.5) and the parameters in Table 5.1.

$$D(u) \sim \text{Normal}\left(\text{loglogistic}(u;\ \alpha, \beta), \sigma_D\right) \tag{5.4}$$

$$\text{loglogistic}(u;\ \alpha, \beta) = \frac{(u/\alpha)^{\beta}}{1 + (u/\alpha)^{\beta}} \tag{5.5}$$

The parameters α, β, σ_D are fit to probabilities of turbine tower buckling calculated by comparing simulated stresses on a 5-MW offshore wind turbine designed by the U.S. National Renewable Energy Laboratory [36] to the stochastic resistance to buckling proposed by Sørensen et al. [38] The simulations are described in more detail by Rose et al. [17] The predictive distribution given in (5.4) is fitted to simulations of wind turbine buckling at 36 10-min average wind speeds from 77.8 – 213.8 knots (40 – 110 m/s, in 2 m/s steps) using Metropolis-Hastings (MH) sampling, a special case of Markov Chain Monte Carlo (MCMC) methods [39]; additional detail is given in Appendix B. We give summary statistics for the empirical distribution of each parameter from MH sampling in Table 5.1 considering two load cases: a non-yawing turbine hit broadside by the wind and a yawing turbine hit head-on by the wind.

Table 5.1: Descriptive statistics for the parameters of the predictive distribution for the wind turbine damage function, which models the probability that a turbine will buckle at a given 10-min average wind speed *u*. These parameters are fit to simulations of wind turbine shut down with blades feathered. **(p < 0.05), *(p < 0.01)**

		Mean	Median	Std. Dev.	Correlation coefficients for α, β, σ_D
Non-yawing turbine (broadside to wind)	α (scale)	139.6	139.6	0.455	$\begin{bmatrix} 1 & & \\ -0.072^{**} & 1 & \\ 0.000 & 0.070^{**} & 1 \end{bmatrix}$
	β (shape)	18.6	18.5	0.998	
	σ_D (std. dev.)	0.0356	0.0352	0.0044	
Yawing turbine (head-on to wind)	α (scale)	174.0	174.0	0.842	$\begin{bmatrix} 1 & & \\ 0.086^{***} & 1 & \\ 0.113 & 0.119^{***} & 1 \end{bmatrix}$
	β (shape)	19.6	19.6	0.411	
	σ_D (std. dev.)	0.0295	0.0292	0.0038	

5.3 Results

5.3.1 Wind Power Simultaneously Offline

We estimate the return periods for fractions of the wind power in a region simultaneously offline due to hurricane damage for fifty 5,000-year periods. The return period is the inverse of the annual probability of a given fraction of wind power being offline. We assume it takes 2 years to rebuild turbines buckled by hurricanes, so the damage from multiple hurricanes within 2 years is cumulative; we plot the sensitivity of the results to rebuilding time in Figure 5.7. In Texas (Figure 5.5) the median amount of wind power offline with a 100-year return period is 11% with a range of 8.3–16% for non-yawing turbines. For a 50-year return period, the median fraction offline is 6.3% with a range of 4.7 – 8.1%. If the turbines were able to yaw to track the wind direction, the median amount of wind power offline in Texas is 0.37% with a 100-year return period and 0.10% with a 50-year return period. In the Southeast (GA, SC, and NC), shown in Figure 5.6, the median amount of wind power offline with a 100-year return period is 1.9%, with a range of 1.2% – 3.0% for non-yawing turbines. For a 50-year return period in the Southeast, the median fraction offline is 0.65% with a range of 0.38 – 0.98%. We do not show results for the Southeast if turbines were able to yaw; the median wind power offline is 0.01% with a 100-year return period and 0% with a 50-year return period. We also do not show results for the Mid-Atlantic and New England because the risks are too small to estimate with the 3,285 simulated landfalling hurricanes we used in our simulations.

Our damage model predicts that historical hurricanes would have been similarly destructive if offshore wind turbines had existed in the locations we describe above. The most destructive would have been Hurricane Carla, which struck Texas in 1961. It would have buckled 7.9% of the turbines (6.8 GW) in Texas if they were unable to yaw and 0.4% (0.38 GW) if they could yaw fast enough to always point into the wind. Similarly, Hurricane Helene in 1958 would have destroyed 1.8% of the non-yawing turbines (1.8 GW) in the Southeast and Hurricane Gloria in 1985 would have destroyed 0.2% of the non-yawing turbines (0.1 GW) in the Mid-Atlantic. The one exception is Hurricane Gerda in 1969, which would have destroyed 8.8% of the non-yawing turbines (3.4 GW) in New England, significantly more than our simulations predict for even a 1,000-year return period (we predict a median of 1.5% and maximum of 4.2%). For comparison, the only other historical hurricane that would have caused measureable simulated damage in New England was Hurricane Esther in 1961, which would have destroyed 0.2% (0.08 GW) of the non-yawing turbines.

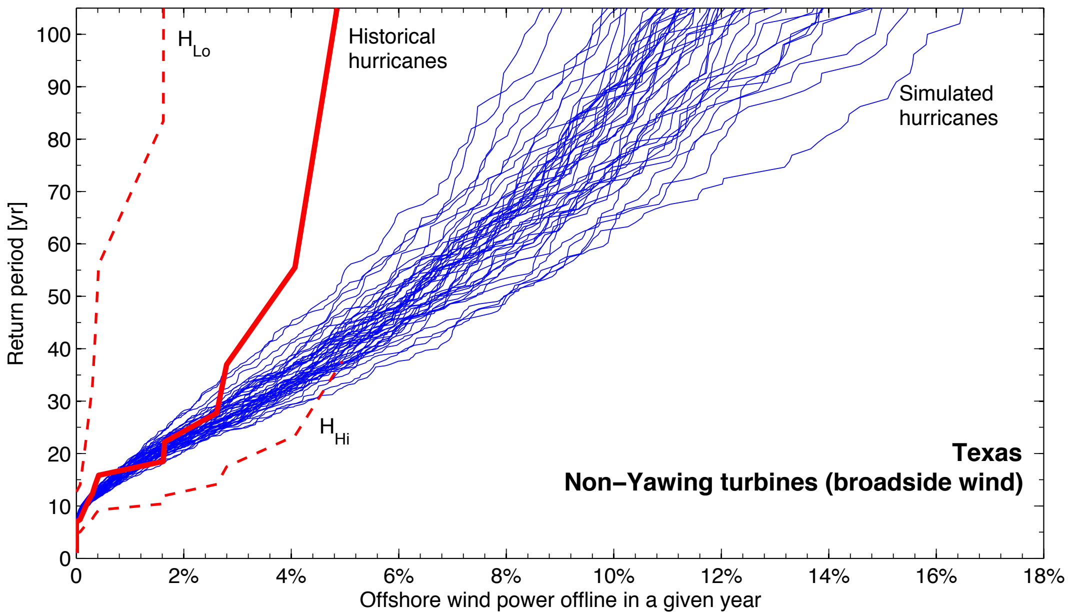

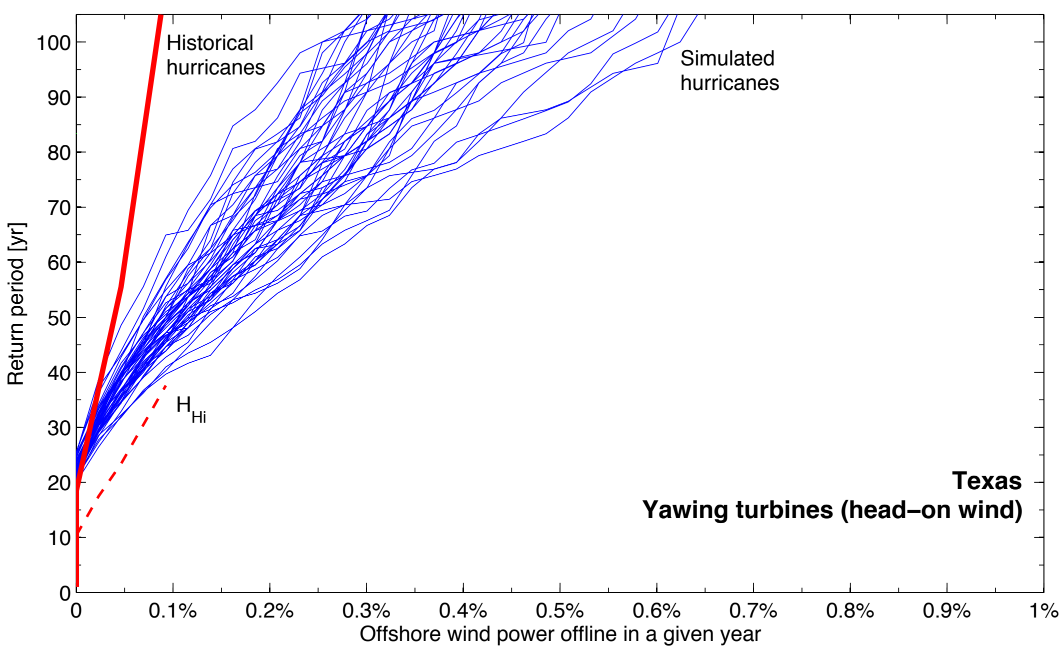

Figure 5.5: Return period for fraction of wind power offline due to hurricane damage in the Texas, assuming turbines are placed in all locations described above (total capacity of 87 GW). The top plot gives risks for non-yawing turbines; the bottom gives risks for yawing turbines. Each of the "Simulated hurricanes" lines represents one of the fifty 5,000-year periods of simulated hurricanes. The "Historical hurricane" line represents risk calculated from the historical hurricane record (1900 - 2011) and "H_{Lo}" and "H_{Hi}" represent the lower and upper confidence bounds for the historically-based estimates.

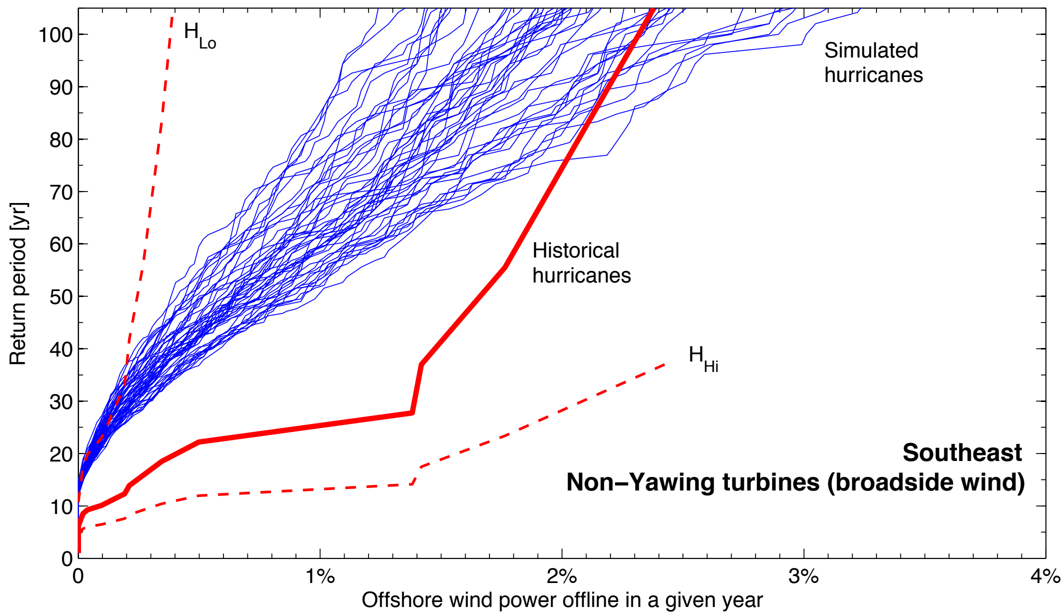

Figure 5.6: Return period for fraction of wind power offline due to hurricane damage in the Southeast (GA, SC, NC), assuming turbines are placed in all locations described above (total capacity of 104 GW) and the turbines cannot yaw. We do not show the results for yawing turbines because the risks are negligible. Each of the "Simulated hurricanes" lines represents one of the fifty 5,000-year periods of simulated hurricanes. The "Historical hurricane" line represents risk calculated from the historical hurricane record (1900 - 2011) and "H_{Lo}" and "H_{Hi}" represent the lower and upper confidence bounds for the historically-based estimates.

The lines labeled "Historical hurricanes" in Figure 5.5 and Figure 5.6 show damage that would have been caused by historical hurricanes if offshore turbines had existed in the locations we describe above. The lines labeled H_{Lo} and H_{Hi} represent the lower and upper confidence bounds for the empirical CDF of historically-based risks, calculated using Greenwood's formula [40].

These results are most sensitive to the uncertainty in the size of hurricanes and the turbine rebuilding time. Sensitivity of wind power simultaneously offline to rebuilding time is shown in Figure 5.7 for the 100-year return period in Texas.

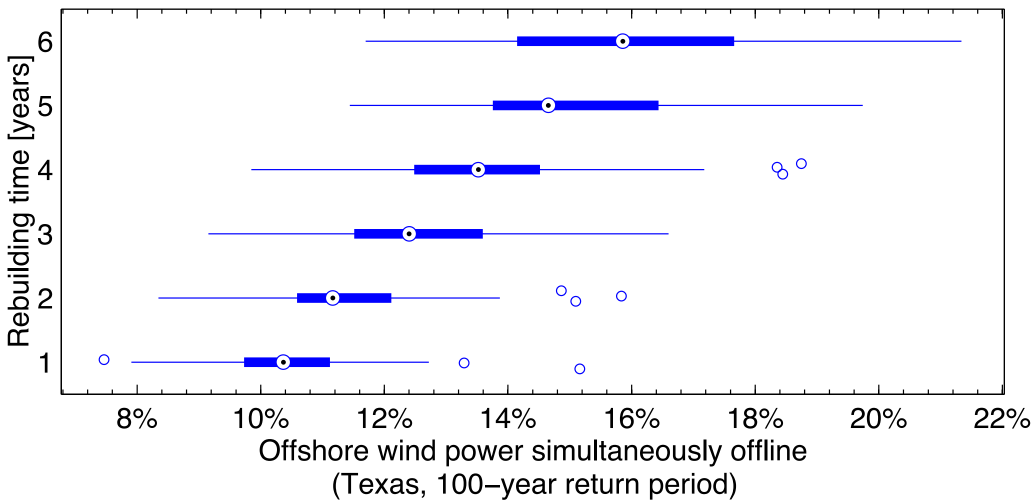

Figure 5.7: Sensitivity of results to rebuilding time. These results are the percentage of Texas offshore wind power simultaneously offline with a 100-year return period. The boxes represent the 25th and 75th percentiles of the simulation results, the whiskers represent the maximum extent of the simulated predictions not classed as outliers, and circles are the outliers.

5.3.2 Cumulative Damage

In the previous section, we showed that only a small fraction of offshore wind power in a region would be offline simultaneously due to buckling by hurricanes. However, the cumulative damage over several years can be significantly larger. We estimate the cumulative damage to offshore wind power in each region and in the entire eastern U.S. for periods of 2, 5, and 10 years, assuming turbines designed to existing standards. The results, plotted in Figure 5.8, show that the cumulative damage increases with the length of the period and that Texas is likely to see the most cumulative damage.

For Texas and the entire Atlantic coast except Florida ("All U.S."), we predict a 10% probability that more than 0.7% of offshore wind power will be destroyed in any 2-year period, more than 2.9% in any 5-year period, and more than 5.7% in any 10-year period if the turbines cannot yaw. For Texas alone, there is a 10% probability that more than 0.9% of offshore wind power will be destroyed in any 2-year period, more than 4.8% in any 5-year period, and more than 10% in any 10-year period if the turbines cannot yaw. For the Southeast (GA, SC, NC), there is a 90% probability that more than 0.04% of offshore wind power will be destroyed in any 2-year period, more than 0.5% in any 5-year period, and more than 1.6% in any 10-year period if the turbines cannot yaw. If the turbines can yaw to point directly into the wind, the cumulative damages are lower by at least a factor of 10. We do not show results for the Mid-Atlantic and New England because the simulated cumulative damages are too small to estimate with the 3,285 simulated landfalling hurricanes we used in our simulations.

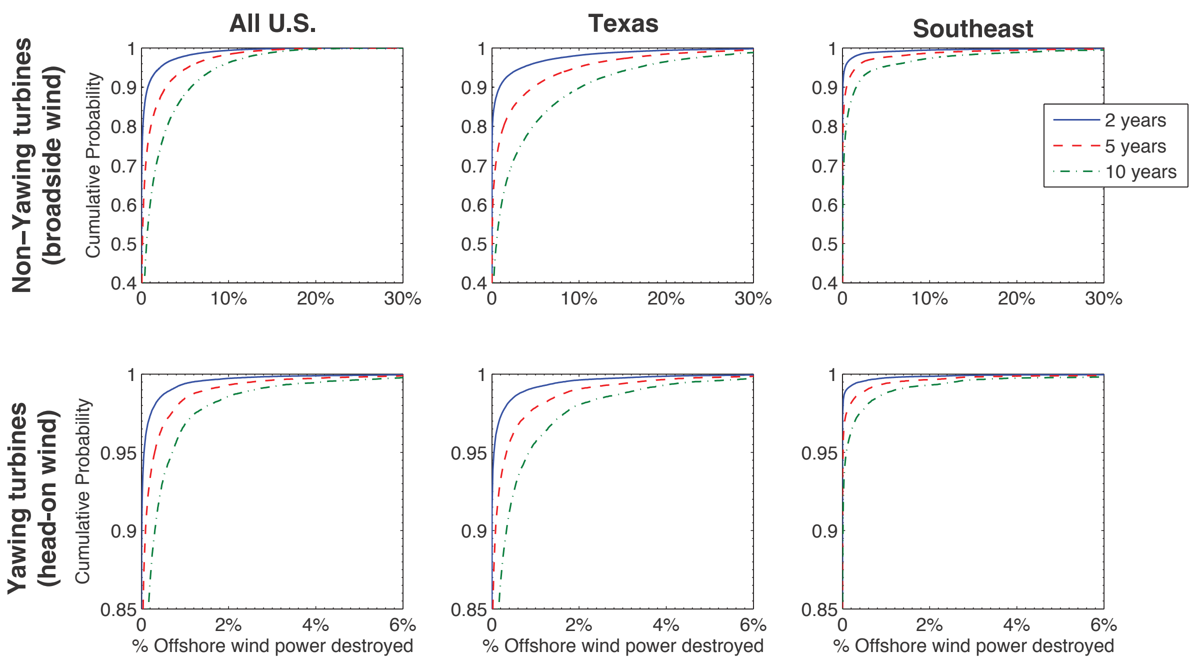

Figure 5.8: Predicted cumulative fraction of offshore wind turbines destroyed in periods of 2, 5, and 10 years. The top row shows cumulative damage for non-yawing turbines and the bottom row for yawing turbines. The left-most column shows cumulative damage for the entire eastern U.S. coast, the center column for Texas, and the right-most column for the Southeast region (GA, SC, NC).

5.3.3 Lifetime Risk to a Single Wind Farm

We estimate the lifetime hurricane risk to a single wind farm in four locations: Galveston County, TX; Dare County, NC; Atlantic County, NJ; Dukes County, MA. For each location, we calculate the lifetime risk as the distribution of the simulated number of turbine towers buckled by hurricanes in 20 years, the typical design life of wind turbines, if buckled turbines are not replaced. For each county, we simulate 5 x 10^4 years of hurricane activity at several possible offshore wind farm locations using hurricanes simulated with a method proposed by Emanuel et al. [20]; the exact wind farm locations are given in the online Supporting Information. The results for Galveston and Dare counties are shown in Figure 5.9 and Figure 5.10, where the lines plot the median risk for all periods and all wind farm sites near a particular county; the error bars represent the 5th and 95th percentile risks. Solid lines plot the risk to non-yawing turbines and dashed lines plot the risk to yawing turbines. Results for Atlantic and Dukes counties are given in Appendix B.

We present these results (labeled "New results (this paper)") for comparison with results for the same four locations presented in Rose et al. [17] (labeled "Rose et al.") and a correction of those earlier results that converts 1-min average wind speeds to 10-min average wind speeds, described in Rose et al. [41] (labeled "Rose et al. corrected") and Section 4.1. There are several important differences between the methods used in the current paper and the methods for previous results. First, the new results are based on the simulated hurricanes described above; previous results are based on probability distributions fitted to historical hurricanes. Second, the new results model the wind field of a hurricane near shore, whereas the previous did not. Third, the new results correct an error in the previous results described by Powell and Cocke [18] that confused 1-min and 10-min average wind speeds; the results labeled "Rose et al. corrected" correct that error but use probability distributions fitted to historical hurricanes. Table 5.2 compares selected results for Galveston, TX calculated with three methods described above; Table 5.3 compares selected results for Dare County, NC calculated with the same three methods. The comparisons in Table 5.2 and Table 5.3 show that the hurricane risks to offshore wind turbines we predict with the more sophisticated method in this paper are slightly lower than risks predicted by the simplified method developed by Rose et al. [17], if the corrections for wind speed averaging period described by Rose et al. [41] are applied.

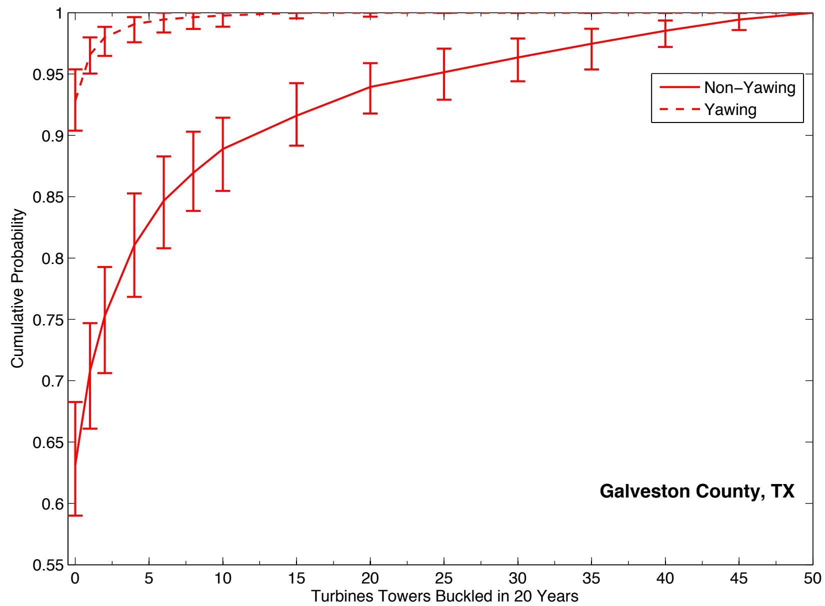

Figure 5.9: Cumulative distribution of number of turbine towers buckled in Galveston County, TX by hurricanes in 20 years if buckled towers are not replaced. Dashed lines plot the distribution for the case that the turbines can yaw to track the wind direction, and solid lines plot the distribution for the cast that turbines cannot yaw.

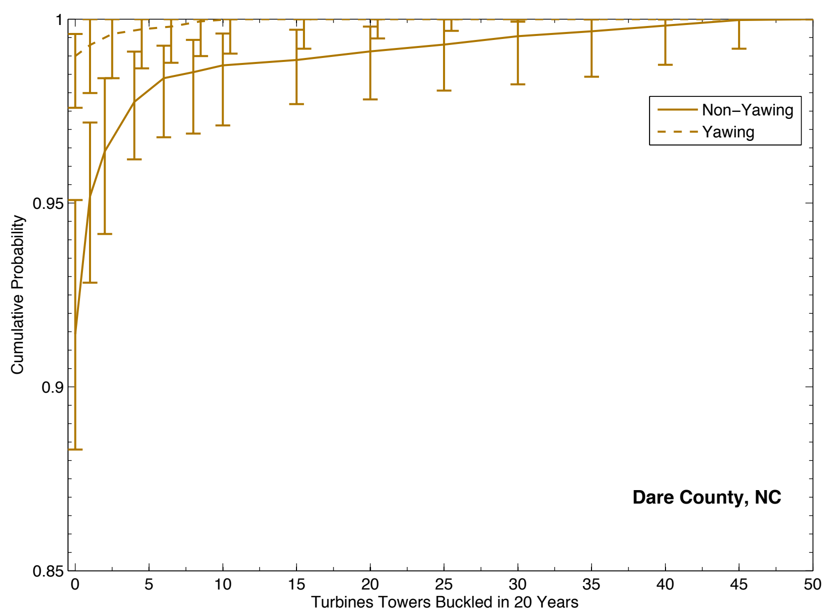

Figure 5.10: Cumulative distribution of number of turbine towers buckled in Dare County, NC by hurricanes in 20 years if buckled towers are not replaced. Dashed lines plot the distribution for the case that the turbines can yaw to track the wind direction, and solid lines plot the distribution for the cast that turbines cannot yaw.

In Atlantic County, NJ, there is a 0.4 - 3% probability and in Dukes County, MA, a 0.2 – 2% probability that at least one tower will buckle in 20 years if the turbines cannot yaw. The probability of more than half the turbines buckling in the non-yawing case or any turbines buckling in the yawing case in Atlantic County and Dukes County are too small to estimate with the 3,285 simulated landfalling hurricanes we used in our simulations.

Table 5.2: Comparison of results for Galveston County with no rebuilding of buckled turbines.

Galveston County, TX

		≥ 1 turbine buckled in 20 years	> 25 turbines buckled in 20 years
Non-yawing turbine (broadside to wind)	New results (this paper)	32 - 41%	3 – 7%
	Rose et al. corrected [41]	43%	18%
	Rose et al. [17]	60%	30%
Yawing turbine (head-on to wind)	New results (this paper)	5 – 10%	0%
	Rose et al. corrected [41]	16%	6%
	Rose et al. [17]	25%	10%

Table 5.3: Comparison of results for Dare County, NC if buckled turbines are not rebuilt.

Dare County, NC

		≥ 1 turbine buckled in 20 years	> 25 turbines buckled in 20 years
Non-yawing turbine (broadside to wind)	New results (this paper)	5 - 12%	0.01 - 2%
	Rose et al. corrected [41]	34%	1%
	Rose et al. [17]	60%	9%
Yawing turbine (head-on to wind)	New results (this paper)	0.4 - 2%	< 0.3%
	Rose et al. corrected [41]	4%	< 0.1%
	Rose et al. [17]	15%	< 0.1%

5.4 Discussion

Our results suggest that hurricanes will pose a non-negligible, but likely manageable risk to grid operators in coastal regions should they become dependent on offshore wind power, though hurricanes in the Gulf of Mexico may pose a significant risk to insurers. Grid operators in areas prone to intense hurricanes should account for the hurricane risk when calculating capacity value for offshore wind power if they use existing wind turbine designs. Insurers should carefully assess the spatial and temporal correlation of hurricane risk to offshore wind power in areas prone to intense hurricanes. Hurricane risk can be mitigated by strengthening turbine designs or ensuring that turbines can yaw to track the wind direction even if grid power is lost. These risks may change as the climate changes, but it is unclear whether the risks will increase or decrease.

From the perspective of an electrical grid operator, the hurricane risk to offshore wind power may affect two aspects of electrical grid reliability: system security and system adequacy. Security is a measure of the ability of the power grid to continue operating normally in case of the loss of a major component, such as a power plant or transmission line. The U.S. grid has experience in dealing with temporary losses of major components as a result of hurricanes, and there are established communication protocols that require generators to inform the power grid operators of any generation assets loses [42]. Furthermore, the scale of expected offshore wind power losses, even in extreme events, is similar to the reserve margin used to maintain system security. For example, ERCOT, the Texas grid operator, has a minimum reserve margin target of 13.75% of system load [43], but a 100-year hurricane event would take 9 – 14% of the offshore wind power offline simultaneously.

Adequacy is a measure of the generation and transmission capacity to meet future load. Wind power can contribute only a fraction of its rated power output, known as "capacity value", to system adequacy because wind is a variable resource. There has been significant work on estimating the capacity value of wind power [44]-[46], but none has considered the risk of losses in wind farm installations resulting from natural hazards. Unlike conventional generators, which can see short-term outages as a result of hurricanes [47], long term loses of offshore wind resources could result from hurricanes. These long-term losses can affect the adequacy of the grid, which in turn would affect security. The results we present in this paper suggests that there is a risk associated with installing significant amounts of offshore wind power in the Gulf of Mexico if the turbines are designed to current standards. Figure 5.5 shows, for example, that there is a 2% probability of having 4.7 – 8.1% of installed wind capacity offline simultaneously in any given year and a 1% probability of 9 – 14% offline. We thus suggest that methods for calculating the capacity value of offshore wind resources in the Gulf Cost should incorporate the risk of losses due to hurricanes. This will ensure that appropriate long-term reserve margins are maintained and available to maintain security of the grid.

From the perspective of insurers, the hurricane risk to offshore wind power may be significant because offshore turbines are expensive and current turbine designs are vulnerable. For example, a 100-year event (hurricane or series of hurricanes) could cause $31 – 49 billion in damages to offshore wind turbines and a 50-year event could cause $17 – 27 billion if turbines are installed in all feasible locations along the Texas coast (87 GW and assuming an overnight capital cost for offshore wind turbines of $4,000/kW [30]). That 100-year event would rank as one of the ten costliest two-year periods in U.S. history in terms of hurricane damage and the 50-year event would rank as one of the fifteen costliest 2-year periods. For comparison, Hurricane Ike, one of the costliest hurricanes in U.S. history after Katrina, caused approximately $29.5 billion in damages [6]. It is unlikely that the entire Texas coastline will be developed, but the insurance exposure could be in the billions of dollars if there is significant offshore wind power development in the Gulf of Mexico with current wind turbine designs.

To mitigate the risks of hurricanes, offshore wind turbines can be designed for higher maximum wind speeds, designed to track the wind direction (yaw) quickly enough to match wind changes in a hurricane even if grid power is cut off, or placed in areas with lower hurricane risk, as discussed by Rose et al. [17]. Efforts are underway to determine design standards for offshore wind turbines in hurricane prone areas [48]. Battery backup is a low-cost way to maintain yawing capability when grid power is interrupted [17]. Nearly all planned offshore wind development in the U.S. in the next 10 – 20 years will occur in low-risk areas such as New England and the Mid-Atlantic states. A U.S Department of Energy report envisions a scenario with 54 GW of offshore wind from North Carolina to Maine by 2030 [4] and the U.S. Bureau of Ocean Energy Management (BOEM) is planning to auction offshore wind leases from Massachusetts to Virginia [49]. However, the state of Texas has strongly encouraged onshore wind development and has signed a lease for a wind power development near Galveston [50].

The model developed for this paper uses simulated hurricane tracks and intensities based on climatological conditions from 1979 to 2011; it does not assess the effects of climate change. There has been significant work on evaluating the implications of climate change on hurricane occurrence [21], [51]-[53]. Studies suggest the frequency of hurricanes may not increase in the future and may even decrease, but the intensity of these tropical cyclones is likely to increase as a result of climate change. These conflicting trends will affect the risk hurricanes pose on the large-scale deployment of offshore wind resources in the Gulf Coast, where we find the current risk is the greatest. While a reduction in hurricane frequency may mean there is a reduction in risk, the increased intensity will result in increased damages by individual storms. It is hard to measure, however, which of these two mechanisms will affect the risk to offshore wind farms the most.

5.5 Acknowledgements

This work was supported in part by the EPA STAR fellowship program, a grant from the Alfred P. Sloan Foundation and EPRI to the Carnegie Mellon Electricity Industry Center, and by the Doris Duke Charitable Foundation, the R.K. Mellon Foundation and the Heinz Endowments for support of the RenewElec program at Carnegie Mellon University. This research was also supported in part by the Climate and Energy Decision Making (CEDM) center. This Center has been created through a cooperative agreement between the National Science Foundation (SES-0949710) and Carnegie Mellon University.

5.6 References

[1] R. Wiser and M. Bolinger, "2011 Wind Technologies Market Report," U.S. Department of Energy, Oak Ridge, TN, DOE/GO-102012-3472, Jul. 2012.

[2] M. Schwartz, D. Heimiller, S. Haymes, and W. Musial, "Assessment of Offshore Wind Energy Resources for the United States," National Renewable Energy Laboratory, Golden, CO, NREL/TP-500-45889, Jun. 2010.

[3] "OffshoreWind.net," *offshorewind.net*. [Online]. Available: http://www.offshorewind.net. [Accessed: 18-Nov-2012].

[4] DOE, “20% Wind Energy by 2030,” U.S. Department of Energy, DOE/GO-102008-2567, Jul. 2008.
[5] EIA, “Electric Power Annual 2010,” U.S. Energy Infomation Administration, Washington, DC, Nov. 2011.
[6] E. S. Blake, C. W. Landsea, and E. J. Gibney, “The Deadliest, Costliest, and Most Intense United States Tropical Cyclones From 1851 to 2010 (and Other Frequently Requested Hurricane Facts),” National Hurricane Center, Miami, NWS NHC-6, Aug. 2011.
[7] S. A. Changnon, “Characteristics of severe Atlantic hurricanes in the United States: 1949–2006,” *Nat Hazards*, vol. 48, no. 3, pp. 329–337, 2009.
[8] K. Takahara, T. Mekaru, F. Shinjo, T. Ishihara, A. Yamaguchi, and S. Matsuura, “Damages of wind turbine on Miyakojima Island by Typhoon Maemi in 2003,” *2004 European Wind Energy Conference and Exhibition*, 2004.
[9] N. E. Clausen, A. Candelaria, S. Gjerding, S. Hernando, P. Nørgård, S. Ott, and N. Tarp-Johansen, “Wind farms in regions exposed to tropical cyclones,” *2007 European Wind Energy Conference and Exhibition*, 2007.
[10] S. A. Cauffman, “Performance of Physical Structures in Hurricane Katrina and Hurricane Rita: A Reconnaissance Report,” National Institute of Standards and Technology, Gaithersburgh, MD, NIST Technical Note 1476, Jul. 2006.
[11] T. Johnson, “New Jersey's Aging Power Plants, Another Casualty of Superstorm Sandy,” *njspotlight.com*, 16-Nov-2012. [Online]. Available: http://www.njspotlight.com/stories/12/11/16/new-jersey-s-aging-power-plants-another-casualty-of-superstorm-sandy/. [Accessed: 18-Nov-2012].
[12] *Power Reactor Information System*, 2012. [Online]. Available: http://www.iaea.org/pris/CountryStatistics/CountryDetails.aspx?current=JP. [Accessed: 18-Oct-2012].
[13] A. Sagawa, “Coal for Power Generation: Supply and Demand Following the Great East Japan Earthquake,” *Institute of Energy Economics, Japan*, Aug-2012.
[14] O. Tsukimori, “Tohoku: Haramachi plant to resume before summer 2013,” *Reuters*, 27-Jan-2012. [Online]. Available: http://www.reuters.com/article/2012/01/27/japan-power-tohoku-idUST9E7NL01L20120127. [Accessed: 13-Aug-2012].
[15] IEA, “IEA Wind 2011 Annual Report,” International Energy Agency, Jul. 2012.
[16] NERC, “1998 System Disturbances,” North American Electric Reliability Council, Princeton, NJ, May 2001.
[17] S. Rose, P. Jaramillo, M. J. Small, I. Grossmann, and J. Apt, “Quantifying the hurricane risk to offshore wind turbines,” *Proceedings of the National Academy of Science*, vol. 109, no. 9, pp. 3247–3252, Feb. 2012.
[18] M. D. Powell and S. Cocke, “Hurricane wind fields needed to assess risk to offshore wind farms,” *Proc Natl Acad Sci U S A*, vol. 109, no. 33, pp. E2192–E2192, Aug. 2012.
[19] M. Mahdyiar and B. Porter, “The Risk Assessment Process: The Role of Catastrophe Modeling in Dealing with Natural Hazards,” in *Catastrophe Modeling: A New Approach to Managing Risk*, P. Grossi and H. Kunreuther, Eds. New York: Springer, 2005, pp. 45–68.
[20] K. A. Emanuel, S. Ravela, E. Vivant, and C. Risi, “A statistical deterministic approach to hurricane risk assessment,” *Bull. Amer. Meteor. Soc.*, vol. 87, no. 3, pp. 299–314, Mar. 2006.
[21] K. A. Emanuel, R. Sundararajan, and J. Williams, “Hurricanes and Global Warming: Results from Downscaling IPCC AR4 Simulations,” *Bull. Amer. Meteor. Soc.*, vol. 89, no. 3, pp. 347–367, Mar. 2008.
[22] K. A. Emanuel, “Tropical Cyclone Energetics and Structure,” in *Atmospheric Turbulence and Mesoscale Meteorology*, no. 8, Cambridge: Cambridge University Press, 2004, pp. 165–191.

[23] K. A. Emanuel, R. Sundararajan, and J. Williams, "Downscaling hurricane climatologies from global models and re-analyses," presented at the 28th Conference on Hurricanes and Tropical Meteorology, Orlando, 2008.
[24] G. J. Holland, J. I. Belanger, and A. Fritz, "A Revised Model for Radial Profiles of Hurricane Winds," *Mon. Wea. Rev.*, vol. 138, no. 12, pp. 4393–4401, Dec. 2010.
[25] K. A. Emanuel, "Personal communication," 19-Apr-2012.
[26] J. L. Demuth, M. DeMaria, and J. A. Knaff, "Improvement of advanced microwave sounding unit tropical cyclone intensity and size estimation algorithms," *Journal of Applied Meteorology and Climatology*, vol. 45, no. 11, pp. 1573–1581, 2006.
[27] M. Powell, G. Soukup, S. Cocke, S. Gulati, N. Morisseau-Leroy, S. Hamid, N. Dorst, and L. Axe, "State of Florida hurricane loss projection model: Atmospheric science component," *Journal of Wind Engineering and Industrial Aerodynamics*, vol. 93, no. 8, pp. 651–674, Aug. 2005.
[28] F. P. Ho, J. C. Su, K. L. Hanevich, R. J. Smith, and F. P. Richards, "NOAA Technical Report NWS 38: Hurricane Climatology for the Atlantic and Gulf Coasts of the United States," National Weather Service, Silver Spring, MD, NOAA Technical Report NWS 38, Apr. 1987.
[29] M. Brower, "Development of Eastern Regional Wind Resource and Wind Plant Output Datasets," National Renewable Energy Laboratory, Golden, CO, NREL/SR-550-46764, Dec. 2009.
[30] W. Musial and B. Ram, "Large-Scale Offshore Wind Power in the United States: Assessment of Opportunities and Barriers, NREL (National Renewable Energy Laboratory)," Sep. 2010.
[31] K. A. Emanuel, C. DesAutels, C. Holloway, and R. Korty, "Environmental control of tropical cyclone intensity," *Journal of the Atmospheric Sciences*, vol. 61, no. 7, pp. 843–858, 2004.
[32] M. H. DeGroot and M. J. Schervish, *Probability and Statistics*, 3rd ed. Boston: Addison Wesley, 2002.
[33] H. E. Willoughby and M. E. Rahn, "Parametric Representation of the Primary Hurricane Vortex. Part I: Observations and Evaluation of the Holland (1980) Model," *Mon. Wea. Rev.*, vol. 132, no. 12, pp. 3033–3048, Dec. 2004.
[34] B. D. Keim, R. A. Muller, and G. W. Stone, "Spatiotemporal Patterns and Return Periods of Tropical Storm and Hurricane Strikes from Texas to Maine," *J. Climate*, vol. 20, no. 14, pp. 3498–3509, Jul. 2007.
[35] K. A. Emanuel and T. Jagger, "On Estimating Hurricane Return Periods," *Journal of Applied Meteorology and Climatology*, vol. 49, no. 5, pp. 837–844, 2010.
[36] J. Jonkman, S. Butterfield, W. Musial, and G. Scott, "Definition of a 5-MW reference wind turbine for offshore system development," National Renewable Energy Laboratory, Golden, CO, NREL/TP-500-38060, Feb. 2009.
[37] B. A. Harper, J. Kepert, and J. Ginger, "Guidelines for converting between different wind averaging periods in tropical cyclone conditions," World Meteorological Organization, Oct. 2008.
[38] J. D. Sørensen and N. J. Tarp-Johansen, "Reliability-based optimization and optimal reliability level of offshore wind turbines," *International Journal of Offshore and Polar Engineering*, vol. 15, no. 2, pp. 141–146, 2005.
[39] D. Gamerman and H. F. Lopes, *Markov Chain Monte Carlo*, 2nd ed. Boca Raton, FL: Chapman & Call/CRC, 2006.
[40] M. Greenwood, "A Report on the Natural Duration of Cancer," UK Ministry of Health, London, 33, 1926.
[41] S. Rose, P. Jaramillo, M. J. Small, I. Grossmann, and J. Apt, "Reply to Powell and Cocke:

On the probability of catastrophic damage to offshore wind farms from hurricanes in the US Gulf Coast," *Proc Natl Acad Sci U S A*, vol. 109, no. 33, pp. E2193–E2194, Aug. 2012.
[42] NERC, "Standard COM-002-2: Communications and Coordination," Washington, DC, COM-002-2, Jan. 2007.
[43] ERCOT, "ERCOT 10-year outlook indicates need for additional generation," *ercot.com*, no. 512. ERCOT, Austin, 01-Dec-2011.
[44] C. Ensslin, M. Milligan, H. Holttinen, M. O'Malley, and A. Keane, "Current methods to calculate capacity credit of wind power, IEA collaboration," presented at the IEEE Power and Energy Society General Meeting, 2008, pp. 1–3.
[45] B. Hasche, A. Keane, and M. O'Malley, "Capacity Value of Wind Power, Calculation, and Data Requirements: the Irish Power System Case," *IEEE Transactions on Power Systems*, vol. 26, no. 1, pp. 420–430, Feb. 2011.
[46] A. Keane, M. Milligan, C. J. Dent, B. Hasche, C. D'Annunzio, K. Dragoon, H. Holttinen, N. Samaan, L. Soder, and M. O'malley, "Capacity Value of Wind Power," *IEEE Transactions on Power Systems*, vol. 26, no. 2, pp. 564–572, 2011.
[47] A. Lippert, M. Farber-DeAnda, K. SeCorla-souza, R. Laramey, J. T. J. Ostrich, C. Lewandowski, M. Scott, and C. Hackett, "Comparing the Impacts of the 2005 and 2008 Hurricanes on U.S. Energy Infrastructure," US Department of Energy, Office of Electricity Delivery and Energy Reliability, Washington, DC, Feb. 2009.
[48] Q. Yu, L. Samuelsson, and P.-L. Tan, "Design Considerations for Offshore Wind Turbines in US Waters - The American Way," presented at the Offshore Technology Conference, Houston, 2011, pp. 1–13.
[49] P. Brannen, "Offshore wind farms will be encouraged in tracts along the East Coast," *Washington Post*, Washington, DC, 23-Jul-2012.
[50] DOE, "Company Plans Large Wind Plant Offshore of Galveston, Texas," *Energy Efficiency & Renewable Energy Network News*. [Online]. Available: http://apps1.eere.energy.gov/news/news_detail.cfm/news_id=9502. [Accessed: 02-Nov-2005].
[51] T. R. Knutson, J. L. McBride, J. Chan, K. A. Emanuel, G. Holland, C. Landsea, I. Held, J. P. Kossin, A. K. Srivastava, and M. Sugi, "Tropical cyclones and climate change," *Nat Geosci*, vol. 3, no. 3, pp. 157–163, Feb. 2010.
[52] K. Trenberth, "CLIMATE: Uncertainty in Hurricanes and Global Warming," *Science*, vol. 308, no. 5729, pp. 1753–1754, Jun. 2005.
[53] S. T. Tokdar, I. Grossmann, J. B. Kadane, A.-S. Charest, and M. J. Small, "Impact of Beliefs About Atlantic Tropical Cyclone Detection on Conclusions About Trends in Tropical Cyclone Numbers," *Bayesian Analysis*, vol. 6, no. 4, pp. 547–572, 2011.

B Appendix

B.1 Wind Turbine Placement Details

Wind turbines are placed in areas that meet the following criteria:

- Water depth shallower than 30 meters
- Mean annual wind speed greater than 7.4 m/s at 90 m height (http://www.nrel.gov/gis/data_wind.html)
- Distance from shore greater than 8 km and less than 93 km.

Wind turbines are excluded from the following areas:

- Marine sanctuaries
  - Descibed by shapefiles labeled "Marine Protected Areas" from http://www.cec.org/Page.asp?PageID=924&ContentID=2336
- Military practice areas
  - Described by shapefiles labeled "COASTAL.MIPARE_POLYGON" from http://ocs-spatial.ncd.noaa.gov/SpatialDirect/translationServlet?SSFunction=prepareFetch
- Military aviation warning areas with floor below 1000 ft
  - Shapefiles retrieved by querying http://www.csc.noaa.gov/ArcGISPUB/rest/services/MultipurposeMarineCadastre/MultipurposeMarineCadastre/MapServer/27/query with the following parameters:
    - Filter Geometry: `{xmin: -125, ymin: 29, xmax: -70, ymax: 47}`
    - Geometry Type: `Envelope`
    - Return Fields: `"NAME", "LOWER_ALT"`
- Shipping lanes
  - Described by shapefiles labeled "COASTAL_FAIRWAY" and "COASTAL_TSEZNE" from http://ocs-spatial.ncd.noaa.gov/SpatialDirect/translationServlet?SSFunction=prepareFetch
- Active oil and gas leases

    - Described by shapefiles retrieved from http://csc.noaa.gov/mmcviewer/
- Bays and inland waterways
    - Matagorda Bay, Galveston Bay, Pamlico Sound, Cheasapeake Bay, Delaware Bay, Long Island Sound, and Cape Cod Bay

B.2 Total Installed Wind Capacity Used in This Paper

Table B-1: Total installed offshore wind power capacity that could be developed in each state within the constraints described in Section B.1, assuming a density of 5 MW/km^2. Mississippi, Alabama, and Florida are excluded because wind resource estimates are not available for those states. Connecticut is excluded because nearly all its coastline is on Long Island Sound, are area we assumed was unlikely to be developed.

	State	Capacity (MW)
Gulf of Mexico	Texas	86,520
	Louisiana	68,100
Southeast	Georgia	45,740
	South Carolina	21,200
	North Carolina	37,380
Mid-Atlantic	Virginia	15,160
	Maryland	720
	Delaware	6,760
	New Jersey	18,400
	New York	9,940
New England	Rhode Island	3,000
	Massachusetts	29,140
	New Hampshire	40
	Maine	6,840

B.3 Lifetime Risk to a Single Wind Farm

B.3.1 Wind Farm Locations

Table B-2: Locations of the wind farms used to calculate results in Section 5.3.3 and Section B.3.2.

	Wind Farm Locations
Galveston County, TX	29.09°N, 94.90°W
	29.25°N, 94.71°W
	29.41°N, 94.41°W
	28.76°N, 94.63°W
	28.82°N, 94.32°W
	28.96°N, 94.18°W
Dare County, NC	35.09°N, 75.93°W
	35.21°N, 75.57°W
	35.50°N, 75.34°W
	35.73°N, 75.41°W
	36.17°N, 75.61°W
Atlantic County, NJ	39.24°N, 74.34°W
	39.31°N, 74.26°W
	39.40°N, 74.24°W
Dukes County, MA	41.45°N, 70.96°W
	41.23°N, 70.73°W
	41.27°N, 70.42°W
	41.48°N, 70.37°W

B.3.2 Additional Results

Figure B-1 and Figure B-2 plot results for the lifetime (20-year) risk to a single wind farm in Atlantic County, NJ and Dukes County, MA, and Table B-3 and Table B-4 compare those results to previously-published results.

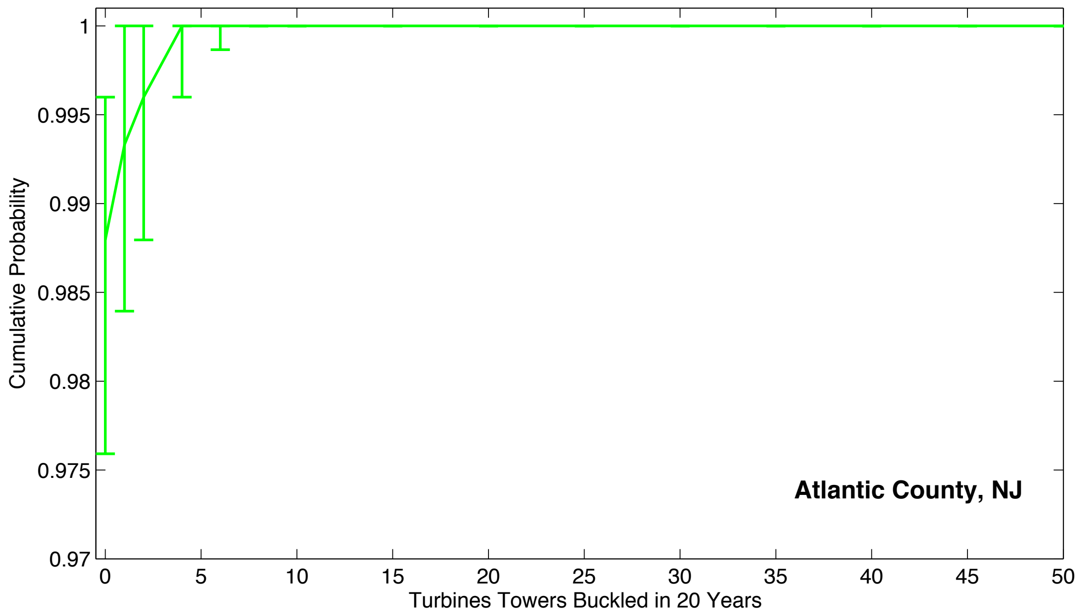

Figure B-1: Cumulative distribution of number of turbine towers buckled in Atlantic County, NJ by hurricanes in 20 years if buckled towers are not replaced. Solid lines plot the distribution for the cast that turbines cannot yaw. Results for yawing turbines are not shown because the risks are too small to calculate with the method in this paper.

Table B-3: Comparison of results for Atlantic County with no rebuilding of buckled turbines.

Atlantic County, NJ			
		≥ 1 turbine buckled in 20 years	**> 25 turbines buckled in 20 years**
Non-yawing turbine (broadside to wind)	New results (this paper)	0.4 – 2.4%	0%
	Rose et al. corrected [1]	7%	< 1%
	Rose et al. [2]	15%	1%
Yawing turbine (head-on to wind)	New results (this paper)	0%	0%
	Rose et al. corrected [1]	<1%	<1%
	Rose et al. [2]	1%	0%

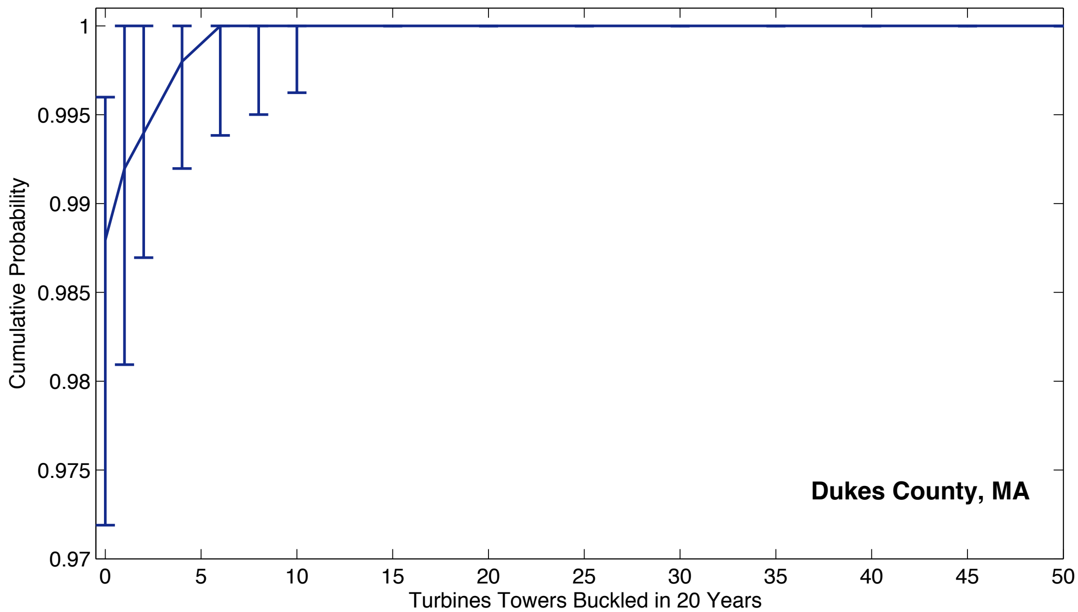

Figure B-2: Cumulative distribution of number of turbine towers buckled in Dukes County, MA by hurricanes in 20 years if buckled towers are not replaced. Solid lines plot the distribution for the cast that turbines cannot yaw. Results for yawing turbines are not shown because the risks are too small to calculate with the method in this paper.

Table B-4: Comparison of results for Dukes County with no rebuilding of buckled turbines.

Dukes County, MA			
		≥ 1 turbine buckled in 20 years	**> 25 turbines buckled in 20 years**
Non-yawing turbine (broadside to wind)	New results (this paper)	0.4 – 2.8%	0%
	Rose et al. corrected [1]	5%	<1%
	Rose et al. [2]	10%	< 1%
Yawing turbine (head-on to wind)	New results (this paper)	0%	0%
	Rose et al. corrected [1]	1%	< 0.1%
	Rose et al. [2]	1%	0%

B.4 Metropolis-Hastings Algorithm for Damage Function Distribution

We use a Metropolis-Hastings algorithm (a special case of Markov Chain Monte Carlo methods) to estimate the three parameters $\theta_1 = \alpha$, $\theta_2 = \beta$, $\theta_3 = \sigma$ for the turbine damage function. Specifically, we use the Metropolis-Hastings algorithm with component wise updating of the parameters[3], according to the following steps:

1. Initialize an iteration counter $j = 1$ and set initial values of the parameters $\boldsymbol{\theta}^{(0)}$. It helps to choose initial parameter values relatively close to the expected final values because the MH algorithm will converge faster that way.
2. For each parameter θ_i:
    a. Propose a new parameter value θ_i^* as a function of the previous parameter value $\theta_i^{(j-1)}$ according to the proposal distribution q:

    $$\theta_i^* \sim q\left(\theta_i^{(j)} | \theta_i^{(j-1)}\right) = \text{Gamma}\left(\tau_i \theta_i^{(j-1)},\ 1/\tau_i\right)$$

    b. Calculate the proposal ratio:

    $$\text{prop. ratio} = \frac{q\left(\theta_i^{(j-1)} | \theta_i^*\right)}{q\left(\theta_i^* | \theta_i^{(j-1)}\right)}$$

    c. Calculate the likelihood ratio, which is the ratio of the likelihood function with 3 parameters: the proposed value for the i^{th} parameter θ_i^* and the values for the two other parameters from the previous step $\theta_{\neg i}^{(j-1)}$:

    $$\text{like. ratio} = \frac{p\left(\theta_i^*,\ \theta_{\neg i}^{(j-1)}\right)}{p\left(\theta_i^{(j-1)},\ \theta_{\neg i}^{(j-1)}\right)}$$

    where the likelihood function based on equation (4) in the body of the paper is the product of the probability density value of the residuals (difference between measured turbine buckling probability and loglogistic model) for the K measured turbine buckling probabilities $y(u_k)$ that are a function of wind speed u_k:. For example:

$$p(\theta_2^*, \theta_{\neg 2}^{(j-1)}) = p(\theta_1^{(j-1)}, \theta_2^*, \theta_3^{(j-1)})$$
$$= \prod_{k-1}^{K} f\left(\left(y(u_k) - \text{loglogistic}(u_k; \alpha^{(j-1)}, \beta^*) \right);\ 0, \sigma_D^{(j-1)} \right)$$

where f(x; μ, σ) is the PDF of the Normal distribution:

$$f(x;\ \mu, \sigma) = \frac{1}{\sqrt{2\pi\sigma^2}} \exp\left(\frac{-(x-\mu)^2}{2\sigma^2} \right)$$

d. Calculate the acceptance probability α as the minimum of the proposal ration and the likelihood ratio:

$$\alpha = \min\{1, \text{prop. ratio}, \text{like. ratio}\}$$

e. If the proposal is accepted (α > uniform random number), $\theta_i^{(j)} = \theta_i^*$, otherwise $\theta_i^{(j)} = \theta_i^{(j-1)}$ and go to the next parameter θ_{i+1}.

3. Increment the iteration counter $j = j+1$

In the Gamma distribution in step 2a, τ is a parameter that must be tuned to improve the convergence speed of the algorithm; we set $\tau_\alpha = 100$, $\tau_\beta = 5$, and $\tau_{\sigma D} = 1000$. In the likelihood function in step 2c, y_k is the simulated probability of tower buckling at wind speed u_k. Each pair (u_k, y_k) corresponds to a point in Figure 7 in the body of the paper. We simulated turbine buckling at K = 36 different 10-min average wind speeds from 77.6 – 213.8 knots (40 – 110 m/s, in 2 m/s steps). The details of the turbine buckling simulation are given in the Supporting Information of work by Rose et al. [2]

We assume informationless priors, i.e. uniform distributions.

B.5 Model Validation

Emanuel et al. have shown that the simulated hurricanes we use as the basis for our analysis have statistical properties similar to historical hurricanes [4]. However, we transform those simulated hurricanes by modeling uncertainty in their return rate and size. We validate the transformed hurricanes by calculating the return periods of three different storm intensities at 45 locations along the U.S. coast (Section B.5.1 below) and return periods of a range of wind speeds in New Orleans and Miami (Section B.5.2 below).

*B.5.1 **Return Period of Storms Along the U.S. Coast***

We estimate return periods of intense hurricanes, all hurricanes, and all tropical storms for 45 points along the Gulf and Atlantic coasts using the simulated hurricanes described in the body of the paper. For each point, the return periods are calculated within 20 km of the point for storms that pass within 240 km of the point, using the simulated hurricanes described in the body of the paper. We present these results for comparison with results based on historical hurricane data in a paper by Keim et al. [5]

In Figure B-3 we plot our estimates of the return periods of winds greater than intense-hurricane (> 96 knots), which are comparable to the historically-based return periods given by Keim et al. for most locations. This is important because offshore wind turbines designed to existing standards are most vulnerable to intense hurricanes. Our simulations predict shorter return periods for intense-hurricane-force winds along the coasts of Georgia, northeastern Florida, and northwestern Florida, but the historical record is not long enough to accurately estimate return periods for those regions.

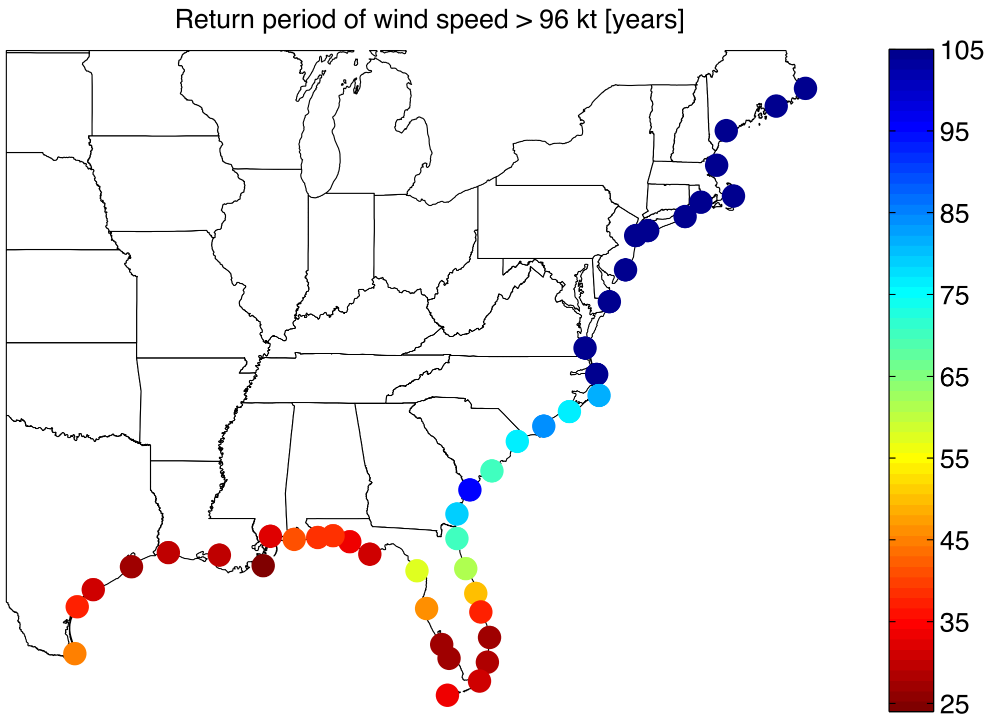

Figure B-3: Return periods of wind speeds greater than 96 knots (intense hurricanes) within 20 km of each point, calculated with the simulation method described in the body of the paper.

In Figure B-4 we plot our estimates of return periods for winds greater than hurricanes strength (> 64 knots), which predict shorter return periods than the historical record. Although our results over-predict the frequency of all hurricanes relative to historical data, we expect this has little effect on our turbine risk results because most of risk comes from intense hurricanes and we show in Figure B-3 that we model the return period of those well.

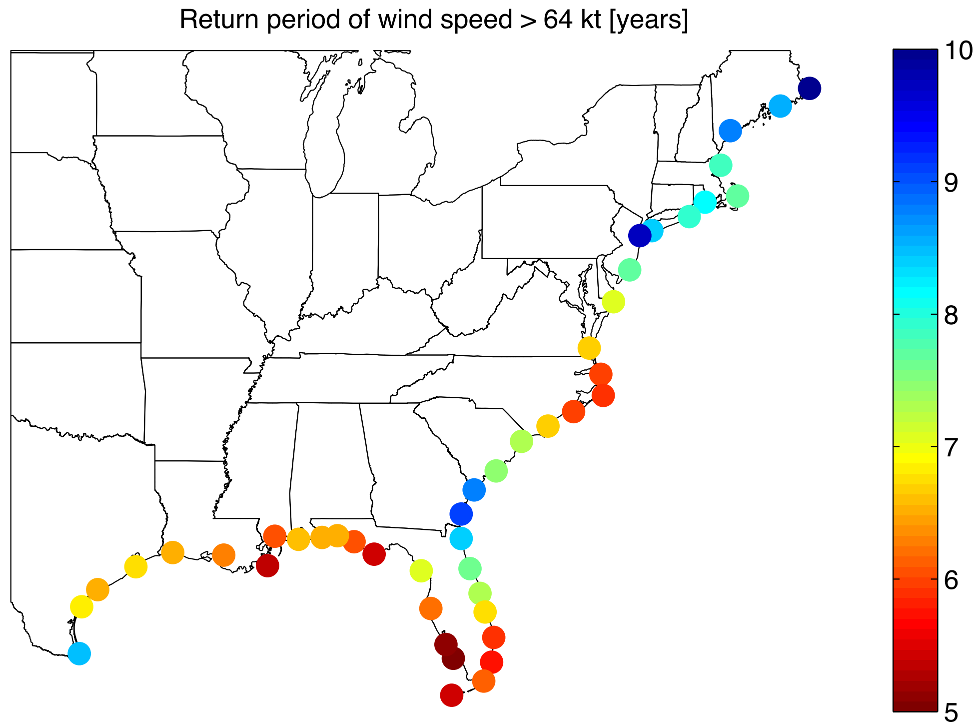

Figure B-4: Return period of wind speeds greater than 64 knots (hurricanes) within 20 km of each point, calculated with the simulation method described in the body of the paper.

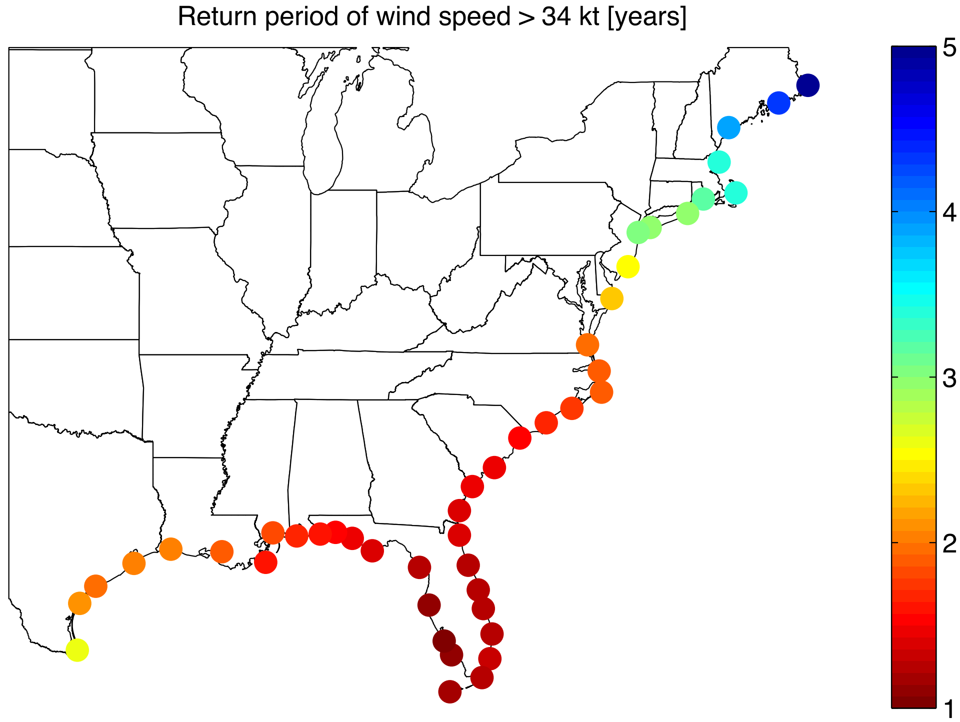

Figure B-5: Return period of wind speeds greater than 34 knots (tropical storms) within 20 km of each point, calculated with the simulation method described in the body of the paper.

In Figure B-5 we plot our estimates of return periods for tropical-storm-force winds, which predict shorter return periods than the historical record. As with the return periods of all hurricanes in Figure B-4, we expect this has little effect on our turbine risk results because most of risk comes from intense hurricanes and we show in Figure B-3 that we model the return period of those well.

B.5.2 ***Return Periods of Maximum Total Wind Speed for Select Locations***

We estimate the distribution of return periods for a range of maximum total wind speeds for New Orleans and Miami, shown in Figure B-6 and Figure B-7. For each point of interest, the return periods are calculated within 100 km of the point for storms that pass within 100 km of the point, using the simulated hurricanes described in the body of the paper. We present these results for comparison with results based on historical hurricane data in a paper by Emanuel and Jagger.[5]

We find the return periods we estimate for total maximum wind speed in New Orleans (Figure B-6) are somewhat shorter than the return periods Emanuel and Jagger estimate. For example we estimate 100-knot winds have approximately a 25-year return period but Emanuel and Jagger estimate approximately 30 years. We estimate 120-knot winds have a return period of approximately 45 years but Emanuel and Jagger estimate approximately 65 years. Both our estimates and Emanuel and Jagger's both fall within the confidence interval for return periods estimated from historical hurricane records. We believe our estimates differ from Emanuel and Jagger's even though we use the same model to simulate hurricanes because our hurricanes are have larger radii of maximum winds that better match the distribution of sizes of historical hurricanes.

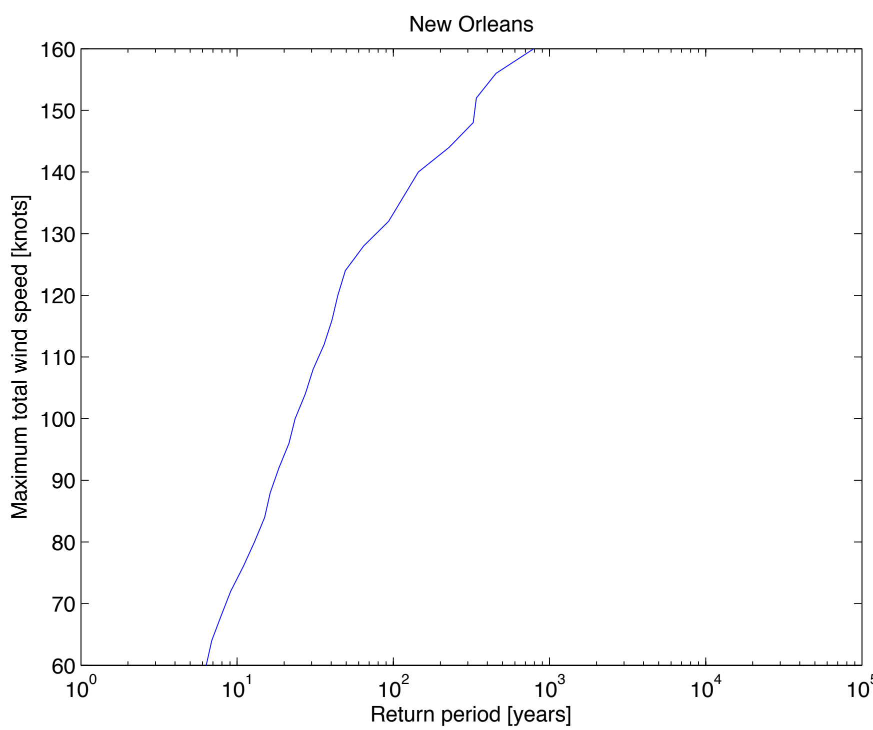

Figure B-6: Return periods for maximum total wind speeds within 100 km of New Orleans, calculated from the simulated hurricanes described in the body of the paper.

We find the return periods we estimate for total maximum wind speed in Miami (Figure B-7) are somewhat different from the return periods Emanuel and Jagger estimate. For example we estimate 100-knot winds have approximately a 24-year return period but Emanuel and Jagger estimate approximately 17 years. We estimate 120-knot winds have a return period of approximately 55 years but Emanuel and Jagger estimate approximately 38 years. Both our estimates and Emanuel and Jagger's both fall within the confidence interval for return periods estimated from historical hurricane records.

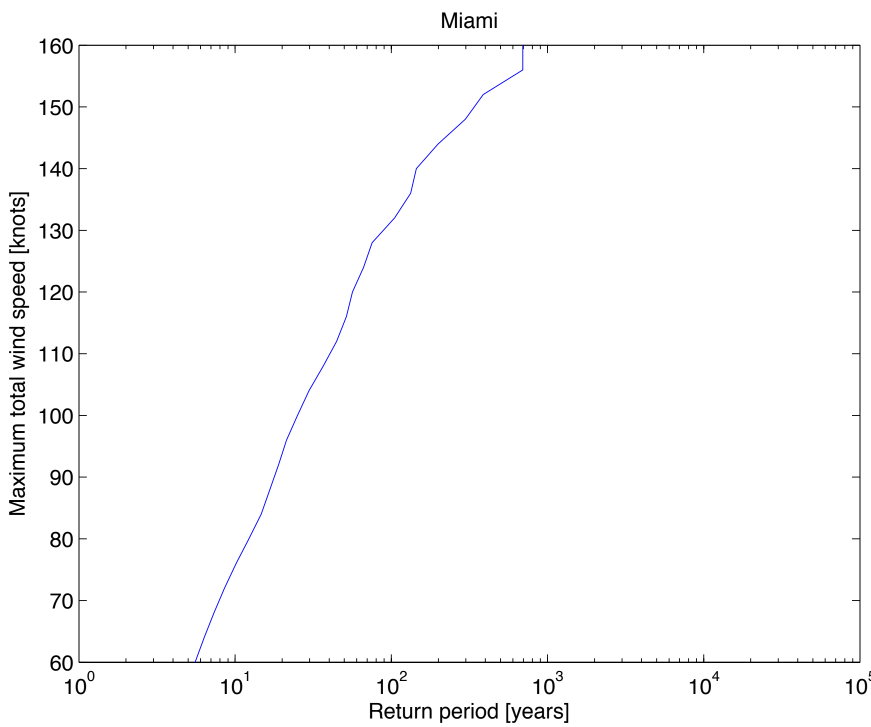

Figure B-7: Return periods for maximum total wind speeds within 100 km of Miami, calculated from the simulated hurricanes described in the body of the paper.

B.6 Appendix References

[1] S. Rose, P. Jaramillo, M. J. Small, I. Grossmann, and J. Apt, "Reply to Powell and Cocke: On the probability of catastrophic damage to offshore wind farms from hurricanes in the US Gulf Coast," *Proc Natl Acad Sci U S A*, vol. 109, no. 33, pp. E2193–E2194, Aug. 2012.

[2] S. Rose, P. Jaramillo, M. J. Small, I. Grossmann, and J. Apt, "Quantifying the hurricane risk to offshore wind turbines," *Proceedings of the National Academy of Science*, vol. 109, no. 9, pp. 3247–3252, Feb. 2012.

[3] D. Gamerman and H. F. Lopes, *Markov Chain Monte Carlo*, 2nd ed. Boca Raton, FL: Chapman

& Call/CRC, 2006.

[4] K. A. Emanuel, S. Ravela, E. Vivant, and C. Risi, "A statistical deterministic approach to hurricane risk assessment," *Bull. Amer. Meteor. Soc.*, vol. 87, no. 3, pp. 299–314, Mar. 2006.

[5] B. D. Keim, R. A. Muller, and G. W. Stone, "Spatiotemporal Patterns and Return Periods of Tropical Storm and Hurricane Strikes from Texas to Maine," *J. Climate*, vol. 20, no. 14, pp. 3498–3509, Jul. 2007.